CHARACTERIZATION OF INTERACTIONS OF THE TYPE IV SECRETION SYSTEM CORE COMPONENT VIRB8

CHARACTERIZATION OF INTERACTIONS OF THE TYPE IV SECRETION SYSTEM CORE COMPONENT VIRB8

By

DURGA SIVANESAN, H.BSc., MSc.

A Thesis

Submitted to the School of Graduate Studies

in Partial Fulfilment of the Requirements

for the Degree

Doctor of Philosophy

McMaster University

DOCTOR OF PHILOSOPHY (2010) McMaster University
(Biology) Hamilton, Ontario

TITLE: Characterization of interactions of the Type IV secretion system core component VirB8

AUTHOR: Durga Sivanesan, H.BSc. (McMaster University), MSc. (Brock University)

SUPERVISOR: Dr. Christian Baron

NUMBER OF PAGES: xii, 171

ABSTRACT

Type IV secretion systems (T4SS) are essential for the virulence of many gram-negative pathogens. The systems studied here comprise eleven VirB proteins in case of *Agrobacterium tumefaciens* and twelve in case of *Brucella suis*. The VirB proteins associate in the cell envelope and form a complex that mediates the translocation of virulence factors into host cells. In this report, VirB8, a core component of T4SS, is characterized with regards to its interaction with itself and with other VirB proteins.

VirB8 was found to exist in monomer-dimer equilibrium and the self-association was demonstrated by analytical ultracentrifugation, analytical gel filtration, surface plasmon resonance and bacterial two-hybrid assay. The above experiments demonstrated that residues M102, Y105 and E214 of VirB8 from *B. suis* are involved in self-association and mutagenesis of these residues led to the impairment of T4SS function in *B. suis*. Furthermore, this information was utilized to unravel the contribution of VirB8 self-association towards T4SS assembly and function. To this end dimerization variants of VirB8 from *Agrobacterium tumefaciens* were created and the effects were assessed with purified proteins *in vitro*. Following this, the effects of VirB8 dimer site changes were assessed *in vivo*. Introduction of a cysteine residue at the predicted interface (V97C) supported DNA transfer but not T-pilus formation. Variants that reduced the self-association did not support T4SS functions and T-pilus formation. Moreover, VirB2-VirB5 co-fractionated with high molecular mass components from membranes of *A. tumefaciens* and VirB8 dimerization was shown to be necessary for VirB2 association with the high molecular mass components. Using purified VirB8 and VirB5 it was shown

that VirB5 interacts with VirB8 via its globular domain and this interaction dissociates VirB8 dimers. Taking these results together, a mechanistic contribution of VirB8 dimerization to T4SS assembly was proposed.

Next, the interactions of VirB8 with other core components (VirB9 and VirB10) were analyzed by using various *in vitro* and *in vivo* experiments. Purified soluble periplasmic domains of VirB8, VirB9 and VirB10 were used in enzyme-linked immunosorbent assays, circular dichroism, and surface plasmon resonance experiments. The pair-wise interactions and self-association of VirB8, VirB9 and VirB10 were demonstrated with the *in vitro* experiments. In addition, a ternary complex formation between VirB8, VirB9, and VirB10 was identified. Using the bacterial two-hybrid system, the dynamics of the interactions between VirB8-VirB9-VirB10 full-length proteins were analyzed demonstrating that VirB9 stimulates VirB8 self-association, but that it inhibits the VirB10-VirB10 as well as the VirB8-VirB10 interaction. Based on these results, a dynamic model for secretion system assembly is proposed where VirB8 plays a role as an assembly factor that is not closely associated with the functional core complex comprising VirB9 and VirB10.

The work reported in this thesis advances the understanding of VirB8 self-association and its contribution to T4SS assembly and function. Furthermore, the establishment of the bacterial two-hybrid system to detect VirB interactions has helped identify inhibitors for the VirB8 dimerization through collaboration with Dr. Athanasios Paschos. Moreover, techniques such as ELISA, analytical ultracentrifugation, circular

dichroism and surface plasmon resonance will be utilized routinely to characterize other VirB-VirB interactions in future.

ACKNOWLEDGEMENTS

Writing the acknowledgement page is the hardest and most important as I have quite a lot of people to thank for their help and support throughout my Ph.D. First, I would like to thank my colleagues at McMaster University (Dr. Athanasios Paschos, Dr. Qing Yuan, Chan Gao, Michelle Melone, and Gregory Rekas) for the daily encouragement, collaborations and discussions over coffee. Special thank you to my colleagues (Dr. Mark Andrew Smith, Dr. Ana Villamil Giraldo, Benoit Bessette, and Gaelle Mawambo) at the Université de Montréal who were extremely supportive at the end stage of my Ph.D. tenure and for helping with proof reading the chapters of my thesis.

Co-workers from Dr. James Coulton's laborartory (McGill University) especially Dr. Maria Plesa and Ernuo Cheung are thanked for help with the phage display experiments. It was a great opportunity to work briefly under Dr. James Coulton's supervision as his love for science and great mentoring was highly motivational. Special mention to Dr. Mark Hancock, form Sheldon Biotechnology (McGill University) with whom I collaborated to perform surface plasmon resonance experiments. Dr. Mark Hanacock's guidance and advice was extremely helpful and will always be remembered.

I would like to thank Drs. George Sorger and Raquel Epand for providing me with motivation and scientific discussions. I admire their love for scientific research and hope that I would be able to emulate their work ethics.

I would like to extend my appreciation to my graduate committee members (Dr. Gerry Wright and Dr. Xu-Dong Zhu) who have provided me with excellent guidance through the years of my Ph.D. training and for encouraging me to develop into a scholar.

Most importantly, I would like to acknowledge my sincere gratitude to my supervisor, Dr. Christian Baron. Being trained under his supervision, I have learnt various important technical skills and most importantly the ability to conduct independent research. He has not only been instrumental in my success but also his mentorship, encouragement, patience and guidance will never be forgotten nor surpassed.

TABLE OF CONTENTS

LIST OF FIGURES

Page

LIST OF TABLES

CHAPTER ONE: An overview to Type IV secretion systems

1.1 Secretion systems in prokaryotes

Protein export and secretion systems are essential for bacteria as virulence factors and for survival (Alvarez-Martinez & Christie, 2009; Marlovits & Stebbins, 2009; Mudrak & Kuehn, 2010; Rambow-Larsen, Petersen, Gourley, & Splitter, 2009). Eight different secretion systems have been reported to date (Desvaux, Hebraud, Talon, & Henderson, 2009). Since Gram-positive bacteria differ from Gram-negative bacteria in their cell envelope, the nomenclature to describe export and translocation differs between them (Figure 1.1). Translocation of a protein occurs when there is change in location due to active transport across a lipid bilayer. Protein export is the active transport of a protein from cytoplasm to the periplasm. Protein secretion is the active transport of a protein from the cytoplasm to the exterior of the cell where an outer membrane protein is involved. Protein secretion systems Sec (secretion), Tat (twin-arginine translocation), FEA (flagella export apparatus), FPE (fimbrilin-protein exporter), holin (hole forming) and Wss (WXG100) are used for both Gram negative and Gram positive bacteria, while Type I to Type VIII applies only for Gram-negative bacteria (Desvaux et al., 2009).

1.2. Types of Secretion systems

There are eight different types of secretion systems that have been grouped according to gene organization and sequence similarity. The type I secretion system (T1SS) is a system composed of three proteins, the ATP binding cassette transporter (ABC) which forms a dimer, and an oligomeric membrane fusion protein (MFP) that associates with the outer membrane protein (OMP) (Balakrishnan, Hughes, & Koronakis,

2001). The coding sequences for this secretion system are found in an operon that is tightly regulated to ascertain that delivery of secreted substrates occurs at the right time and in large amounts (Mourino et al., 1994). Substrates of T1SS are translocated in an unfolded state and the C-terminal signal sequence found in the substrate is important for secretion (Letoffe, Ghigo, & Wandersman, 1994).

The type II secretion system (T2SS) is more commonly found in γ-proteobacteria but also been identified in α-proteobacteria. T2SSs are encoded by 12-16 genes organized into an operon. Diverse substrates are translocated by T2SSs ranging from virulence factors to enzymes that allow the bacteria to survive in various environments (Cianciotto, 2005). The proteins secreted by T2SSs are characterized by the presence of a signal peptide at their N-terminus and are secreted into the extracellular medium in a 2-step process. First, the protein is translocated to the periplasm and this requires either the Sec or Tat pathway for translocating the substrates across the inner membrane (Filloux, 2004). The transport of the protein across the outer membrane then requires the specialized assembly of the T2SS (Brok et al., 1999).

The type III secretion system (T3SS) is related to the flagellar system and delivers proteins directly into the cytoplasm to subvert the host cell defense. T3SS-associated chaperones sequester their specific substrates inside the cell and export them to the periplasm and the chaperones themselves never get secreted but recycled (Parsot, Hamiaux, & Page, 2003). A large number of T3SS substrates are secreted by various animal and plant pathogens (Mota & Cornelis, 2005).

The type IV secretion system (T4SS) is classified as such due to the sequence similarities between the protein components of systems used for conjugation of plasmids and for the delivery of virulence factors from bacterial pathogens to their hosts (Salmond, 1994). T4SS similar to other types of secretion systems span the inner to the outer membrane to deliver various substrates to hosts (DNA, DNA-protein and protein alone). T4SSs are not only important for DNA secretion but also for import. This secretion system will be discussed in detail in the following sections of this chapter.

The type V secretion system (T5SS) has been proposed to be less 'complex' than other secretion systems (Henderson, Cappello, & Nataro, 2000). Each protein secreted by the T5SS contains an N-terminal signal sequence that targets the protein to the Sec machinery to direct its export across the inner membrane. The signature component of this system is the outer membrane β-barrel protein domain allowing the secretion of the effector molecules. The T5SS is subdivided into three subtypes: autotransporter (AT), T5aSS; a two-partner secretion system, T5bSS; and a trimeric autotransporter, T5cSS. The autotransporter (T5aSS) is encoded by one transcript and it contains all the necessary elements for secretion of the effector protein. Autotransporters consist of three domains: a signal sequence targeting Sec dependent export, a C-terminal translocator domain, and a secreted effector also known as the passenger domain (Jose, Jahnig, & Meyer, 1995). The two-partner secretion system (T5bSS) is similar to T5aSS but there are two transcripts, one encoding the passenger domain and one encoding the translocator domain. Each contain their own signal sequence for inner membrane translocation (Henderson et al., 2000). The trimeric AT (T5cSS) is very similar to the T5aSS and

T5bSS; however, this group is characterized by ATs containing a very short C-terminal translocator domain compared to other ATs (Surana, Cutter, Barenkamp, & St Geme, 2004).

The type VI secretion systems are encoded within gene clusters that vary in organization. The systems in this group were initially named as IAHP for IcmF-associated homologous proteins because they contain a gene encoding an Icm (intracellular multiplication) F-like component. *Legionella pneumophilia* requires Icm genes along with other effectors to inhibit phagosome-lysosome fusion inside host cells (Filloux, Hachani, & Bleves, 2008). The type VII secretion system (T7SS), otherwise known as the chaperone-usher pathway, is similar to T1SS to T4SS and T6SS but the distinction of this secretion system is that a periplasmic chaperone is identified that works in conjunction with an integral outer membrane protein, usher (Hung, Knight, Woods, Pinkner, & Hultgren, 1996) to assemble pili (also known as fimbria). Finally, the type VIII secretion system (T8SS) comprises the extracellular nucleation/precipitation pathway, also known as 'curli'. 'Curli' are thin aggregative fimbriae that assemble in Gram-negative bacteria to provide adhesion to biological and non-biological surfaces (Austin, Sanders, Kay, & Collinson, 1998). The focus of the studies reported in this thesis is the Type IV secretion system. Therefore the rest of this chapter will review the literature pertinent to Type IV secretion.

1.3 Type IV secretion system- introduction

Type IV secretion systems (T4SS) are characterized by their ability to transport DNA/protein and protein alone into host cells and import of DNA from other bacteria or

extracellular mileu. T4SSs were classified on the basis of their ancestral relation to conjugative machineries found in Gram-negative bacteria (P.J. Christie, 2004). T4SSs are often encoded by conjugative plasmids such as R388 (IncW), pKM101 (IncN) and RP4 (IncP). These systems allow the dissemination of plasmids between bacterial pathogens, which ultimately leads to increase in antibiotic resistance (P. J. Christie, 2001; Seubert, Hiestand, de la Cruz, & Dehio, 2003). Many Gram negative pathogens such as the plant pathogen *Agrobacterium tumefaciens* (causing crown gall) and animal pathogens such as *Brucella sp.* (brucellosis), *Helicobacter pylori* (gastric ulcers), *L. pneumophilia* (legionnaire's disease), *Bordetella pertussis* (whooping cough), and *Bartonella henselae* (cat-scratch disease) also possess the T4SSs that are utilized for virulence (Cascales & Christie, 2003).

There are three subgroups of T4SS: conjugation systems that translocate DNA, effector translocation systems that primarily deliver proteins to host cells, and DNA uptake/release systems that take up or deliver DNA into the extracellular space (Alvarez-Martinez & Christie, 2009). Recently, the conjugative group was further divided into six groups based on the architecture of the relaxase domain, sequence similarities within the catalytic centre and the 'nic' DNA targeting sequences (Garcillan-Barcia, Francia, & de la Cruz, 2009). Previously, the conjugative group was subdivided based on incompatibility (Inc) groups that were based on the predisposition of the residing plasmid to inhibit the replication of 'incoming' plasmids that are either identical or closely related (Novick, 1987). There are limitations to this strategy as many plasmids have undergone genetic recombination and thus cannot be easily grouped by phylogeny-based classification. An

alternative approach is to subdivide T4SS based on function. However, there are T4SSs that can perform both DNA and effector transfer independently of each other (Alvarez-Martinez & Christie, 2009). The classification of T4SSs that is commonly used is based on the sequence similarity to conjugative systems.

1.4 Architecture of T4SS

Many studies have been conducted to resolve the assembly mechanism of T4SS and most of these studies provide a low-resolution view of T4SS assembly. However, very recently, the x-ray crystal structure of the outer membrane core complex (VirB7-VirB9-VirB10) was resolved to 2.6 Å resolution (Chandran et al., 2009; Fronzes, Schafer et al., 2009). Incorporating this information with other interaction network studies such as yeast two-hybrid and biochemical analysis of the T4SS complex and *in vitro* experiments such as peptide array and other protein-protein interaction studies (Höppner, Carle, Sivanesan, Hoeppner, & Baron, 2005; D. Ward, Draper, Zupan, & Zambryski, 2002; Yuan et al., 2005), has provided a static view of the assembly as shown in Figure 1.2. Transfer immunoprecipitation assay (TrIP, formaldehyde cross-linking imuno-precipitation assay) allows identification of transfer steps at which T-DNA (substrate) is arrested in the absence of a T4SS component or sequence tags in the various components. This assay revealed that there is a dynamic interplay between the subunits of the T4SS to transfer the T-DNA from the cytoplasm to the outer membrane (Cascales & Christie, 2004b). However, the sequence of interactions that precede assembly and the understanding of how the complete T4SS complex assembles is still limited. The

complex macromolecular structure of T4SS can be divided into three groups of proteins: NTPases, core components and extracellular pilus (surface) components.

NTPases of T4SSs

The first group of proteins is comprised of the energetic components of the system: VirD4, VirB4 and VirB11. T4SS uses one or two of the ATPases for T4SSs assembly or substrate transfer. VirB4 and VirB11 contain the Walker A motifs indicative of NTPase activity. **VirD4**, a Type IV secretion system coupling protein (T4CP) that is used for recognizing the substrate and for translocation across the cytoplasmic membrane also contains the Walker A motifs. However, *B. suis* lacks the VirD4-like coupling protein which links the DNA processing complexes, and the relaxosomes to the membrane-bound secretion systems of plasmid translocation T4SS (Hamilton et al., 2001; Schröder & Dehio, 2005). The absence of such a coupling component is suggestive that the effectors of the *B. suis* T4SS are most likely proteins, similar to *B. pertussis* (PT toxin) and may be translocated via a periplasmic route. **VirB4** is a component that is found in all T4SSs identified to date and it is characterized by its large size (94 kDa) and NTP binding motif domain, though the ATPase activity has not been conclusively shown (Alvarez-Martinez & Christie, 2009). VirB4 is localized on the cytoplasmic face of the inner-membrane (Middleton, Sjölander, Krishnamurthy, Foley, & Zambryski, 2005), and regions of *A. tumefaciens* VirB4 were shown to be exposed in the periplasm (Dang & Christie, 1997). Interestingly, using the TrIP assay, it was shown that the T4CP directs the transfer of the T-DNA to VirB4 and VirB11, thus the energizers mediate the transfer of the substrate to the T4SS structural components (Atmakuri, Cascales, & Christie,

2004). The X-ray structure of **VirB11** homolog, HP0525 (H. J. Yeo, Savvides, Herr, Lanka, & Waksman, 2000) and the recent structure of VirB11 from *B. suis* (Hare, Bayliss, Baron, & Waksman, 2006) revealed that these proteins are hexamers, and that they are structurally related to the ATPases commonly associated with other secretion systems such as T2SS, T3SS, and the flagellar biogenesis systems. VirB11 is essential for the assembly of secretion channels as well as pili (Sagulenko, Sagulenko, Chen, & Christie, 2001). Mutational variants of VirB11 were affected in either pilus assembly or substrate transfer providing evidence that VirB11 is important for both functions and that these may be independent of each other. VirB11 hydrolyzes ATP and this activity is enhanced in the presence of lipids suggesting that VirB11 associates with the membranes (Krause, Pansegrau, Lurz, de la Cruz, & Lanka, 2000). The ATPase activity of VirB11 creates conformational changes in VirB10 (core component, inner membrane protein) that were determined by protease susceptibility tests (Cascales & Christie, 2004a). In addition, an interaction of VirB11 with VirB9 (core component, periplasmic protein) was identified using a yeast two hybrid peptide library (D. Ward, Draper, Zupan, & Zambryski, 2002). This puts forward the notion that through ATP utilization and changes of its conformation (Savvides et al., 2003), the interaction of VirB11 with core components promotes either substrate transfer, and/or pilus assembly.

Core components (VirB1, VirB3, VirB6, VirB7, VirB8, VirB9 and VirB10)

The second group of proteins in the T4SS complex is that of the core components composed of VirB1 (lytic transglycosylase), VirB3, VirB6, VirB8 and VirB10 (inner-membrane proteins), VirB7 (lipoprotein) and VirB9 (periplasmic protein). **VirB1** is a

lytic transglycosylase (degrades peptidoglycan) that promotes DNA competence for *A. tumefaciens* T4SS by assisting in T4SS complex formation, but it is not an essential component for T4SS virulence (Höppner, Liu, Domke, Binns, & Baron, 2004). Lytic transglycosylases cleave β-1,4 glycosidic bonds between N-acetylmuramic acid (MurNAc) and N-acetylglucosamine (GlcNAc). Direct evidence for VirB1s lytic transglycosylase activity has been provided (Zahrl et al., 2005a) and VirB1 derivatives with alterations in the putative active site exhibit reduced virulence (Höppner et al., 2004). VirB1 was shown to interact with VirB8, VirB9 and VirB11 (Höppner et al., 2005) which puts forward the notion that VirB1 may be targeted to T4SS assembly through interactions with the structural VirB components. A proteolytically cleaved VirB1 product (VirB1*) is found outside the cell, though the exact role of this VirB1* product remains to be elucidated (Zupan, Hackworth, Aguilar, Ward, & Zambryski, 2007).

VirB3 is a protein predicted to contain transmembrane domains, which suggests that it is located at the inner-membrane, though previous evidence suggested that this protein localizes predominantly at the outer membrane (Jones, Shirasu, & Kado, 1994; Shirasu & Kado, 1993). Recent evidence suggests that VirB3 likely localizes in the inner membrane, since the VirB4, an inner-membrane/cytoplasmic protein influences accumulation of VirB3 (Jones et al., 1994; Yuan et al., 2005). Furthermore, VirB6, an inner-membrane protein, co-localizes with VirB3, which provides evidence that VirB3 likely is an inner-membrane protein too (Judd, Kumar, & Das, 2005b). **VirB6** is a polytopic inner membrane protein with five transmembrane domains (S.J. Jakubowski, Krishnamoorthy, Cascales, & Christie, 2004) with the members of VirB6 family having

low sequence similarities (Alvarez-Martinez & Christie, 2009). In the absence of VirB6, VirB5 and VirB3 accumulation are affected suggesting that these proteins may interact (Hapfelmeier, Domke, Zambryski, & Baron, 2000). Results of the TrIP assay suggested that VirB6 co-ordinates with VirB8 and obtains the DNA substrate from VirB11 to transfer it to other VirB core components (Cascales & Christie, 2004b; S.J. Jakubowski et al., 2004).

VirB8 and VirB10 are bi-topic inner membrane proteins (A. Das & Y.-H. Xie, 1998). X-ray crystal structures of **VirB8** from both *A. tumefaciens* and *B. suis* have been solved and their structure suggest that it is a homo-dimer (Figure 1.3). Each VirB8 monomer consists of large four β-strands linked to five α-helices (Bailey, Ward, Middleton, Grossmann, & Zambryski, 2006; Terradot et al., 2005) (Figure 1.3). The structures are similar to nuclear transport factor 2 (NTF2) that is involved in transport of cargo to and from the nucleus (Chaillan-Huntington et al., 2001). VirB8 has received a large amount of attention and it has been proposed that VirB8 is a scaffolding protein that targets many VirB proteins to provide polar localization and hence T4SS assembly (Judd, Kumar, & Das, 2005a). In accordance with this view, VirB8 interacts with multiple partners, namely VirB1, VirB4, VirB5, VirB8, VirB9, VirB10 and VirB11 (Das & Xie, 2000; Höppner et al., 2005; D. Ward et al., 2002; Yuan et al., 2005) and there is indirect evidence that VirB8 interacts with VirB6 (S.J. Jakubowski et al., 2004; D. Ward et al., 2002; Yuan et al., 2005). Though VirB8 is a central protein in T4SS assembly and function, it requires VirB4 for its stability *in vivo* (Yuan et al., 2005). Interestingly, attempts to pull-down VirB8 along with VirB7-VirB9 and VirB10 were not successful,

which suggests that VirB8 interaction with VirB9 and VirB10 may be weak (Chandran et al., 2009; Fronzes, Schafer et al., 2009). As mentioned before, VirB8 can be cross-linked to the DNA substrate and it also interacts with VirB10 and many other VirB proteins, it may therefore be a very good drug target (Baron, 2006).

VirB10, another bitopic protein of the T4SSs is found to exist as a homo-dimer as suggested by the crystal structure of a homologue in *H. pylori* ComB10 (Terradot et al., 2005). The ComB10 structure comprises an extensively modified β-barallel with a α-helix projecting to one side and a second flexible helix-loop-helix projecting to the top. VirB10 contains a proline rich domain (coiled-coiled) followed by a large C-terminal domain that extends into the periplasm (S. J. Jakubowski et al., 2009). VirB10 interactions with itself, VirB8, VirB9 and VirB11 were shown before (Das & Xie, 2000; D. Ward et al., 2002). It is proposed that VirB10 undergoes a conformational change upon ATP utilization by the ATPase VirB11 and mediates contact with VirB7-VirB9 to form the VirB7-VirB9-VirB10 complex *in vivo* (Cascales & Christie, 2004a). Recent structural information on the core complex of VirB7-VirB9-VirB10 has advanced our understanding on how these proteins form a core complex at the molecular level (Chandran et al., 2009; Fronzes, Schafer et al., 2009).

VirB7 and VirB9. VirB7 proteins are lipoproteins and in *A. tumefaciens*, it localizes at the outer membrane and forms a disulfide linkage with VirB9 (Baron, Thorstenson, & Zambryski, 1997; Fernandez, Dang et al., 1996). Periplasmic VirB9 is a hydrophilic protein and it was originally thought to multimerize and form pores as secretin to secrete effectors (Cascales & Christie, 2004b) but recently this was proven to

be incorrect (Chandran et al., 2009). VirB7 interacts with VirB9 to form VirB7-VirB9 heterodimers, which stabilize other type IV components (Fernandez, Spudich, Zhou, & Christie, 1996). The NMR structure of VirB7-VirB9 from the pKM101 conjugative plasmid showed that VirB9 has a β-'sandwich' fold consisting of nine β-strands and a short region of 3_{10} helix between the first and second strands. VirB7 is present as an extended structure that wraps around VirB9 (Bayliss et al., 2007). A 1 MDa complex between VirB7-VirB9-VirB10 proteins was solved by cryo-electron microscopy (Fronzes, Schafer et al., 2009). This core complex consists of 14 copies of each protein and it is composed of two layers I (inner) and O (outer). Following on this cyro-EM structure, a X-ray crystal structure of the core complex (VirB7-VirB9-VirB10 from pKM101) after chymotryptic cleavage was solved recently (Chandran et al., 2009). This 590 kDa complex contains 14 copies of each of the C-terminal domain of VirB10, C-terminal domain of VirB9 and full length VirB7. Unlike predictions of the cryo-electron microscopy structure, in the crystal structure of the core complex VirB10 forms a ring inside that is surrounded by VirB9 and VirB7 (Figure 1.4). Interestingly, it is VirB10 and not VirB9 that forms the channel, and VirB10 is found to insert into the outer membrane as well into the inner membrane. The crystal structure also shows that there is more order to VirB9 when bound to VirB10 compared to the NMR structure of VirB9-VirB7 complex indicating that upon interaction with VirB10, VirB9 undergoes conformational changes. Moreover, the X-ray structure shows that VirB7 winds around VirB9 more than what was observed in the NMR structure (Chandran et al., 2009). The structure of the VirB7-VirB9-VirB10 complex is a decisive step forward towards understanding the

assembly of T4SS core complex. However, the major question that still remains regards VirB8's role in the core complex. Since VirB8 and VirB6 were reported to cross-link to the DNA substrate (Cascales & Christie, 2004b), either one protein would most likely be involved in forming the core at the inner membrane (Fronzes, Christie, & Waksman, 2009).

Outer membrane components (VirB2 and VirB5)

The third group of T4SSs comprises the extracellular or pilus components, VirB2 and VirB5. **VirB2** is the major component and VirB5 is the minor component of the T-pilus (Schmidt-Eisenlohr, Domke, & Baron, 1999). VirB2 contains a signal peptide that gets cleaved and becomes a 7.2 kDa product and this VirB2 product links itself between the amino and carboxyl terminal residues to become cyclized (E. M. Lai, Eisenbrandt, Kalkum, Lanka, & Kado, 2002). The cyclization of *A. tumefaciens* VirB2 is specific to the host and this process is VirB independent. VirB2-VirB5 constitutes the T-pilus and it is important in providing attachment for virulence and for conjugation. **VirB5** was found to localize at the tips of the pili (Aly & Baron, 2007; H.-J. Yeo, Yuan, Beck, Baron, & Waksman, 2003). The X-ray structure of the VirB5 homolog TraC from pKM101 was solved (H.-J. Yeo et al., 2003). Mutational anlaysis of TraC, in addition to its structural similarity to focal adhesion targeting (FAT) domain suggests that VirB5 may play a role as an adhesion protein (Backert, Fronzes, & Waksman, 2008). However, there is no direct experimental evidence for VirB5 as receptor. In contrast, plant receptor proteins for VirB2 were identified by yeast-two hybrid analysis (Hwang & Gelvin, 2004).

1.5 Regulation of T4SS

In order to circumvent unnecessary expression of the virulence genes, bacteria possess factors that tightly control their expression. In this thesis, the focus is on two bacterial pathogens, *B. suis* (mammalian pathogen), and *A. tumefaciens* (plant pathogen). Persistent infection of mammalian cells requires expression of functional T4SS in *Brucella* sp (O'Callaghan et al., 1999). *Brucella* sp. are facultative intracellular pathogens of many animals and causes zoonotic disease in humans. The survival of the pathogen in macrophage cells occurs via secretion of effector proteins such as VceA and VceC using T4SS (de Jong, Sun, den Hartigh, van Dijl, & Tsolis, 2008b). The VirB system of *B. suis* is regulated by two proteins VjbR and BlxR (Delrue et al., 2005). These regulators belong to the family of LuxR quorum sensing (QS) regulators that contain acylhomoserine lactone binding motifs. The quorum sensing pheromone N-dodecanoylhomoserine lactone (C_{12}-HSL) inhibits the activation of *virB* genes via VjbR (Delrue et al., 2005). VjbR binds *virB* promoters directly and another regulator, known as integration host factor (IHF), that is regulated by Rsh (stringent response mediator) under nutrient limitation conditions was identified to bend DNA to form the correct promoter structure for action of additional transcriptional regulators. In addition, low pH was also found to activate T4SS of *B. suis*. However, the intermediate factor involved in this pathway is still unknown.

Similarly, the *A. tumefaciens* T4SS virulence genes are induced by three factors: phenolic compounds, monosaccharides, and low pH using the two-component regulator VirA/VirG system (Winans, 1992). *A. tumefaciens* infects plant cells at wound sites

where the above signals such as phenolic compounds (acetosyringone) and monomers of plant cells wall polysaccharides are secreted. T4SS virulence genes in *A. tumefaciens* strains are induced by VirA and VirG (Stachel & Zambryski, 1986). VirA undergoes autophosphorylation upon sensing phenolic compounds, which then transfers the phosphate to VirG. Phosphorylated VirG binds *vir* promoters and activates transcription and induction by sugars require the presence of ChvE that is encoded in the chromosome of the bacteria (Winans, 1992).

1.6 Functional importance of T4SS

T4SSs are found to be essential virulence factors in many bacterial pathogens (Cascales & Christie, 2003; Llosa, Roy, & Dehio, 2009). The model system for this multi-component secretion machinery is from the plant pathogen *A. tumefaciens*. *A. tumefaciens* uses the VirB/D4 system to transport T-DNA/protein (VirD2) complex into the plant cells. The T-DNA moves to the plant nucleus and gets incorporated into the chromosome. The T-DNA encodes enzymes that allow for synthesis of auxins and cytokinins that is responsible for tumor formation; and opines which is synthesized by the plant cells that is taken up by *A. tumefaciens* as carbon and nitrogen sources (Alvarez-Martinez & Christie, 2009; Zupan, Muth, Draper, & Zambryski, 2000).

Another function of T4SS is conjugation. There are three steps involved in conjugation of DNA: DNA substrate processing, substrate recruitment and translocation of the DNA substrate (Alvarez-Martinez & Christie, 2009). The DNA processing system is conserved for all conjugative machineries. DNA transfer and replication proteins (Dtr) proteins start processing by binding a cognate origin of transfer (oriT) sequence.

Relaxase (VirD1 and VirD2) binds oriT sequence (5' end of the T-DNA) and nicks the DNA that is to be translocated (T-DNA). The relaxase targets the T-DNA to the translocation channel by interacting with T4CP (VirD4) that specifically recruits the substrate. Translocation of the T-DNA occurs via the T4SS VirB components and the relaxase that is bound to the 5' end of the T-DNA in the recipient cell starts the re-circularization of the T-DNA to initiate second strand synthesis or insert into the chromosome of the host or recipient cell (Alvarez-Martinez & Christie, 2009) (Figure 1.5).

In the mammalian pathogen *B. suis* the *virB* region of *B. suis* is essential for virulence as independent *virB5*, *virB9*, or *virB10* mutations attenuated infection of human macrophage cells, and infection was restored to wild type levels when complemented with respective *virB* genes *in trans* (O´Callaghan et al., 1999). This suggests that the *B. suis* utilizes the *virB* operon for its intracellular survival and multiplication in human macrophages. Signature-tagged transposon mutagenesis has revealed that mutants of *virB* region in *B. suis* are attenuated in HeLa and THP-1 macrophage cell infections (Foulongne, Bourg, Cazevieille, Michaux-Charachon, & O'Callaghan, 2000). The mutants within the *virB* operon fail to display wild type *Brucella* behavior, such as failure to recruit actin polymerization, failure to form macropinosomes and they do not sustain interactions with the host ER and are killed by fusion with lysosomes (Celli et al., 2003; Watarai, Makino, Fujii, Okamoto, & Shirahata, 2002). *B. pertussis* and *H. pylori* use T4SS to deliver PT toxin and Cag A toxin to host cells, respectively. Therefore, T4SS is harnessed for two major functions in Gram negative bacteria, for pathogenesis and

plasmid transfer (leading to antimicrobial resistance). Understanding the contribution of each of the VirB components towards T4SS assembly and function would lead to identification of novel targets for control of diseases and to reduce the spread of antibiotic resistant bacteria.

The objectives of this thesis were to identify the protein-protein interaction between VirB5 and VirB8, to characterize VirB8 self-association, to identify the mechanism of VirB8 self-association *in vivo* and finally, to characterize the core complex formation betweenVirB8-VirB9-VirB10.

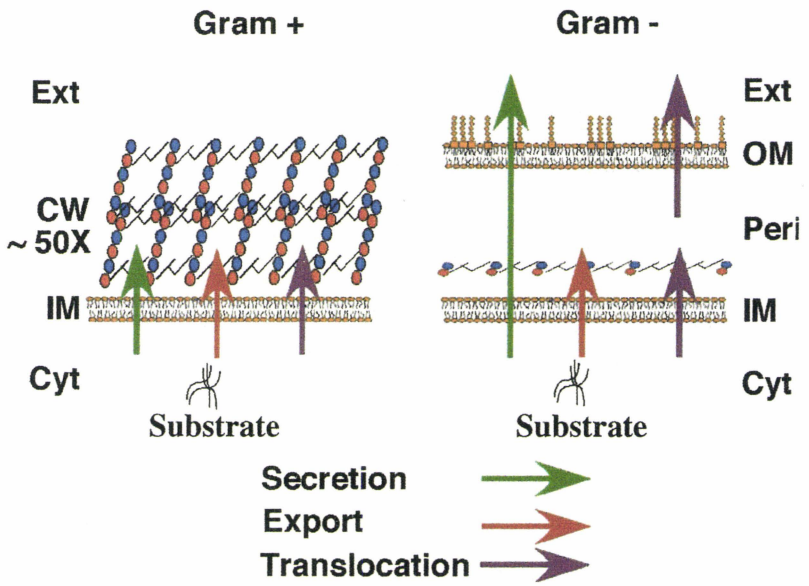

Figure 1.1 Difference in cell envelope composition between Gram-negative and Gram-positive bacteria. Cyt, cytoplasm; IM, inner membrane; Peri, periplasm; OM, outer membrane; Ext, extra-cellular space; CW, cell wall. The CW of Gram-positive bacteria is roughly consists of 50 layers of peptidoglycan.

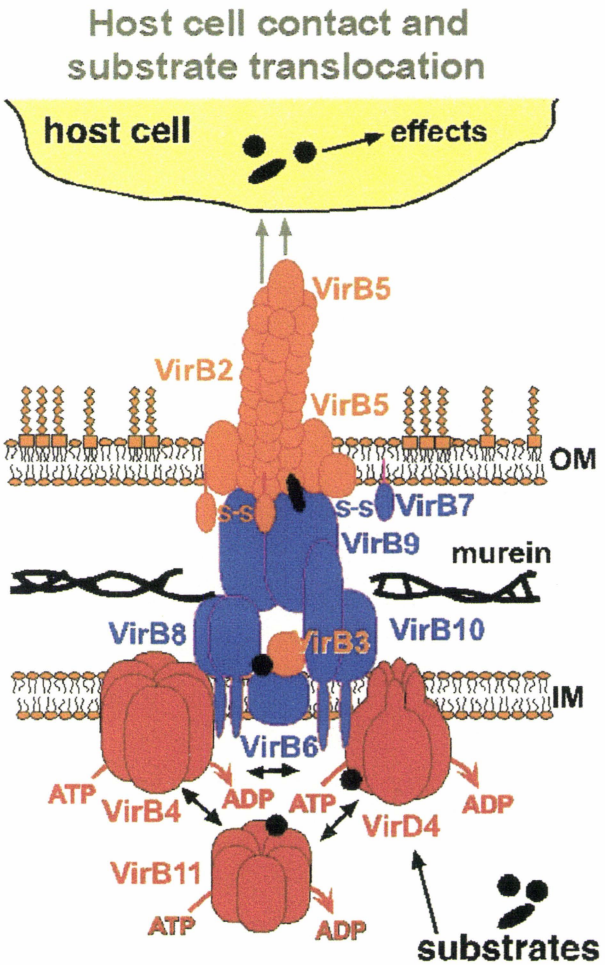

Figure 1.2 Type IV secretion system (T4SS) complex model. The T4SS is grouped into three major groups of components: energizers colored in red provide energy for substrate transfer and T4SS assembly, core components colored in blue that transverse the inner membrane to the periplasm, and pilus associated proteins colored in orange that make contact with the host. IM, corresponds to inner membrane and OM, corresponds to outer membrane. This figure was kindly provided by Dr. Christian Baron (Baron, 2006). Permission to reproduce this figure was obtained from NRC Research Press.

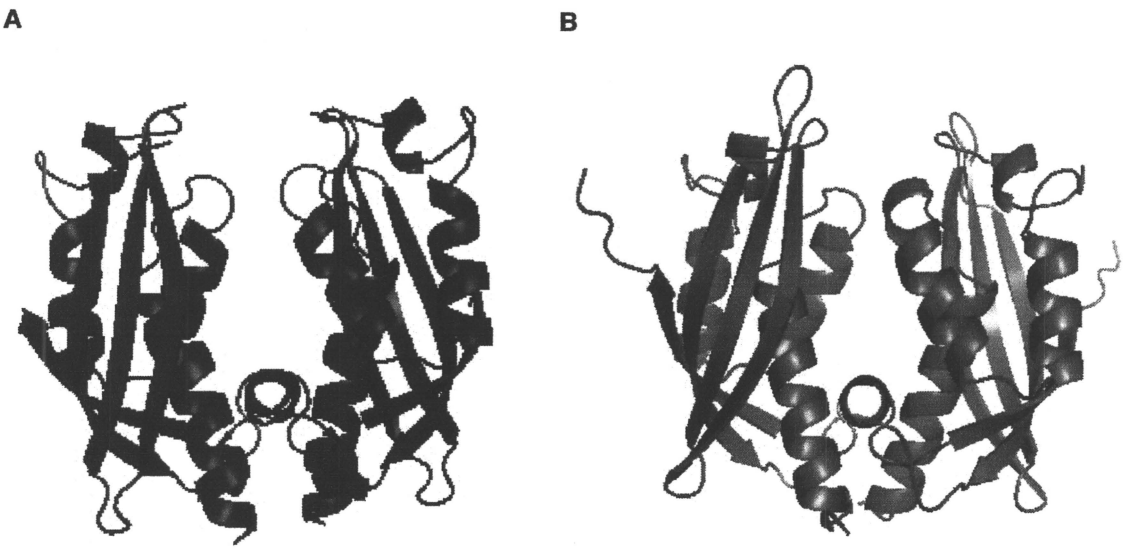

Figure 1.3 Ribbon diagrams of VirB8 from *B. suis* (VirB8sp) and *A. tumefaciens* (VirB8ap). The VirB8sp model **(A)** was generated based on the data base file (2BHM.pdb) and **(B)** the VirB8ap (2CC3.pdb) by MacPymol (pymol.sourceforge.net).

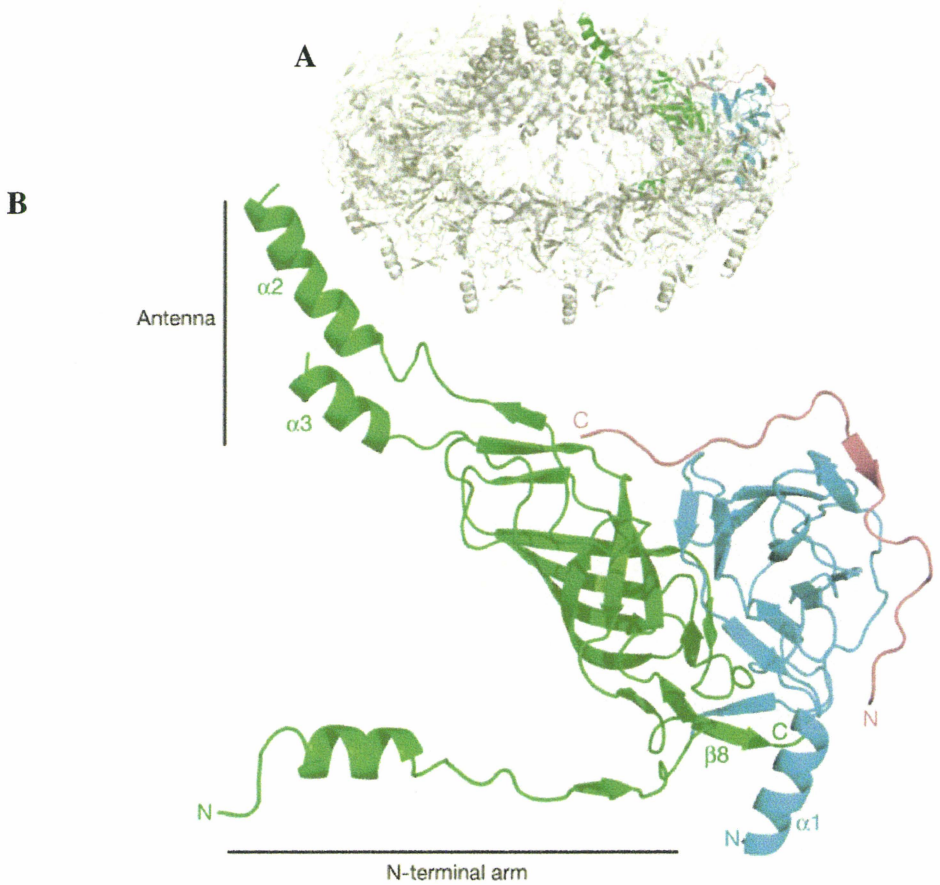

Figure 1.4 The cartoon diagram of the VirB7-VirB9-VirB10 complex of the heterodimer unit of the T4SS core complex. The structure in green corresponds to VirB10 C-terminus; the structure in blue shows VirB9 C-terminus and the structure in magenta shows VirB7. The entire outer-membrane core complex structure is shown above **(A)** in grey where one heterodimer unit is represented within the outer-membrane core complex **(B)** (Chandran et al., 2009). Permission to reproduce this figure was obtained from Nature Publishing Group.

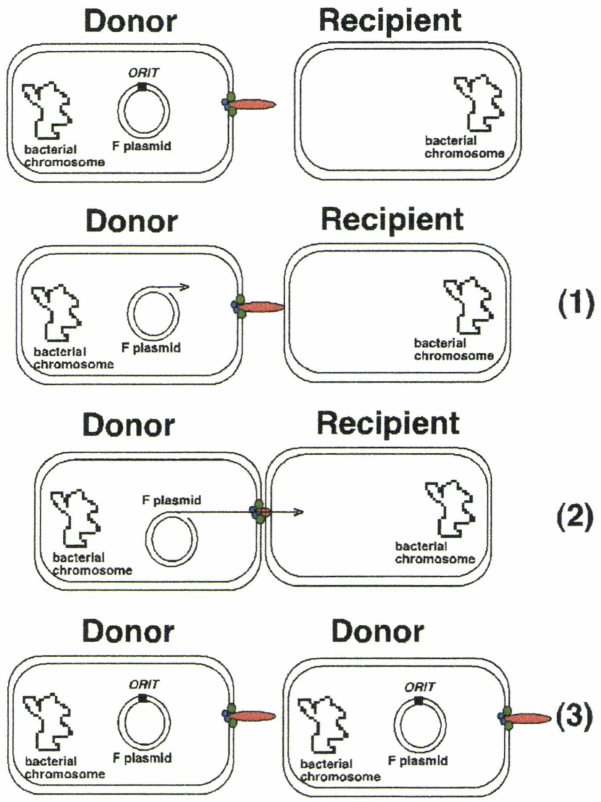

Figure 1.5 Conjugation mechanism in bacteria. (1) The donor cell makes contacts with the recipient cell using the pilus structure. (2) The F-plasmid is nicked at the origin of transfer and ssDNA is transferred into the recipient cell and second strand of DNA is synthesized in the recipient cell and the DNA is nicked and released in the recipient cell. (3) Once the plasmid is completely transferred the cells separate and now the recipient cell becomes a donor cell. This model is believed to reflect the basic mechanism of all conjugation systems, it was adapted from the following website: http://www.sci.sdsu.edu/~smaloy/MicrobialGenetics/topics/plasmids/conjugation-mech.html

CHAPTER TWO: Characterization of the VirB5-VirB8 interaction.

Preface:

Dr. Anna Carle performed the pull down experiment during her Ph.D. tenure in Germany under the supervision of Dr. Christian Baron. The results presented in Figure 2.1A were confirmed by me at the beginning of my Ph.D. tenure. Dr. Anna Carle conducted the peptide array experiments in this chapter that are presented in Figure 2.2B. Dr. Athanasios Paschos, a previous research associate in Dr. Christian Baron's laboratory at McMaster University performed the peptide competition (cross-linking experiments) that are presented in Figure 2.3A. Figure 2.1 was contributed towards a co-authored publication and this research was published in Journal of Biological Chemistry [Qing Yuan, Anna Carle, Chan Gao, Durga Sivanesan, Khaled Ahmed Aly, Christoph Hoppner, Lilian Krall, Natalie Domke, and Christian Baron. Identification of the VirB4-VirB8-VirB5-VirB2 pilus assembly sequence of Type IV secretion systems. Journal of Biological Chemistry. 2005; 280, 26349-26359. Figures 2.2, and 2.3 were contributed towards a manuscript to be submitted where I am first author (Durga Sivanesan, Athanasios Paschos, Anna Carle, Ernuo Cheung, James Coulton and Christian Baron).

CHAPTER Two: Characterization of the VirB5-VirB8 interaction

Abstract

Type IV secretion systems are essential for the virulence of many gram-negative pathogens. The systems studied here comprise eleven VirB proteins in case of *A. tumefaciens* and twelve in case of *B. suis*. The VirB proteins associate in the cell envelope and form a complex that mediates the translocation of virulence factors into host cells. VirB5, VirB8, VirB9 and VirB10 proteins from the *B. suis* T4SS were purified and analyses using pull down and cross-linking revealed that VirB5 directly binds VirB8 and VirB10, but not VirB9. The minimal domain of *B. suis* VirB5 required for interaction with VirB8 was identified. Domain deletion and peptide array analysis showed that a globular appendage of VirB5 is the likely interaction site with VirB8. Peptide competition and affinity precipitation experiments of VirB5 wild type and of variants in the putative interaction domain identified the VirB5 domain required for the interaction with VirB8. The identification of the minimal VirB5-VirB8 interaction domain greatly advances our understanding of the dynamic interplay between these essential virulence factors and opens avenues for development of inhibitors of protein-protein interactions.

2.1 Introduction

Protein-protein interactions between subunits of complex translocation machineries such as secretion systems play key roles in providing stability and function. The best characterized T4SS model is from the plant pathogen *A. tumefaciens*, but work reported in this chapter was conducted with *B. suis* VirB proteins (named VirBs in the following and VirBsp to indicate their periplasmic domains) as they are more suited for purification and *in vitro* biochemical studies (Höppner et al., 2005; Yuan et al., 2005). The secretion system of the mammalian pathogen *B. suis* is encoded in an operon similar to *A. tumefaciens* but it encodes twelve VirBs proteins instead of eleven like *A. tumefaciens* (O´Callaghan et al., 1999). Also, *B. suis* lacks a VirD4-like coupling protein (Paulsen et al., 2002). These proteins link the DNA processing complexes, the relaxosomes, to the membrane-bound translocation complexes of plasmid-translocating T4SSs (Hamilton et al., 2001; Schröder & Lanka, 2005). The absence of such a coupling component suggests that the effectors of the *B. suis* T4SS are most likely proteins, and similar to *Bordetella pertussis*, they may be translocated via a periplasmic route.

B. suis requires its T4SS for infection (survival and replication) of mammalian cells (Celli & Gorvel, 2004) and similarly, T4SSs are required for the virulence of many other pathogens and for the transfer of antibiotic resistance gene-carrying plasmids. The broad distribution of T4SSs suggests that they may be excellent targets for the development of inhibitors, which would disarm many pathogens and reduce resistance gene spread (Baron, 2005). The protein-protein interactions studied here constitute novel targets for the development of such drugs. The VirB protein interaction network has been studied

using different approaches aimed at defining the mechanism of substrate transport and T4SS assembly (Ding et al., 2002; Judd et al., 2005a; Krall et al., 2002; D. Ward et al., 2002).

In our laboratory, we identified a pilus assembly sequence in *A. tumefaciens* that is dependent on stabilization of VirB4 but not on its nucleotide hydrolase activity (Yuan et al., 2005). Using biochemical methods we showed that VirB4s directly interacts with VirB8sp, which explained the stabilizing effect in the *A. tumefaciens* system. Thus, we proposed that VirB5 may interact with VirB8, VirB9 and VirB10 preceding the formation of the VirB2-VirB5 complex and its incorporation into pili. As VirB5-like proteins localize extracellularly in the pilus (Schmidt-Eisenlohr, Domke, Angerer et al., 1999; Schmidt-Eisenlohr, Domke, & Baron, 1999), VirB5sp interaction with the periplasmic parts of the bitopic inner-membrane proteins VirB8sp, VirB9sp and VirB10sp (A. Das & Y.-H. Xie, 1998) could identify an intermediate step prior to incorporation into pili. The availability of crystal structures of VirB8sp (Terradot et al., 2005) and of the VirB5 ortholog TraC (H.-J. Yeo et al., 2003) greatly facilitated the structure-function analysis reported here.

VirB5-like proteins comprise a bundle of three α-helices and a globular appendage. Mutational studies of TraC identified several residues important for incorporation into pili and for its function in plasmid transfer (H.-J. Yeo et al., 2003). We here analyzed the effects of similar changes introduced into VirB5sp. In this study, we performed high-resolution peptide array, peptide competition and mutational analysis of VirB5sp to identify the minimal domain necessary for interaction with VirB8sp. The

results from this study will set the stage for the development of peptide aptamers or small molecules as inhibitors of T4SS functions.

2.2 Materials and Methods

2.2.1 Cultivation of bacteria.

The strains and plasmids used in this study are listed in Table 2.1. Cultures of *E. coli* JM109 for cloning experiments were grown at 37°C in LB (1% tryptone, 0.5% yeast extract, 0.5% NaCl) in the presence of antibiotics for plasmid propagation (spectinomycin [spc], 50 μg/ml; streptomycin [str], 50 μg/ml; carbenicillin [car], 100 μg/ml; kanamycin [kan], 50 μg/ml).

For protein overproduction, *E. coli* strain GJ1158 was grown under aerobic conditions at 37°C in LBON medium (1% tryptone, 0.5% yeast extract) to an OD_{600} of 0.4-0.8, followed by the addition of NaCl at 0.3 M. Cultivation under aerobic conditions proceeded at 26°C for 16 h after induction.

2.2.2 Plasmid, strain constructions and mutagenesis.

DNA manipulations followed standard procedures (Maniatis, Fritsch, & Sambrook, 1982). Site directed mutagenesis and deletions of *virB5* were performed using pT7-7StrepIIVirB5sp as a template for inverse PCR (Ansaldi, Lepelletier, & Mejean, 1996). Here, the use of overlapping sequences of PCR primers (Table 2.2) along with *Dpn*I treatment of the PCR product at 37°C for 2 h allowed direct cloning in *E. coli* without the need for ligation.

For creation of pTrcSC, 5'-phosphorylated oligonucleotides (Table 2.2) encoding the calmodulin binding peptide were cloned into *Bst*BI/*Hind*III sites of pTrcStrep. This vector permits the expression of proteins with a C-terminal double tag (Strep-tag II and calmodulin binding protein) for detection with specific antisera and purification via

affinity chromatography. For creation of pTrcSP-SC, 5'-phosphorylated oligonucleotides encoding the VirB5s signal peptide (SP) were ligated into *Nco*I/*Pac*I of pTrcSC. This vector was used to subclone the genes encoding VirB5sp and variants from pT7-7StrepII constructs, which did not encode the signal peptide. The resulting genes encoding VirB5s and variants with the signal peptide were sub-cloned into pSDM200 to complement the defect of pTrc300B1+3-12$^{\Delta virB5}$ in trans.

To create constrained peptide aptamers, the gene fragment encoding thioredoxin (TrxA) from *E. coli* was PCR amplified and sub-cloned into pTrcSP-SC downstream of the SP sequence to create pTrcSP-TrxA-SC construct. The 5'-phosphorylated oligonucleotides corresponding to peptide IV or I+II (Table 2.2) were sub-cloned into the *Rsr*II restriction site found in the gene at a position corresponding to the active site of TrxA. The resulting DNA encoding SP-TrxA (peptide IV or I+II) SC was sub-cloned into pUT18CB8+SD for expression. All of the fragments that were PCR amplified and sub-cloned were confirmed by DNA sequencing.

2.2.3 Purification of fusion proteins.

N-terminally StrepII-tagged proteins (StrepIIVirB5sp and derivatives, StrepIIVirB8sp, StrepIIVirB9sp, and StrepIIVirB10sp), and (H_6TrxAVirB8sp, H_6TrxAVirB9sp and H_6TrxAVirB10sp) were overproduced in GJ1158 *E. coli* expression strain. The cells harvested from expression of the plasmid H_6TrxAVirB constructs were lysed using a French Press Cell (Aminco) at 18,000 psi (pounds per square inch) in lysis buffer (50 mM Hepes pH 7.5, 200 mM KCl, 5 mM $MgCl_2$) with 0.5 mM phenyl methyl sulfonyl fluoride (PMSF). The lysate was clarified by centrifugation twice at 13,000

rpm at 4 °C for 30 min, followed by flowing over a HPLC Nickel chelated IMAC column (Talon™ Superflow, BD Biosciences Clontech). A step gradient method was used to isolate the hexa-histidyl (6xHis) tagged proteins where first the column was washed with 5 column volumes (CV) of Buffer A (50 mM Hepes pH 7.5, 1 M NaCl), followed by washing with 2.5 CV of buffer A plus 20 mM imidazole and then the protein was eluted with a step gradient using buffer B (buffer A with 400 mM imidazole). The fractions containing the isolated protein were then dialyzed overnight at 4 °C in H1B (50 mM Hepes pH 7.5, 200 mM NaCl). The fractions were then subjected to a second dialysis step overnight at 4 °C in H2B (H1B with 50% glycerol and 2 mM DTT) for storage at -20 °C.

N-terminally strepII-tagged proteins were lysed in Buffer W (100 mM Tris-HCl pH 8.0, 150 mM NaCl, 1 mM EDTA) in the presence of 0.5 mM PMSF as described above. The clarified supernatant after lysis was flowed over a 1 mL Strep-Tactin Superflow column (IBA, Göttingen, Germany). The column was then washed with 5CV of Buffer W follwed by elution with Buffer W plus 2.5 mM desthiobiotin. The isolated proteins were then further purified using size exclusion chromatography (Superdex 75 or Superdex 200, Amersham Biosciences) using S2B at a flow rate of 0.5 ml/min. The strepII-tagged proteins were then dialyzed overnight at 4 °C in Buffer W with 50% glycerol and 2 mM DTT (PSB) for storage at -20 °C.

2.2.4 Peptide array analysis.

The methodology used for peptide array analysis was followed as described before (Höppner et al., 2005). The sequence of VirB5sp from *B. suis* (Genbank

accession: AAD56615) without the signal peptide was displayed on a cellulose membrane as N-terminally acetylated 13-mer peptides covalently bound at the C-terminus. The sequence shifted by three amino acid positions each, beginning with peptide 1:AHAQLPVTDAGSI, peptide 2: QLPVTDAGSIAQN etc. to peptide 70:YPQPKALEAAY. The protocol for "Mapping of discontinuous epitopes" from the supplier was applied (Jerini, Berlin, Germany). The peptide array membranes were pre-incubated for 30 min in TBS-T (20 mM Tris/HCl, 137 mM NaCl, 0.1% Tween-20, pH 8.0), transferred into blocking solution (Roche) for 1 h, washed with TBS-T for 10 min and then incubated in blocking solution containing 1-5 μg/ml of the different proteins (StrepIIVirB8sp, StrepIIVirB9sp, and StrepIIVirB10sp) for 12 h at 4 °C. The membranes were then washed three times in TBS-T for 10 sec to remove non-specifically bound protein, transferred onto PVDF membranes with a semi-dry blot device (Fast-Blot, Biometra) followed by Western blotting.

2.2.5 SDS-PAGE and Western blotting.

Cells and protein samples were incubated in Laemmli sample buffer (SB) for 5 min at 100 °C, followed by SDS-PAGE (Laemmli, 1970; Schägger & von Jagow, 1987). Western blotting was performed following standard protocols (Harlow & Lane, 1988), with VirBs protein-specific antisera.

2.2.6 Assays for protein-protein interactions: pulldown and cross-linking experiments.

Biochemical analyses of StrepIIVirB5sp interaction with VirB8sp, VirB9sp and VirB10 sp fusion proteins via cross-linking and pulldown assays were conducted as previously described (Yuan et al., 2005). Pulldown experiments were performed by

mixing 10 μL (5 pmol/ μL) of each strepII-taggedVirB5sp and H_6-tagged VirB proteins together, followed by the addition of 80 μL of S2B buffer and incubation for 30 min at 22°C. The protein mixture was then incubated for 15 min at 22°C with 20 μL of Strep-Tactin Superflow beads (IBA, G Göttingen, Germany). The Strep-Tactin Superflow beads were centrifuged and washed three times with 200 μL of S2B. StrepII-tagged VirB5sp co-precipitated proteins were eluted with 50 μL of S2B buffer with 1 mM biotin. One volume of Laemmli sample buffer was added to the eluted fraction and it was further analyzed by SDS-PAGE and Western blotting. In this study, we further analyzed the ability of StrepIIVirB5sp variants to bind to H_6TrxAVirB8sp in pulldown assays, where the above procedure was followed.

For chemical cross-linking, 5 μl each of 10 pmol/μl stock solutions of purified StrepII-tagged proteins in PSB (Buffer W with 50% glycerol and 2mM DTT) or 5 μl PSB as negative control, were mixed for 5 min at 22°C, 90 μl of CLB (50 mM MES-KOH, 150 mM NaCl, 1 mM EDTA, pH 6.5) was added and the mixture was incubated for 30 min. The cross-linking agent DSS (disuccinimidyl suberate, 10 mM stock in DMSO; Pierce, Rockford IL, USA) was added in different concentrations (0.05 mM and 0.1 mM) and the samples were incubated for 1 h at 22°C, followed by the addition of one volume of Laemmli sample buffer and analysis by SDS-PAGE and Western blotting (Yuan et al., 2005).

For experiments involving competitive inhibition of VirB5sp-VirB8sp cross-links and VirB8sp dimerization, the above described methodology was followed. To assess the potency of VirB5sp peptides to impact protein-protein interactions, different amounts

(0.05, 0.5, 5 and 25 nmol) were added to mixtures of StrepIIVirB5sp and StrepIIVirB8sp or to StrepIIVirB8sp (50 pmol each) and incubated at 22°C for 30 min. DSS at a concentration of 0.1 mM was added, the mixtures were incubated for 1 h, the reactions were stopped by the addition of one volume of SB, followed by SDS-PAGE and Western blotting. The four peptides used in the peptide competition assay (Jerini, Berlin, Germany) corresponded to sequences from VirB5sp (peptide I: TGYRGLGDILRDPTL, peptide II: YLPHNWRDLYEAVMS, peptide III, EAKVVKPVQDKVMTS, and peptide IV, ARRGYPQPKALEAAY).

2.2.7 Bacterial two-hybrid assay testing the effects of VirB5 peptides on VirB8 dimerization.

Competitive inhibition experiments of VirB8-VirB8 interaction *in vivo* using VirB5sp peptides were conducted by using the bacterial two hybrid system (G. Karimova, Josette Pidoux, Agnes Ullmann and Daniel Ladant, 1998). The full sequence encoding length VirB8 was fused to the T18 and T25 fragments (catalytic domain of *Bordetella pertussis* adenylate cyclase) that were co-expressed in the BTH101 (cya deficient) cells. Interaction was detected using the functional complementation of the two catalytic fragments that leads to the production of cAMP, which triggers the beta-galactosidase production. The strains harboring various combinations of the T25 and T18 plasmids were grown in liquid LB culture with kanamycin (50 μg/mL), carbenicillin (100 μg/mL) and 1 mM IPTG for 16 h at 26°C. Aliquots (20 μl) of the cultures were mixed with 80 μl detection buffer (modified from (Cowie, 2006)) (8 mg/ml 2-nitrophenyl-β-D-galactopyranoside dissolved in 11 μl 10% SDS, 26 μl β-mercaptoethanol in 9 ml Z-buffer

(0.06 M Na_2HPO_4 x $7H_20$, 0.04 M $NaH_2PO_4xH_20$, 0.01 M KCl, 0.001 M $MgSO_4$)). After 0.5 h incubation at room temperature, reactions were stopped with 100 µl 1 M Na_2CO_3. The end products were measured at 420 nm and 550 nm with a SPECTRAmax®PLUS^{384} Microplate Spectrophotometer Reader (Molecular Devices). Specific activities were calculated as Miller Units = $[OD_{420} - (1.75 \times OD_{550})] / [(t) \times OD_{600} \times (\text{vol in ml})] \times 1000$ (OD_{600} = after 12h incubation; (t) = time needed for the color formation).

The interaction was monitored by measurement of ß-galactosidase activity using ONPG as the substrate (Cowie, 2006). The VirB5 peptides (IV and I & II) were expressed N-terminally linked to VirB5 signal peptide (SP) sequence in order to facilitate export into the periplasm for detection and eventual purification and C-terminally linked to tandem affinity tags, SC (strep tagII and calmodulin). In order to minimize flexible folding of the peptides, the SP-VirB5peptides-SC were constrained by insertion into the Thiredoxin A (TrxA) active site. To test the effects of the peptides on VirB8 self-association, bi-cistronic constructs were created in the vector containing the VirB8 fused to the T18 fragment. The bi-cistronic constructs were then co-expressed with the T25 VirB8 encoding construct to analyze the effects of the various VirB5sp peptides on VirB8 dimerization.

2.2.8 CD spectroscopy and deconvolution

Purified protein samples were dialyzed into 10 mM sodium phosphate buffer pH 7.5 containing 100 mM NaCl and 1 mM EDTA. Circular dichroism (CD) spectroscopy was performed using an AVIV spectropolarimeter at 25°C in a 1 mm path length cell, a time constant of 1 sec and a bandwidth of 1 nm. The spectra obtained for the protein

samples were corrected by subtracting the signal from that obtained with buffer alone. The CD measurements were made from 260 nm to 195 nm. Molar ellipticity of the protein was expressed as deg. cm^2/ dmol using the extinction coefficient of StrepIIVirB5sp (23880 M^{-1} cm^{-1}) and of StrepIIVirB5sp$^{\Delta gb}$ (12650 M^{-1} cm^{-1}), the number of total residues and the concentration of the protein sample. The quantification of secondary structures was calculated by using three methods, SELCON3, CONTINLL, and CDSSTR, which were downloaded from the software package CDPro available at http://lamar.colostate.edu/~sreeram/CDPro (Sreerama & Woody, 2000). The quantification was performed as described (Taneva, 2003).

2.3 Results

2.3.1 VirB5sp binds VirB8sp and VirB10sp.

A previous study in our laboratory showed that VirB4, an NTPase of the T4SS directly interacts with VirB8 and stabilizes VirB8 and VirB3 in *A. tumefaciens* cells (Yuan et al., 2005). In the absence of VirB4, VirB5 and VirB2 do not form high molecular mass complexes in the membranes of *A. tumefaciens* cells and thus do not form pili. In order to determine the interactions of the minor component VirB5 prior to pilus formation, biochemical analyses were performed. Purified strepIIVirB5sp was mixed with H_6VirB8sp, or H_6VirB9sp, or H_6VirB10sp and co-affinity precipitation on Streptactin Superflow Sepharose beads showed that VirB5 binds VirB8 and VirB10 but not VirB9 (Figure 2.1A; (Yuan et al., 2005)). As another method to detect binding among the proteins, DSS, a chemical cross-linker was incubated with purified VirB5sp, VirB8sp, VirB9sp and VirB10sp. Analysis of the cross-linking pattern of individual proteins in pair-wise mixtures showed that VirB5 interacts with VirB8 and VirB10 (presence of novel complex that corresponded to the sum of the molecular mass of interacting proteins) but not VirB9 (Figure 2.1B; (Yuan et al., 2005)). Amongst these interactions, that of VirB5 with VirB8 is very interesting since VirB8 is required for polar localization of other VirB proteins (Judd et al., 2005a). Therefore, the result is in accordance with the notion that the interaction with VirB5 may be necessary to target VirB5 to the core T4SS followed by incorporation into pili. To further identify the minimal domain of VirB5 that is required for interaction with VirB8, peptide array experiments were performed next.

2.3.2 The globular domain of VirB5 interacts with VirB8.

First, we incubated purified VirB8 with the cross-linking agent disuccinimidyl suberate (DSS) and observed higher molecular mass complexes indicating the formation of multimers (Figure 2.2A). The inclusion of increasing amounts of purified VirB5 successively reduced the amounts of VirB8 multimers and a novel complex was observed that might correspond to a VirB8-VirB5 complex as reported before (Yuan et al., 2005); inclusion of BSA control protein did not have such an effect (Figure 2.2A).

To narrow down the region that interferes with the VirB8-VirB8 interaction, we next identified the interacting domain on VirB5. To this end, we used a peptide array that displayed the sequence of VirB5 on cellulose membranes in 13-mer peptides overlapping by three amino acids (Höppner et al., 2005). After incubation of the peptide array membranes with VirB8, we detected binding to overlapping peptides in the globular region of VirB5 predicted using the Phyre server based on the structure of its homolog TraC (H.-J. Yeo et al., 2003). These peptides 16, 18 and 22-23 (Figure 2.2B) were not recognized by the negative control protein VirB9 (bound only peptide 21, data not shown) and corresponded to amino acids 66-78 and 72-84 of VirB5. To further test the notion that the globular domain of VirB5 interacts with VirB8, we conducted pulldown assays with VirB5 wildtype and variants deleted for the globular domain (Δgb, amino acids 71-138) and the C-terminal domain (Δcd, deleted for 18 amino acids) as negative control. VirB5 deleted for the globular domain did not pull down VirB8, which further supported the notion that this domain is necessary for the interaction (Figure 2.2C). In addition, we recently performed phage display experiments with VirB8 as bait and found

that overlapping peptides in the globular domain of VirB5 bound to VirB8 (not shown). Thus, the globular domain of VirB5 binds to VirB8 and the sequences of the peptides identified by these experiments are displayed in the model of the VirB5 structure generated by Phyre *(http://www.cmpharm.ucsf.edu/cgi-bin/webmol.pl)* shown in Figure 2.2D.

2.3.3 Peptides from the globular domain of VirB5 inhibit VirB8-VirB8 interactions.

Peptides have been described as powerful inhibitors of protein-protein interactions (41-43) and we next determined whether peptides derived from the globular domain of VirB5 reduce VirB8 dimerization. We synthesized four peptides derived from the VirB5 sequence, peptide I (amino acids 66-80) and peptide II (amino acids 83-97) derive from the globular domain of VirB5 and they bound VirB8 in peptide array experiments. Peptide III (amino acids 133-147) and peptide IV (amino acids 224-238) derive from other regions of the protein and served as negative controls. These peptides were added in increasing concentrations to VirB8 cross-linking experiments, and addition of peptides I and II strongly inhibited the formation of higher molecular mass cross-linking products (Figure 2.3A). In contrast, addition of the negative control peptides III and IV did not have such an effect further substantiating that the globular domain of VirB5 inhibits VirB8-VirB8 interactions (Figure 2.3A).

Finally we assessed whether VirB5-derived peptides have such an effect *in vivo* using the bacterial two-hybrid system we have previously applied to analyze the effect of VirB9 and VirB10 on VirB8 dimerization (Sivanesan, Hancock, Villamil Giraldo, & Baron, 2010). The gene encoding VirB8 was fused to a vectors encoding the two domains of the *Bordetella pertussis* adenylate cyclase, and interaction between the expressed

fusion protein restored cAMP formation and β-galactosidase formation in *E. coli* strain BTH101 (G. Karimova, Josette Pidoux, Agnes Ullmann and Daniel Ladant, 1998) indicating the VirB8-VirB8 interaction. When peptides I and II were co-expressed with VirB8, we observed a statistically significant reduction of dimerization, whereas expression of negative control peptide IV did not have such an effect (Figure 2.3B). This result constitutes additional evidence for the notion that VirB5 inhibits the dimerization of VirB8.

2.3.4 Analysis of secondary structures of VirB5sp variants

In order to assess whether the reduced binding of VirB5Δgb could be due to conformational changes of the variant, the secondary structures of StrepIIVirB5sp and of its variants were analyzed using circular dicroism (CD) spectroscopy. The CD spectrum of StrepIIVirB5sp indicated a predominantly α-helical protein, which is in accord with the X-ray structure of the VirB5-like protein TraC (Figure 2.4). The spectra of VirB5Δcd was essentially identical to the wild type (not shown). However, analysis of the Δgb variant revealed a significantly different spectrum (Figure 2.4). Quantitative analysis of the data revealed that this variant had more α-helix content than the wild type (Table 2.3). This result was expected based on the TraC X-ray structure showing that VirB5-like proteins consist of a bundle of three α-helices and the globular appendage missing in Δgb (H.-J. Yeo et al., 2003). Taken together, the CD spectroscopy did not reveal any major structural changes of VirB5sp variants suggesting that their reduced functionality is due to changes at the interaction site with VirB8sp.

2.4 Discussion

The work presented here gives detailed insights into the molecular requirements for the interaction between two essential T4SS components. We demonstrated that VirB5sp interacts with VirB8sp and VirB10sp (Figure 2.1) (Yuan et al., 2005). This suggested a sequence of interactions in pilus assembly. VirB4 stabilizes VirB8 and VirB3, followed by VirB5 binding to VirB8 and VirB10 and this precedes VirB5 incorporation into pili (VirB2-VirB5 complex) (Yuan et al., 2005). In the *A. tumefaciens* system, VirB8 was shown to be necessary for VirB8-VirB9-VirB10 complex formation and for polar localization of VirB5 and of four other VirB proteins (Judd et al., 2005a; Kumar, Xie, & Das, 2000). VirB8-like proteins may therefore act as assembly and nucleating factors and undergo transient interactions with several T4SS components. This function is reminiscent of PapD, the periplasmic chaperone in the P-pilus system (Sauer, Remaut, Hultgren, & Waksman, 2004). PapD forms soluble but transient complexes with pilin subunits, which stabilizes these proteins and targets them to the outer membrane-localized usher PapC. Whereas PapD has an immunoglobulin-like fold, VirB8sp has structural similarity to the protein nuclear transport factor 2 (NTF2) (Terradot et al., 2005), which mediates protein translocation to the nucleus. VirB8 could bind transiently to VirB5, direct its interaction with VirB2 and incorporation into pili (Yuan et al., 2005).

The region in VirB5sp required for the interaction with VirB8sp was identified here. Peptide array results showed that the globular region containing the 3_{10} and $\propto$a helix comprises VirB8sp binding sites. These results were substantiated by competition analysis with peptides from the globular region of VirB5sp. The formation of cross-links

between VirB5sp and VirB8sp was inhibited by peptides (I and II) that correspond in sequence to the 3_{10} and ∝a helix. In contrast, negative controls with peptides III and IV derived from regions of VirB5sp not bound strongly by VirB8sp did not inhibit crosslink formation, suggesting that the results obtained with peptides I and II were not due to non-specific competition. Moreover, peptides III and IV but not I and II contained K residues, which could, in principle, bind to the cross-linking agent and quench the reaction. That inclusion of peptides III and IV did not have such an effect further supports the hypothesis that peptides I and II specifically inhibited the protein-protein interaction. Therefore, we conclude that peptides I and II mimic the binding site of VirB8sp on VirB5sp and their inclusion inhibits complex formation between the two proteins.

During the cross-linking experiments we made the interesting observation that peptides I and II also inhibited the formation of dimers and higher molecular mass multimers of VirB8sp. Peptides III and IV did not have such an effect, suggesting that peptides I and II bind to VirB8sp and prevent its self-interaction. Dimer formation of VirB8sp was proposed based on protein contacts observed in the X-ray analysis (Terradot et al., 2005) and the results of cross-linking studies (Yuan et al., 2005). We recently showed that VirB8sp dimer formation occurs *in vitro* and that it is important for its functionality *in vivo* (Paschos et al., 2006). Peptides from the VirB8sp binding sites apparently mimic the action of VirB5sp and dissociate the VirB8sp dimer. Similarly, using a bacterial two-hybrid system-based *in vivo* assay, we observed that VirB5 peptides from the interaction domain reduced VirB8 dimerization. Thus, VirB5 reduces VirB8 dimerization and in turn, we conclude that dissociation of the dimer may be necessary for

the VirB8-VirB5 interaction. It is intriguing to speculate that a dissociation-association cycle of VirB8-like proteins could be functionally important during its function as assembly factor for VirB5 and other T4SS components. This hypothesis is presented and tested in the following chapter 3 of this thesis.

Following up on the peptide competition experiments, VirB5sp variant with the globular domain and C-terminus deleted were purified and their interaction with VirB8sp was determined by pull down assays. The pull down results were in very good agreement with those of the peptide competition assays and further substantiated that the globular region of VirB5 contribute to VirB8sp binding. The results of CD spectroscopy showed that VirB5sp variants did not have major alterations of the overall structure of the proteins.

The availability of the X-ray structure of TraC enabled the structure-function analysis reported here (H.-J. Yeo et al., 2003). TraC is a VirB5 ortholog and it is a single domain protein, composed of three α-helices and a loose globular appendage, which contains four short α-helices and a 3_{10} helix. This appendage is believed to be flexible and it was postulated that it might serve as a site for protein-protein interactions. A model of VirB5sp was derived based on the TraC X-ray structure and is displayed in Figure 2.2D. Analysis of the model further supports the notion that the region encompassing the 3_{10} helix and some residues between the αd and the α2 helix of VirB5sp are involved in VirB8sp binding. Taking all the results together, we conclude that the minimal domain of VirB5sp required for VirB8sp binding is that of peptide I (TGYRGLGDILRDPTL), and of peptide II (YLPHNWRDLYEAVMS).

This work constitutes a platform upon which inhibitors of the VirB5sp-VirB8sp interaction could be developed and similar strategies will be used for other VirB protein interactions *in vivo*. As a first step in this direction we expressed fusion proteins of the inhibitory peptides of VirB5 and directed their export into the periplasm and analyzed the effects using bacterial two hybrid assay (Figure 2.3B). The result from this approach is in accord with those of the *in vitro* peptide competition experiments and further supports that VirB5sp and VirB8sp indeed interact *in vivo*; however, though the peptide aptamer studies seem promising the various technical difficulties could be faced in these studies, such as detection of the level of expression of the peptide aptamer constructs and importantly the expression of the scaffolding protein should not be toxic to cells. This makes the use of synthesized peptides more attractive. Firstly, this would allow experiments to be designed where we would know the amount of peptides (cell penetrating) that would be added to cells. Secondly, synthesized VirB5 peptides could also be used in *in vitro* binding experiments to VirB8sp and so far we have not shown direct binding of VirB5 peptides to VirB8. This *in vitro* study will allow us to calculate the binding constant of this interaction and to develop probes of the roles of VirB protein interactions for T4SS function. This work will also give leads for the development of inhibitors of VirB protein interactions, which disarm T4SS-carrying bacteria and thereby inhibit their virulence functions and plasmid transfer ability.

Table 2.1. Bacterial strains and plasmids.

Strains	Genotype or description	Source or reference
E. coli JM109	*endA1 gyr96 thi hsdR71 supE44 recA1 relA1* (*Δlac-proAB*) (F' *traD36 proAB*$^{+}$ *lacI*^{q} *lacZ*ΔM15)	(Yanisch-Perron, Viera, & Messing, 1985)
E. coli GJ1158	*ompT hsdS gal dcm ΔmalAp510 malP::*(*proUp*-T7 RNAP) *mal*Q::*lacZhyb11* Δ(*zhf-900*::Tn*10*ΔTet)	(Bhandari & Gowrishankar, 1997)
Plasmids		
pT7-7StrepII	car^{r}, T7 promoter expression vector for N-terminal strepII affinity peptide fusions	(Balsinger, Ragaz, Baron, & Narberhaus, 2004)
pT7-H_6TrxFus	car^{r}, T7 promoter expression vector, for N-terminal hexahistidyl-TrxA affinity peptide fusions	(Kromayer, Wilting, Tormay, & Böck, 1996)
pLS1	car^{r}, IncQ plasmid for VirB/D4-mediated conjugative transfer experiments	(Stahl, Jacobs, & Binns, 1998)
pT7-7StrepIIVirB5sp	pT7-7StrepII carrying 666 bp *Acc*65I/*Pst*I *virB5* fragment from *B. suis* (encoding 221 amino acid periplasmic domain)	(Yuan et al., 2005)
pT7-7StrepIIVirB8sp	pT7-7StrepII carrying 492 bp *Acc*65I/*Pst*I *virB8* fragment from *B. suis* (encoding 163 amino acid periplasmic domain)	(Terradot et al., 2005)
pT7-7StrepIIVirB9sp	pT7-7StrepII carrying 813 bp *Acc*65I/*Pst*I *virB9* fragment from *B. suis* (encoding 271 amino acid periplasmic domain)	(Yuan et al., 2005)
pT7-7StrepIIVirB10sp	pT7-7StrepII carrying 1020 bp *Acc*65I/*Pst*I *virB10* fragment from *B. suis* (encoding 339 amino acid periplasmic domain)	(Yuan et al., 2005)
pT7-H_6TrxVirB8sp	pT7-H_6TrxFus carrying 492 bp *Acc*65I/*Pst*I *virB8* fragment from *B. suis* (encoding 163 amino acid periplasmic domain)	(Rouot et al., 2003)
pT7-7StrepIIVirB5sp$^{\Delta gb}$	pT7-7StrepIIVirB5sp modified to encode VirB5sp with amino acid deletion from 71-140 in the globular appendage (gb)	this work

pT7-7StrepIIVirB5sp$^{\Delta cd}$	pT7-7StrepIIVirB5sp modified to encode VirB5sp with deletion of C-terminal amino acids 232-240 (cd)	this work
pTrcStrepII	pTrc200, Strep-tagII encoding sequence cloned into *Pac*I/*Bst*BI	(Aly & Baron, 2007)
pTrcSC	pTrcStrepII, calmodulin binding peptide sequence cloned into *Bst*BI/*Hind*III, for expression of proteins with C-terminal double affinity tag (StrepII-tag and calmodulin binding peptide)	this work
pTrcSP-SC	pTrcSC containing region encoding VirB5sp signal peptide cloned into *Nco*I/*Pst*I	this work
pTrcStrepII	pTrc200, Strep-tagII encoding sequence cloned into *Pac*I/*Bst*BI	(Aly & Baron, 2007)
pTrcSC	pTrcStrepII, calmodulin binding peptide sequence cloned into *Bst*BI/*Hind*III, for expression of proteins with C-terminal double affinity tag (StrepII-tag and calmodulin binding peptide)	this work
pTrcSP-SC	pTrcSC containing region encoding VirB5sp signal peptide cloned into *Nco*I/*Pst*I	this work
pTrcSPTrxASC	pTrcSP-SC carrying 327 bp *Acc651/PstI trxA* from *E.coli* fused to the C-terminal tags (strepII-tag and calmodulin binding peptide)	this work
pSDMSP-SC	pSDM containing region encoding VirB5sp signal peptide and strepII-tag and calmodulin binding peptide sequence cloned into *Nco*I/*Hind*III	this work
pSDMSPTrxASC	pSDMSP-SC carrying 327 bp *Acc651/PstI trxA* from *E.coli* fused to the C-terminal tags (strepII-tag and calmodulin binding peptide)	this work
pUT18CB8s+ SPSC	pUT18CB8s carrying in tandem a shine Dalgarno sequence, followed by signal peptide of VirB5sp fused to tags StrepII and calmodulin binding peptide	this work
pUT18CB8s+ SP(TrxA)pIVCSC	pUT18CB8s+SPSC carrying constrained peptideIV of VirB5sp (peptide IV that corresponds to ARRGYPQPKALEAAY is inserted into active site of TrxA)	this work
pUT18CB8s+ SP(TrxA)pIpIICSC	pUT18CB8s+SPSC carrying constrained peptideI+II of VirB5sp (peptide I+II that corresponds to TGYRGLGDILRDPTLRSYLPHNWRDLYEAVMS is inserted into active site of TrxA)	this work

Table 2.2 Oligonucleotide sequences[a].

Name	Sequence	Constructed plasmid

PCR primers where the underlined sequence corresponds to the restriction enzyme recognition site		
TrxA-5	5'CGGGGTACCCATCACCATCACCATCACAGCGA TAAAATT-3'	pTrcSPTrxASC
TrxA-3	5'AAAACTGCAGGGCCAGGTTAGCGTCGAGGAAC TCTTTCAA-3'	
Inverse PCR primers to create domain deletions in VirB5sp encoding gene		
B5gb-5	5'ACCGGCTACCGTGGCCCGGTCCAGGACAAGGT CATGACG-3'	pT7-7StrepIIVirB5sp$^{\Delta gb}$
B5gb-3	5'CTTGTCCTGGACCGGGCCACGGTAGCCGGTCA GGGCATC-3'	
B5cd-5	5'CACGAATTAGACGCGTAACTGCAGCCCAAGCT TATCGATGAT-3'	pT7-7StrepIIVirB5sp$^{\Delta cd}$
B5cd3	5'AAGCTTGGGCTGCAGTTACGCGTCTAATTCGT GCTGGCGTTC-3'	
5'phosphorylated oligonucleotides		
B5SP-5	5'CATGGCAAAGAAGATAATTCTCAGCTTCGCATT CGCCCTGACTGTAACCAGCACGGCGGTACCTAAT AACTGCAGTTAAT -3'	pTrcSP-SC
B5SP-3	5'TAACTGCAGTTATTAGGTACCGCCGTGCTGGTT ACAGTCAGGGCGAATGCGAAGCTGAGAATTATC TTCTTTGC -3'	
CBP-5	5'CGAAAAGGGCCCGACCACGGCGTCGGAAACCT GTATTTCCAGGGCGAACTGGCGGCGGGCACCAA GCGCCGCTGGAAGAAGAATTTCATCGCCGTCTCG GCAGCCAACCGCTTCAAGAACATCTCGTCCTCCG GGGCGCTCTGA-3'	pTrcSC
CBP-3	5'CGTCAGAGCGCCCCGGAGGACGAGATCTTCTT GAAGCGGTTGGCTGCCGAGACGGCGATGAAATT CTTCTTCCAGCGGCGCTTGGTGCCCGCCGCCAGT TCGCCCTGGAAATACAGGTTTTCCGACGCCGTGG TCGGGCCCTTTT-3'	
B5pIVC-5	5'GTCCCGCCCGGCGCGGCTATCCGCAGCCGAAA GCACTGGAAGCCGCCTATG-3'	pUT18CB8+ SP(TrxA)pIVCSC
B5pIVC-3	5'GACCATAGGCGGCTTCCAGTGCTTTCGGCTGCG GATAGCCGCGCCGGGCGG-3'	
B5pIpIIC-5	5'GTCCCACCGGCTACCGTGGCCTTGGCGATATTC TCCGCGACCCTACGCTGCGTAGCTATCTGCCACA TAACTGGCGAGATCTCTACGAAGCGGTGATGAG CG-3'	pUT18CB8+ SP(TrxA)pIpIICSC
B5pIpIIC-3	5'GACCGCTCATCACCGCTTCGTAGAGATCTCGCC AGTTATGTGGCAGATAGCTACGCAGCGTAGGGT CGCGGAGAATATCGCCAAGGCCACGGTAGCCGG TGG-3'	

Table 2.3: Secondary structure of StrepIIVirB5sp and derivative StrepIIVirB5sp$^{\Delta gb}$.

	Program	StrepIIVirB5sp	StrepIIVirB5sp$^{\Delta gb}$
% Helix	SELCON3	35.5	42
	CONTINLL	39.6	41.7
	CDSSTR	43	52.5
% β-Strand	SELCON3	12.45	6.7
	CONTINLL	7.65	6.7
	CDSSTR	12.1	14.7
% Turn	SELCON3	20.8	23
	CONTINLL	20.5	24.1
	CDSSTR	17.2	13.3
% Un-ordered	SELCON3	31.3	27.2
	CONTINLL	32.3	27.5
	CDSSTR	27.5	19.4

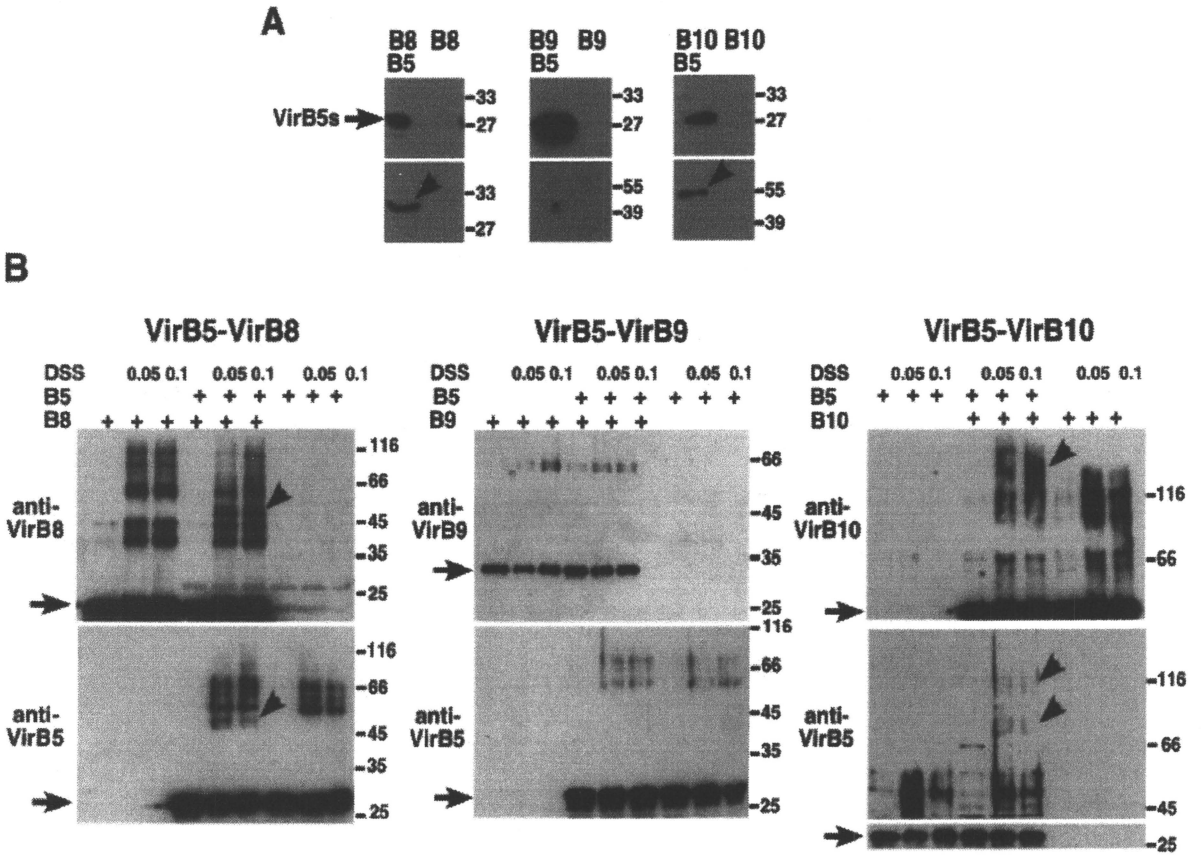

Figure 2.1 Protein-protein interaction assays detect interactions between periplasmic T4SS components. **A.** Affinity precipitation to test the interactions of StrepIIVirB5sp with H_6TrxAVirB8sp, H_6TrxAVirB9sp and H_6TrxAVirB10sp. StrepIIVirB5sp was preincubated with H_6TrxAVirB8sp, H_6TrxAVirB9sp and H_6TrxAVirB10sp before addition to streptactin-Sepharose matrix. The proteins were eluted from the matrix, followed by washing, SDS-PAGE and Western blotting with VirB5sp-, VirB8sp-, VirB9sp-, and VirB10sp-specific antisera. The negative controls of H_6TrxAVirB8sp, H_6TrxAVirB9sp and H_6TrxAVirB10sp alone were incubated with the matrix and is shown in the lanes labeled as (-). Arrowheads indicate StrepIIVirB5, which co-sedimented H_6TrxAVirB8sp and H_6TrxAVirB10sp. Experiments were repeated three times and representative results are shown here. Molecular masses of reference proteins are shown on the right. **B.** Cross-linking experiments to test the interaction of StrepIIVirB5sp with VirB8sp, StrepIIVirB9sp and StrepIIVirB10sp. Equimolar amounts of StrepIIVirB5sp were mixed with StrepIIVirB8sp, StrepIIVirB9sp and StrepIIVirB10sp in 0.05 and 0.1 mM DSS prior to SDS-PAGE and Western blotting with VirB5sp-, VirB8sp-, VirB9sp- and VirB10sp-specific antisera. Arrows indicate monomeric proteins, and arrowheads indicate wild-type cross-linked products. The experiments were repeated three times and representative results are shown. Molecular masses of reference proteins are shown on the right (in kDa).

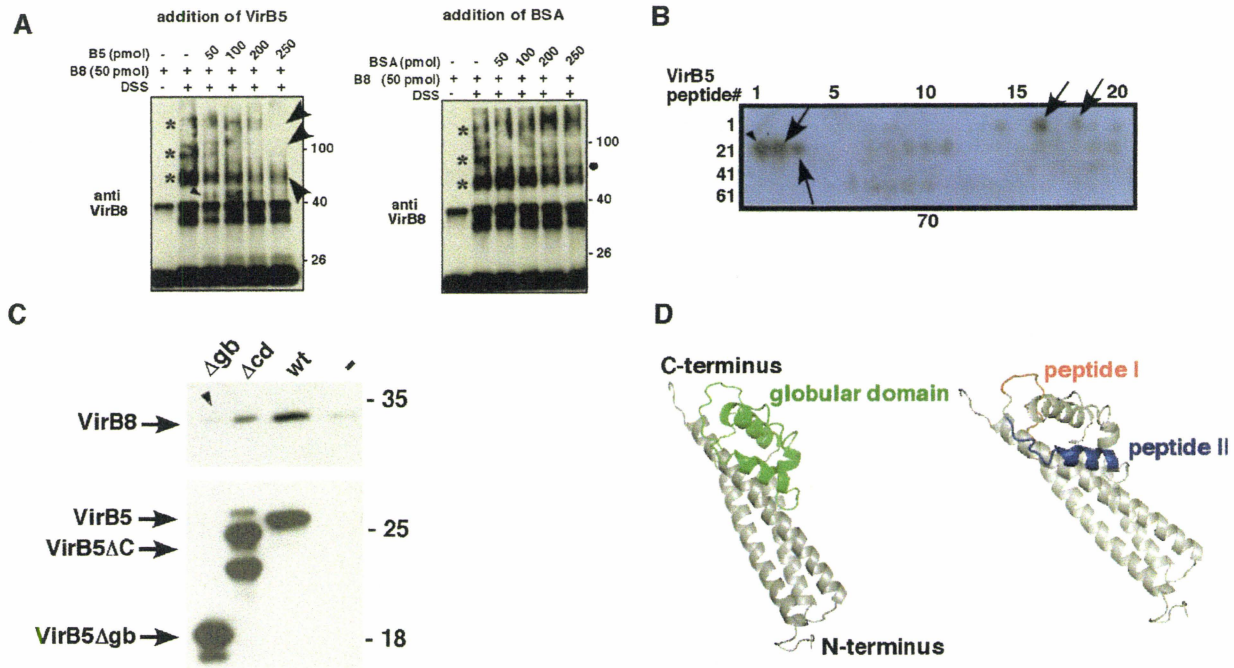

Figure 2.2. Cross-linking assay of VirB8 multimerization and identification of the VirB5 interaction domain. **A**. VirB8 was incubated with 0.1 mM DSS without and with increasing amounts of VirB5 or BSA followed by Western blotting with VirB8-specific antiserum. Stars indicate higher-molecular mass complexes of VirB8 multimers, small arrowheads indicate putative cross-linking products of VirB8 with VirB5, the large arrowheads indicate the reduced or abolished VirB8 cross-linking products, dot indicates a signal presumably representing non-specific recognition of BSA. **B**. Peptide array experiment to assess binding of VirB8 to VirB5 13-mer peptides spotted on membranes. VirB8 was incubated with the peptide array and VirB8 binding to specific peptides was determined by Western blotting with VirB8-specific antiserum. Arrowhead indicates peptide 21 bound by all proteins, arrows indicates peptides bound reproducibly by VirB8. The experiments were performed 4-6 times and overlaid chemoluminograms are shown. **C**. Pulldown assays to test the interactions of VirB5 variants with VirB8. StrepII-tagged VirB5 and variants (deleted for the globular domain Dgb, and C-terminus Dcd) were incubated with VirB8 before pulldown with streptactin-Sepharose matrix, washing, elution, SDS-PAGE and Western blotting with specific antibodies to detect the bait (VirB5 variants) and prey (VirB8). Arrowheads indicate the pulldown of reduced amounts of VirB8 by VirB5 variant as compared to wild type. Experiments were repeated three times and representative results are shown here. Molecular masses of reference proteins are shown on the right. **D**. Ribbon diagrams of VirB5 representing the globular domain (green) and spherical VirB5 structure showing peptide I (red) and peptide II (blue) from the globular domain (ribbon) were generated using Phyre version 2.0 (http://www.sbg.bio.ic.ac.uk/phyre/).

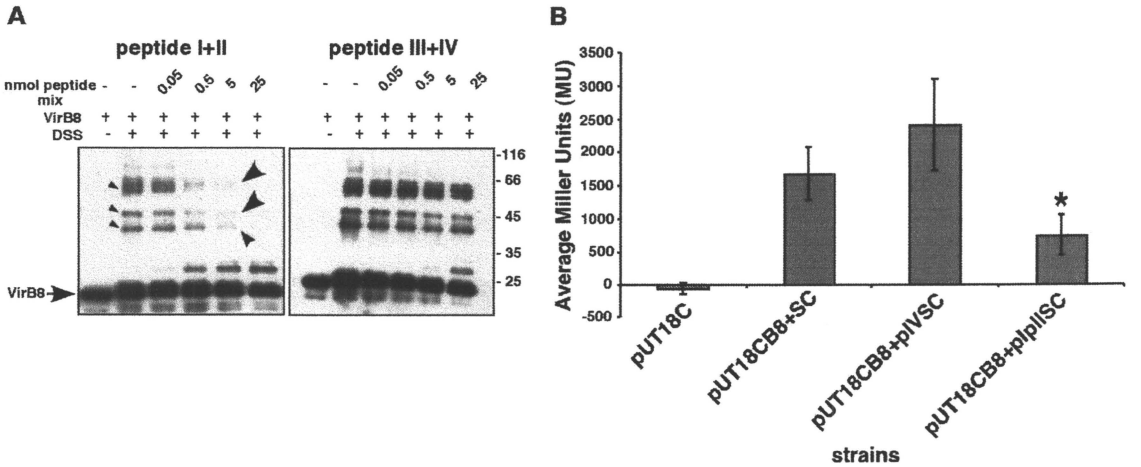

Figure 2.3. Competition of VirB8-VirB8 interactions *in vitro* and *in vivo*. **A.** VirB8sp was incubated in 0.1 mM DSS with increasing amount of peptides I and II from the VirB5 globular domain (0.05, 0.5, 5, 25 nmol) or with equivalent amounts of control peptides III and IV, prior to SDS-PAGE and Western blotting with VirB8-specific antiserum. The stars correspond to signals indicating VirB8sp multimerization, and the arrowheads indicate the inhibition of StrepIIVirB8sp multimer formation by peptides I and II. Molecular masses of reference proteins are shown on the right (in kDa). **B.** Bacterial two-hybrid assay to measure VirB8 dimerization. VirB8 was expressed as fusion to the two domains of adenylate cyclase and b-galactosidase activity indicates dimerization. Effects of co-expression of peptide peptide IV and peptides I&II are tested here. The results of this experiment is from four independent trials and student t-test was performed to show that peptide I&II is statistically significant with a p-value of 0.005 (indicated by star).

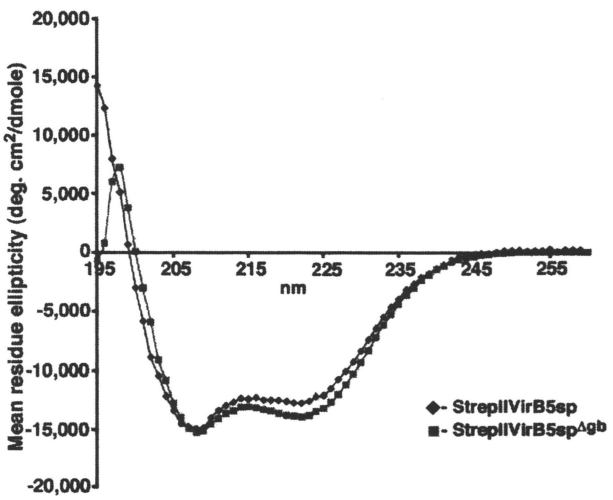

Figure 2.4. Characterization of the secondary structure of StrepIIVirB5sp and StrepIIVirB5sp$^{\Delta gb}$ using circular dichroism spectroscopy. The black line with diamond symbol (◆) corresponds to the CD spectrum of StrepIIVirB5sp and the grey line with square symbol (■) corresponds to the CD spectrum of StrepIIVirB5$^{\Delta gb}$.

CHAPTER THREE: Characterization of VirB8 self-association *in vitro* and *in vivo*: insights into its mechanistic importance for T4SS function.

Preface:

The work in this chapter involves structural and functional characterization of VirB8 self-association from *Brucella suis* and *Agrobacterium tumefaciens*. Figure 3.2 was contributed towards a publication titled 'Dimerization and interactions of *Brucella suis* VirB8 with VirB4 and VirB10 are required for its biological activity' in PNAS (Paschos, A., Patey, G., Sivanesan, D., Bayliss, R., Waksman, G., O'Callaghan, D., and C. Baron. 2006. Dimerization and interactions of *Brucella suis* VirB8 with VirB4 and VirB10 are required for its biological activity. PNAS, USA, 103 (19): 7252-7257), Copyright (2006) National Academy of Sciences, USA. Figure 3.3 was part of the publication titled 'VirB8 dimerization inhibitors inhibit intracellular proliferation of *Brucella*' that was submitted to journal Infection and Immunity (Athanasios Paschos, Andreas den Hartigh, Durga Sivanesan, Renée M. Tsolis and Christian Baron) and is currently under review. In addition, Figures 3.4 to 3.11 of this chapter is essentially a manuscript that was submitted to Journal of Bacteriology where I am the first author (Sivanesan, D and C. Baron) and it is currently under revision. I wrote this manuscript and contributed towards writing of the experimental procedures and results that pertain to my own work in case of the manuscripts where I am a co-author.

CHAPTER Three: Characterization of VirB8 self-association *in vitro* and *in vivo* provides mechanistic insights for T4SS.

Abstract

VirB8 is a component of T4SS that is essential for secretion system function and pilus assembly. The crystal structures of the periplasmic portions of VirB8 from *Brucella suis* and *Agrobacterium tumefaciens* were resolved. In order to identify the residues that are critical for VirB8 self-association, assays were established to test the dimerization. Chemical cross-linking revealed that VirB8 could potentially form higher molecular mass complexes, whereas analytical gel filtration showed that VirB8 is a concentration dependent dimer. Furthermore, analytical ultracentrifugation revealed that VirB8 exists in a monomer-dimer equilibrium with a K_d of 116 +/- 7.5 μM. These experiments identified residues of VirB8 (M102, Y105 and E214) that are important for self-association *in vitro*. Bacterial two-hybrid (BTH) experiments using the full-length protein confirmed that VirB8 self-associates in the periplasm of Gram-negative bacteria. Variants of VirB8 at residues M102, Y105 and E214 were affected in self-association in the BTH assay validating that these residues are important for self-association *in vivo*. Next, in order to assess the role of VirB8 dimerization in T4SS assembly and function, we changed the residues at the predicted dimer interface in order to strengthen or to abolish dimerization, followed by *in vitro* (analytical ultracentrifugation) and *in vivo* analysis (functional assays). Strengthening of the VirB8-VirB8 interaction by introduction of cysteine residues at the dimer interface provided evidence for dimer formation *in vivo*, and this variant supported DNA transfer but not T-pilus formation.

Variants with changes that weaken the dimerization did not support type IV secretion system functions. The analysis of type IV secretion complexes extracted from the membranes revealed that dimerization is important for the association of VirB2 with the core complex proteins (VirB6-VirB8-VirB9-VirB10). These results, along with experiments using purified proteins reported in the previous chapter 2 of this thesis revealed that the globular domain of VirB5 interacts with VirB8 and dissociates the VirB8 dimer, suggesting a mechanistic basis for the contribution of VirB8 dimerization to type IV secretion system function.

3.1 Introduction

The oligomerization of proteins is often important for their stability and function and a dynamic interplay between proteins is necessary for cell functions. VirB8 is a conserved inner-membrane protein of type IV secretion systems (T4SSs) and analysis of its crystal structure and *in vitro* analyses with purified proteins predicted that it is a dimer (Das & Xie, 2000; Paschos et al., 2006). However, the dimerization has not been shown *in vivo* and its mechanistic contribution to T4SS function is not understood. T4SSs are important determinants of virulence in many Gram-negative pathogens e.g. *Agrobacterium tumefaciens*, *Bartonella henselae, Bordetella pertussis*, *Brucella* species, *Helicobacter pylori* and *Legionella pneumophila* (Baron, 2005; Baron, O'Callaghan, & Lanka, 2002; Cascales & Christie, 2003; P.J. Christie, 2004; Llosa & O'Callaghan, 2004). T4SSs systems span the inner and outer membrane and translocate proteins or DNA-protein complexes across the cell envelope (Baron, 2005). The best-characterized T4SS model system is from the plant pathogen *A. tumefaciens* and it translocates proteins and a single-stranded DNA–protein complex into plant cells. T4SS assembly and function are energized by three ATPases (VirB4, VirB11 and VirD4) that localize mainly in the cytoplasm, but they transverse the membrane and contact the core complex. The core components (VirB6, VirB7, VirB8, VirB9 and VirB10) bridge the inner and outer membrane and are linked to the surface-exposed pilus components (VirB2 and VirB5) (Baron, 2005; P.J. Christie, Atmakuri, Krishnamoorthy, Jakubowski, & Cascales, 2005). The interactions between individual VirB proteins have been studied extensively and models of T4SS assembly have been proposed (Chandran et al., 2009; Das & Xie, 2000;

Fronzes, Schafer et al., 2009; Höppner et al., 2005; Krall et al., 2002; D. Ward et al., 2002; Yuan et al., 2005). However, information on the contributions of individual proteins to T4SS assembly and function is largely absent. The availability of X-ray structures of VirB proteins has greatly advanced our ability to study mechanistic questions and we here sought to understand the contribution of VirB8 dimerization to T4SS assembly and function.

VirB8 from *A. tumefaciens* is a bi-topic inner-membrane protein comprising a cytoplasmic N-terminal domain (42 aa), followed by a transmembrane helix (20 aa) and a C-terminal domain in the periplasm (175 aa) (A. Das & Y. H. Xie, 1998). VirB8 was shown to interact with many other T4SS components (VirB1, VirB4, VirB5, and VirB9-11(Das & Xie, 2000; Ding et al., 2002; Höppner et al., 2005; Paschos et al., 2006; D. Ward et al., 2002; Yuan et al., 2005)), and it was proposed to be a nucleating factor enabling the assembly and polar localization of the T4SS complex (Judd et al., 2005a). We provided evidence for a model implying that the VirB8-VirB4 complex is required for the formation of the VirB2-VirB5 pilus-preassembly complex, followed by its incorporation into T-pili (Yuan et al., 2005). Moreover, the crystal structures of the periplasmic portions of VirB8 from *A. tumefaciens* and *B. suis* were resolved (Figure 3.1 & Figure 3.4) (Bailey et al., 2006; Terradot et al., 2005). Both VirB8 proteins consist of four β-sheets and five α-helices and their overall fold is similar to that of the nuclear transport factor 2 (NTF2) (Chaillan-Huntington et al., 2001; Terradot et al., 2005). I first used the information from the *B. suis* VirB8 structure for a structure-function analysis of the dimerization site. Since *Brucella* is a biosafety level 3 pathogen, it was not possible

to carry out detailed mechanistic and functional studies of the consequences of dimer site changes in this system. Comparison of both crystal structures confirmed that the VirB8 homologs have a very similar fold (Bailey et al., 2006). In addition, VirB8 self-association was never confirmed under physiological conditions in *A. tumefaciens* and the mechanistic role of VirB8 self-association was not elucidated. To assess these questions, first I performed *in vitro* analysis on the purified periplasmic portion of VirB8 from *B. suis* to characterize the dimerization site. Next, the information from these experiments was transplanted to VirB8 from *A. tumefaciens*, followed by *in vitro* and *in vivo* analysis of the effects. A *virB8* gene deletion strain was complemented with VirB8 dimer site variants to establish the importance of the dimer site for T4S system function *in vivo* and analytical ultracentrifugation was used to quantify the dimerization *in vitro*.

3.2 Materials and Methods

3.2.1 Cultivation of Bacteria

E. coli strains used for cloning experiments and for bacterial two hybrid interaction experiments were grown at 37°C in LB medium (Yuan et al., 2005). The following antibiotics were added to the media for plasmid propagation (carbenicillin [car], 100 μg/ml; streptomycin [str], 50 μg/ml; spectinomycin [spc], 50 μg/ml; kanamycin [kan], 50 μg/ml; erythromycin [ery] 150 μg/ml). Table 1 lists all the strains and plasmids used in this study.

E. coli strain BL21star DE3 was cultured by shaking at 200 rpm at 37°C in LB medium (1% tryptone, 0.5% yeast extract, 0.5% NaCl) to the exponential phase (OD_{600} of 0.4-0.8), at which point protein production was induced by the addition of 0.5 mM IPTG. Subsequently, the overproduction continued under aerobic conditions at 26°C for 16 h. The *E. coli* strains for bacterial two-hybrid (BTH) experiments were grown in liquid LB culture with kanamycin (50 μg/mL), carbenicillin (100 μg/mL) and 1 mM IPTG for 16 h at 26°C.

A. tumefaciens strains were cultured over night in YEB medium at 26°C as described previously (Yuan et al., 2005). Virulence gene induction was conducted in AB glycerol minimal medium as reported before (Yuan et al., 2005) for 48 h in liquid medium or on AB agar plates for 3 days at 20°C by addition of 200 μM of acetosyringone (AS). Plasmid-encoded genes were expressed by addition of 0.5 mM IPTG. For conjugation experiments, AS was added at a concentration of 500 μM.

3.2.2 Construction of genes encoding protein variants and strains

Standard methods were used for all DNA constructions (Maniatis et al., 1982). The *A. tumefaciens* C58 *virB7-virB8* genes were amplified from plasmid pfullB that contains the *virB* operon with gene specific oligonucleotides (Table 3.2). Site-directed mutagenesis of the *virB8* gene was conducted using pT7-7StrepIIVirB7VirB8a as a template for inverse PCR (Ansaldi et al., 1996). The PCR primers with overlapping sequences used for mutagenesis are listed in Table 3.2. The wild type *virB7-virB8* genes and all the variants were then subcloned into pTrc200 using restriction sites listed in Table 3.2.

3.2.3 Crosslinking, analytical gel filtration and analytical ultracentrifugation

Crosslinking of StrepIIVirB8sp was performed essentially as described in Materials and Methods of Chapter 2.2.6. A Superdex 75 gel filtration column was used to determine the molecular mass of purified StrepIIVirB8sp. StrepIIVirB8sp concentrations from to 0.5 μM to 128 μM were applied to the column in a total volume of 500 μL diluted in buffer W (100 mM Tris-HCl, pH 8.0; 150 mM NaCl, 1 mM EDTA) at 4°C. The Superdex 75 column was calibrated using Low Molecular Weight gel filtration calibration kit (Amersham Biosciences) and Blue Dextran 2000 was used to identify the void volume. A Beckman Coulter XL-A analytical ultracentrifuge was used to perform sedimentation equilibrium studies on VirB8sp and VirB8sp variants. The protein samples were dialyzed twice in the reference buffer (100mM Tris-HCl, pH 8.0; 150mM NaCl, 1mM EDTA) before they were used in the analysis. Sedimentation equilibrium analysis was carried out using three different concentrations of VirB8sp and variants (A_{280} of 0.1, 0.3 and 0.5) in a total volume of 120 μl at 4°C at three different rotor speeds (20,000, 24,000, and 28,000 rpm). Concentration profiles of the samples were obtained

by absorbance scans at 280 nm after 15 and 16 hours at each rotor speed at a radial step of 0.001 cm with five replicates per scan. The sedimentation equilibrium data were analyzed using Origin version 6.0 (Microcal Inc.). The partial specific volume of VirB8sp and solvent density were calculated to be 0.718 and 1.009, respectively, using the SEDENTERP program. The molar dissociation constants K_d of VirB8sp and of its variants were calculated by deriving the concentration dependent association constant from the absorbance based association constant calculated by the Origin program. The following equation was used: $K_{a(conc)} = K_{a(abs)}$ (εl/2), where $K_{a(conc)}$ is the per molar association constant, $K_{a(abs)}$ is the absorbance-based association constant derived by the Origin program, ε is the calculated molar extinction coefficient (37820 cm^{-1} M^{-1}) and l is the path length of the sample cell (1.2cm). K_d was calculated by taking the inverse of $K_{a(conc)}$ (Hudson & Nodwell, 2003). Sedimentation equilibrium studies were performed as described above for StrepIIVirB8ap and variants and the SEDENTERP program was used to calculate the partial specific volumes and solvent density of StrepIIVirB8ap and of its variants. The partial specific volume and solvent densities of StrepIIVirB8ap and its variants were calculated to be 0.718 and 1.009, respectively. The molar extinction coefficient for StrepIIVirB8ap and variants is 29,910 $cm^{-1}M^{-1}$.

3.2.4 Bacterial two-hybrid system

To analyze VirB8 self-association in an '*in vivo*' model the bacterial two-hybrid system was used. The experimental procedure used here is essentially as described in Chapter 2 (2.2.7) (G. Karimova, Josette Pidoux, Agnes Ullmann and Daniel Ladant, 1998).

3.2.5 Analyses of T4SS functions

Experiments involving assessment of T4SS functions (T-pilus formation, conjugation and tumor formation) were conducted as described before (Höppner et al., 2004).

3.2.6 Isolation and fractionation of membrane proteins

Detergent extraction of membranes from *A. tumefaciens* using 2% dodecyl-β-D-maltopyranoside (DDM) were carried out as previously specified (Krall et al., 2002). Blue native gel electrophoresis and gel filtration for fractionation of the isolated membrane proteins were performed as reported before (Yuan et al., 2005).

3.2.7 Protein analysis

The sample preparation for electrophoresis of proteins and cells were essentially performed as described previously (Yuan et al., 2005). Laemmli gels were used for electrophoresis of proteins larger than 20 kDa and the Schägger and v. Jagow system was used for detection of proteins smaller than 20 kDa (Laemmli, 1970; Schägger & von Jagow, 1987). Western blotting was carried out using antisera specific for VirB proteins as per standard protocols (Harlow & Lane, 1988).

3.3 Results

3.3.1 The crystal structure of StrepIIVirB8sp provides information on a potential dimerization site.

The gene encoding the periplasmic portion of VirB8 from *B. suis* was mutagenized based on the X-ray structure and guidance from the group of our collaborator Dr. Gabriel Waksman, London. From the X-ray structure (Figure 3.1), it was suggested that changes such as M102R, Y105R, and E 214R of the VirB8sp be constructed to assess if dimerization will be impacted.

3.3.2 VirB8sp self-associates in vitro and in an in vivo model system.

Purified StrepIIVirB8sp incubated with the chemical cross-linker, disuccinimidyl suberate, formed dimers, trimers and multimers suggesting that VirB8 is able to self-associate (Figure 3.2 A). As alternative approach, we performed analytical gel filtration that showed that VirB8 eluted as a dimer (40.6 kDa) at high concentrations (128 μM) and as a monomer (22.3 kDa) at lower concentration (0.5 μM) (Figure 3.2 B &C). Dr. A. Paschos used this experimental approach to test the VirB8 variants, and found that variants M102R, Y105R and E214R were monomeric or reduced in self-association at all concentrations tested (Figure 3.2C). However, since this approach could be influenced by the shape of the protein, we also used analytical ultracentrifugation to assess the dimer formation of wildtype VirB8 and variants. Three different concentrations and rotor speeds were used in the sedimentation equilibrium experiment. Global anlaysis showed that VirB8sp exits in a monomer/dimer equilibrium with a K_d of 116 +/- 7.5 μM (Figure 3.2D). The variants M102R, Y105R, and E214R did not fit to the monomer/dimer

equilibrium model but fit to the single ideal species model confirming that these variants are indeed monomeric (Figure 3.2 E). CD spectroscopy analysis of the wildtype and variants showed spectra of variants to be very similar to the wildtype (data not shown) indicating that the secondary structures of the variants were not affected by the amino acid changes. These experiments suggested that the M102, Y105 and E214 are residues involved in VirB8sp dimerization.

To complement the *in vitro* experiments, we adopted the bacterial two-hybrid assay (G. Karimova, Josette Pidoux, Agnes Ullmann and Daniel Ladant, 1998) to assess dimer formation in the membranes of Gram-negative bacteria. Self-association was demonstrated for the wildtype VirB8s and as observed in the *in vitro* experiments, VirB8 changes at M102, Y105 and E214 reduced dimerization (Figure 3.3 A & B). The N-terminus of full-length VirB8s showed no dimerization capability using this assay suggesting that the N-terminus of VirB8 comprising the cytoplasmic and transmembrane region do not self-associate determined by this assay. As controls, VirB8 interaction with VirB10 and VirB10 interaction with itself were also tested to show that VirB10 interacts with VirB8 and it self (Figure 3.3 A &B). Taken together, the self-association of VirB8 from *B. suis* was unambigously demonstrated using various *in vitro* experiments and a simplified *in vivo* assay.

3.3.3 Rationale for construction of VirB8 dimer site variants from A. tumefaciens.

There is only 29.2% sequence identity between *Brucella* and *Agrobacterium* VirB8, but their overall fold is very similar (Bailey et al., 2006). However, expression of *Brucella* VirB8 did not complement an *A. tumefaciens virB8* deletion strain (not shown)

and we therefore could not use the previously analyzed variants of the *Brucella* homologue (Paschos et al., 2006) for this study. Therefore, we "transplanted" the dimer site changes identified in *Brucella* VirB8 to the *Agrobacterium* homolog exploiting sequence alignments and the overall very similar structures (Bailey et al., 2006; Terradot et al., 2005). The residues involved in dimerization of *Brucella* VirB8 (M102 and Y105) correspond to V97 and A100 in *Agrobacterium* VirB8 where they form part of the largest contact region. This interface has predominantly hydrophobic character and V97 and A100 from one VirB8 monomer are predicted to bind V97 and A100 of the second monomer of VirB8 (Figure 3.4). In addition, it was proposed that a hydrogen bond between the Q93 of one and E94 of another monomer in the same hydrophobic region contributes to dimerization of *Agrobacterium* VirB8 (Bailey et al., 2006) (Figure 3.4). These residues comprise the likely dimer interface of *Agrobacterium* VirB8 and the gene was subjected to site-directed mutagenesis to change the residues Q93, E94, V97 and A100.

Changes in the *virB8* gene that were predicted to destroy and restore dimer formation were engineered and in addition, we sought to stabilize the VirB8-VirB8 interaction by introducing Cys residues at the interface. The native VirB8 protein contains no Cys and therefore, the formation of Cystine in the oxidative environment of the periplasm (W. C. Lai & Hazelbauer, 2007) would indicate that VirB8 monomers are in close proximity. To test this possibility and to assess the stability of VirB8 variants, the *virB8* gene deletion strain CB1008 was complemented with plasmids expressing VirB8 and variants VirB8^{V97A}, VirB8^{V97R}, VirB8^{V97C}, VirB8^{Q93EE94Q}, and VirB8^{Q93CE94C} under

virulence gene-inducing conditions and the cell lysates were electrophoresed under non-reducing conditions. Analysis by Western blotting showed the presence of a signal at ~54 kDa in case of the VirB8^{V97C} variant that corresponds to twice the molecular mass of the monomer (27 kDa) indicating partial dimer formation (Figure 3.5) and this is consistent with the notion that VirB8^{V97} is involved in dimerization. Functional analyses were performed next to assess the impacts of the changes described above on the T4S.

3.3.4 The postulated dimer site residues of VirB8 are required for T-pilus formation and substrate transfer.

The functionality of VirB8 variants was determined next using a series of assays for the functionality of T4S in *A. tumefaciens*. First, surface-exposed T-pili were isolated from the cells by shearing, followed by ultracentrifugation and the major pilus component VirB2 and the minor component VirB5 were detected by SDS-PAGE and Western blotting. Pilus formation was not observed in CB8 and in CB8 expressing all VirB8^{A100} variants, VirB8^{V97C} and VirB8^{V97R} and in CB1008 expressing VirB8^{Q93CE94C} (Figure 3.6). The other seven VirB8 variants including VirB8^{V97T} complemented T-pilus formation of the *virB8* gene deletion strain even if reduced amounts were produced in case of the VirB8^{Q93D} variants (Figure 3.6). Second, we assessed the ability of CB8 and complemented strains to induce tumor formation after infection of the host plant *Kalanchoë diagremontiana* (Table 3.3). Similar to the results of the T-pilus formation assays, CB8 and the strains expressing VirB8^{A100} variants, VirB8^{V97A}, VirB8^{V97R} and VirB8^{Q93CE94C} did not form tumors reflecting defects in transferring the T-DNA substrate. However, despite its inability to form T-pili at detectable levels, CB8 expressing

VirB8^{V97C} induced tumor formation, albeit at a lower level than the wild type. Third, we used the T4S system-mediated IncQ plasmid pLS1 transfer between *Agrobacterium* cells as quantitative measure of secretion system function. The conjugative transfer of pLS1 was abolished in the *virB8* deletion strain and restored by VirB8. Expression of VirB8^{A100} variants, VirB8^{V97A}, VirB8^{V97R} and VirB8^{Q93CE94C} did not restore the transfer of pLS1 (Table 3.3). In addition, the level of conjugation was substantially reduced in CB1008 expressing VirB8^{Q93D} variants, VirB8^{V97C} and VirB8^{V97T}. The results from the conjugation experiments are similar to those of the tumor formation experiments (T-DNA transfer). The VirB8^{V97C} and VirB8^{V97T} variants are functional in these assays, but VirB8^{V97C} does not form detectable amounts of T-pili. As the variants with the clearest negative and partial defective phenotypes were those with changes of residue V97, we assessed the dimerization state of these variants with purified proteins *in vitro*.

3.3.5 VirB8^{V97} is required for dimerization in vitro.

Analytical ultracentrifugation was used to calculate the dissociation constant of the purified wildtype periplasmic domain of VirB8 and of its V97 variants. The results obtained with the periplasmic domain of VirB8 from *Agrobacterium* fits a monomer/dimer equilibrium and the dissociation constant was determined to be 0.68 mM (Figure 3.7). This is approximately six times weaker than in the case of VirB8 from *B. suis* that has a K_d of 116 μM. Interestingly, the results obtained with the VirB8^{V97A} (not shown) and VirB8^{V97R} variants (Figure 3.7) both fit to the monomer/dimer model, and as expected, these variants were reduced in dimerization with K_d values of 1 mM and 4.64 mM, respectively. VirB8^{V97C} existed predominantly as a dimer with a Kd of 1 μM

(Figure 3.7) and VirB8^{V97T} (not shown) similar to wildtype protein had a K_d of 0.59 mM. Thus as predicted, the variants VirB8^{V97A} and VirB8^{V97R} displayed reduced self-association, VirB8^{V97C} formed significantly tighter dimers and VirB8^{V97T} had wildtype dimerization ability. Analysis of the secondary structure of the VirB8 wildtype and variants using CD spectroscopy suggested that the amino acid changes did not affect the overall folding of the protein (data not shown). Next, we characterized the molecular basis of the effects of V97 dimer site changes in *Agrobacterium.*

3.3.6 VirB8 stabilizes several other VirB proteins.

A common approach to assess the contribution of individual proteins like VirB8 to T4S complex assembly is to determine whether other components are destabilized in their absence. To this end, we cultivated the *virB8* gene deletion strain CB1008 and complemented variants under virulence gene inducing conditions and the levels of other VirB proteins were analyzed by Western blotting. As compared to the wild type C58, the levels of VirB3 and VirB6 were strongly reduced and more modest reductions were observed in the case of VirB1, VirB4, VirB5, VirB7 and VirB11 in CB1008 (Figure 3.8A). Subsequently, we analyzed VirB protein levels in CB1008 expressing the VirB8 dimer variants with changes at V97. The level of VirB8^{V97R} was reduced as compared to the other variants (VirB8^{V97A}, VirB8^{V97C} and VirB8^{V97T}) and we also observed reduced amounts of VirB1, VirB3, VirB5, VirB6, and VirB7 in the cell (Figure 3.8B). Whereas these effects could be explained by the absence of stabilization by VirB8, expression of the other VirB8^{V97} variants did not restore the levels of VirB1, VirB3, VirB5, and VirB6 to wild type. Thus, the mere presence of VirB8 is not sufficient to stabilize these proteins

and the differential effects of the changes (VirB8^{V97A} weaker dimers, VirB8^{V97C} forms more stable dimers, VirB8^{V97T} forms dimers and supports T-pilus formation) have similar impact on the stabilization of these proteins. All of the V97 variants are able to restore VirB7 and VirB11 levels in the cells showing that even reduced amounts of VirB8 are sufficient and that changes in the dimerization state does not impact their stabilization. We next extracted VirB protein complexes from the membranes in order to get further insights into the contribution of VirB8 to T4S complex formation.

3.3.7 VirB8 and its dimerization are required for the association of VirB2 with the T4S core complex.

The VirB8^{V97} variants have differential effects on T4S functions and T-pilus formation (Fig. 3) and this could be due to changes of interactions within the complex for which VirB8 and its dimerization are necessary. To test this possibility, we next assessed whether VirB8 and its dimerization are involved in the formation of VirB2-VirB5 complexes, which we predicted to be incorporated into T-pili following their interaction with the VirB4-VirB8 complex (Krall et al., 2002). To this end, we extracted T4S complexes from CB8 complemented with wildtype VirB8 and the VirB8^{V97} variants with the mild detergent dodecyl-ß-(D)-maltoside (DDM), followed by fractionation by blue native PAGE (BN-PAGE) and gel filtration. To increase the likelihood of isolating T-pilus pre-assembly states, we analyzed strains grown in liquid cultures. Analysis of cell extracts by BN-PAGE revealed that in contrast to the results previously obtained in a *virB4* deletion strain (Krall et al., 2002), the presence of VirB8 is not required for the formation of low molecular mass VirB2-VirB5 complexes of about 100 kDa (Figure 3.9).

However, we noticed that VirB2, and to a lesser extent VirB5, co-fractionated with higher molecular mass complexes that could correspond to complexes of VirB8, VirB8-VirB9 and VirB10 (Yuan et al., 2005). This co-fractionation is not observed in the absence of VirB8 and in CB1008 expressing VirB8^{V97A} and VirB8^{V97R} variants that show reduction in self-association (Figure 3.9). The expression of variants VirB8^{V97C} and VirB8^{V97T} that are able to form dimers restored the co-fractionation of VirB2 with higher molecular proteins (Figure 3.9).

To analyze the localization of membrane-extracted VirB proteins at higher resolution and to detect other proteins that cannot be visualized after BN-PAGE, the extracts were next fractionated by gel filtration. Similar to the results of the BN-PAGE, we detected both VirB2 and VirB5 predominantly in low molecular mass, but also in high molecular mass fractions (Figure 3.10A) In the absence of VirB8, VirB5 levels were significantly reduced and VirB2 accumulated exclusively in the low molecular mass fraction (Figure 3.10B). Expression of VirB8^{V97C} partly restored the co-fractionation of VirB2 with high molecular mass complexes (Figure 3.10C), whereas expression of VirB8^{V97A} resulted in a situation similar to CB8 (Figure 3.10D). Expression of neither variant restored the level of VirB5 to wild type levels and its co-fractionation with high molecular mass complexes. The fractionation patterns of other VirB proteins were not changed in the presence or the absence of VirB8, but we found that some of them were stabilized in the presence of VirB8 as presented before. Taken together, VirB8 and its dimerization impact the association of VirB2 and of VirB5 with high molecular mass complexes and for T-pilus assembly. The direct VirB8-VirB5 interaction we described

earlier (Chapter 2 (Yuan et al., 2005)) may be key to this observation as VirB8 dimers were reduced by VirB5 and VirB5 peptides and so, the VirB8 self-association but also its dissociation is important for correct targeting of VirB2-VirB5 (pilus components) for pilus assembly.

3.4 Discussion

VirB8 is a key T4S component that undergoes multiple interactions with other VirB proteins. A detailed characterization of its contribution to T4S system assembly and function is therefore of high interest for the field (Judd et al., 2005a). In this study we investigated the contribution of VirB8 dimerization towards T4S system assembly and function. Based on the results of the X-ray analysis of *Brucella* and *Agrobacterium* VirB8 (Bailey et al., 2006; Terradot et al., 2005) and our subsequent structure-function analysis of the *Brucella* homolog (Paschos et al., 2006), we conducted a detailed analysis of the functional consequences of changes at the dimer interface in the *Agrobacterium* system. Our results shed light on the mechanistic contribution of this protein towards T-pilus assembly.

Residues that were predicted to localize at the dimer interface and to contribute to the interaction were changed and complementation experiments revealed that many of them (VirB8^{Q93}, VirB8^{V97}, VirB8^{A100}) are indeed required for VirB8 functions. In contrast, changes of VirB8^{E94}, a residue predicted to stabilize the dimer via a hydrogen bond to VirB8^{Q93} on the neighboring VirB8, had no major effects suggesting that this interaction is not important for protein function or that the changes (VirB8^{E94K} and VirB8^{E94Q}) preserved the dimer. Introducing compensatory changes such as VirB8^{Q93DE94K} did not restore function as compared to defective VirB8^{Q93D} alone arguing that VirB8^{Q93} and VirB8^{E94} do not bind to each other, or that these changes had other negative effects, e.g. on protein folding. Changes of VirB8^{A100} abolished VirB8 functions; presumably a consequence of reduced dimerization. This is in line with our

own work on the corresponding change in *Brucella* VirB8 (Paschos et al., 2006) and previous analyses of the *A. tumefaciens* VirB8 variant (Kumar & Das, 2001). We chose residue VirB8^{V97} for a more comprehensive analysis as the spacing between the interacting amino acids at the dimer interface (hydrophobic V97-V97 interaction predicted) permitted interesting possibilities for engineering and modulation of the interaction. The VirB8^{V97A} and VirB8^{V97R} changes were predicted to destroy the interaction and indeed, these variants did not complement the *virB8* deletion. The non-functionality of the VirB8^{V97R} variant could be attributed to the positive charge at the interface that would repel neighboring VirB8 making it a very weak dimer (K_d of 4.64 mM, Fig. 4*C*). In case of VirB8^{V97A} the non-functionality could be attributed to the fact that spacing of the functional residues at the protein interface is increased from 3.56 Å to 5.96 Å also creating a weaker dimer (K_d of 1 mM, Fig. 4*B*). In contrast, the V97T variant that forms dimers at wildtype levels (K_d 0.59 mM, Fig. 4*E*) partly complemented the *virB8* defect in all functional assays, suggesting that the hydrophobic V97-V97 interaction can be replaced by the hydrophilic T97-T97 interaction. Changing V97 to Cys resulted in the formation of a dimer in the oxidative environment of the periplasm showing for the first time that VirB8 does indeed form a dimer under physiological conditions. Interestingly, we did not detect any pili on CB1008 expressing VirB8^{V97C}, but the T4S system translocated substrates to a reduced extent and this makes VirB8^{V97C} a so-called "uncoupling" protein variant that translocates substrates but does not form T-pili. Such variants were already described in the case of VirB6, VirB9 and VirB11 (S.J. Jakubowski, Cascales, Krishnamoorthy, & Christie, 2005; S.J. Jakubowski,

Krishnamoorthy, & Christie, 2003; Sagulenko et al., 2001) and our work adds further evidence to the notion that the dual roles of the T4S system in pilus assembly and substrate translocation can be separated.

The results obtained in case of the partly functional variants VirB8^{V97C} and VirB8^{V97T} raise interesting questions. The overall geometry of the dimer should not be influenced by these changes; the distance at the interface is predicted to be 3.08 Å (VirB8^{V97C}) and 3.73 Å (VirB8^{V97T}), respectively, which is close to the 3.56 Å in the wild type. These changes are predicted to strengthen dimer formation in case of the covalent bond formed by VirB8^{V97C}, whereas the dimer should remain flexible in case of VirB8^{V97T}, similar to what we observed in case of *Brucella* VirB8, a relatively weak dimer with a K_d of 116 +/- 7.5 μM (Paschos et al., 2006). The fact that increasing the strength of dimer formation (VirB8^{V97C}) as well as weakening it (VirB8$^{V97A/R}$) reduced complementation raises the possibility that not only the presence of VirB8 and its self-association, but also the dissociation of the dimer may be important for T4S. The mere presence of VirB8 is required for the stabilization of VirB1, VirB3, VirB4, VirB5, VirB6, VirB7 and VirB11. This is consistent with similar observations on reduced amounts of several VirB proteins in *Brucella* carrying the deletion of *virB8* (A. B. den Hartigh, Rolan, de Jong, & Tsolis, 2008). VirB8 was previously shown to interact with itself, VirB1, VirB4, VirB5, VirB9, VirB10 and VirB11 (Das & Xie, 2000; Ding et al., 2002; Höppner et al., 2005; Paschos et al., 2006; D. Ward et al., 2002; Yuan et al., 2005). VirB8 wild type protein complemented the deletion strain CB8 and restored VirB protein levels, which is consistent with stabilization by direct interactions. However, all the V97

variants did not restore the wild type levels of VirB1, VirB3, VirB5 and VirB6 despite the presence of wild type levels of the VirB8 in most cases (Fig. 5). This result suggests that VirB8 dimer interaction could be important for stabilizing VirB1, VirB3, VirB5 and VirB6 and that both the formation of a dimer (reduced in VirB8$^{V97A/R}$) as well as its dissociation (reduced in VirB8^{V97C}) contribute to stabilization. Moreover, it is intriguing that despite the reduced levels of VirB1, VirB3, VirB5 and VirB6, the VirB8^{V97C} and VirB8^{V97T} variants partly complemented T4S functions. The level of T-pilus formation in CB8 expressing VirB8^{V97T} was at wild type levels, whereas we did not detect T-pili in CB8 expressing VirB8^{V97C} and these results pointed to an involvement of VirB8 dimerization in T-pilus formation.

In our previous work we postulated a VirB4-VirB8-VirB5-VirB2 T-pilus assembly sequence (Yuan et al., 2005). To examine the role of VirB8 and of its dimerization in this sequence, we characterized the T4S complex sub-assemblies in the *virB8* deletion strain CB1008 and after complementation with the V97 variants. This approach revealed that the presence of VirB8 and its dimerization were required for the co-fractionation of VirB2 and VirB5 with a higher molecular mass complex of VirB components (VirB6-VirB8-VirB9-VirB10). In the absence of VirB8, VirB5 levels were reduced, presumably due to lack of a direct stabilizing interaction (Yuan et al., 2005) that may also imply VirB6 (Hapfelmeier et al., 2000). In addition, VirB2 fractionated only in a low molecular mass complex of about 100 kDa together with VirB5 and did not co-fractionate with other VirB proteins in a high molecular mass complex. Whereas in the *virB4* deletion strain CB1004 (Yuan et al., 2005) VirB2 and VirB5 fractionated as

monomers, this was not the case in extracts from CB1008, suggesting that VirB4 is the key factor for the formation of the VirB5-VirB2 complex. VirB8 is required at the next step of the pilus assembly process and mediates their association with the high molecular mass complex. The VirB8^{V97} variants did not restore VirB5 in the cell to wild type levels, but the partly functional variants VirB8^{V97C} and VirB8^{V97T} restored the co-fractionation of VirB2 with high molecular mass proteins, presumably the VirB6-VirB8-VirB9-VirB10 complex (Fig. 3.9 & 3.10) suggesting that dimerization of VirB8 is required at this step of pilus assembly. Moreover, the observation that the VirB8^{V97C} variant did not enable pilus formation provides evidence for the notion that assembly but also dissociation of the VirB8 dimer are required for pilus formation. This raised the possibility that VirB8 may dissociate to enable an interaction with the VirB5-VirB2 complex followed by pilus assembly.

We also conducted experiments with purified proteins to assess whether VirB5 impacts VirB8 dimerization. First, we identified the domain of VirB5 that binds to VirB8 using peptide array and pulldown assays (Chapter 2, Fig. 2.2 & Fig. 2.4). Based on the X-ray structure of the VirB5 homolog TraC (H.-J. Yeo et al., 2003), we modeled the interacting residues to the globular domain of VirB5. Second, we tested the impact of VirB5 and of peptides derived from the interacting domain on VirB8 dimerization and a cross-linking assay revealed strong negative effects on VirB8 multimer formation (Chapter 2, Fig. 2.3). Similarly, using a bacterial two-hybrid system-based *in vivo* assay, we observed that VirB5 peptides from the interaction domain reduced VirB8 dimerization (Chapter 2, Fig. 2.3). Thus, VirB5 reduces VirB8 dimerization and in turn,

we conclude that dissociation of the dimer may be necessary for the VirB8-VirB5 interaction. This would explain the contribution of VirB8 to T-pilus assembly as outlined in the following model.

Taking all the findings together, we propose that the analysis of VirB8 dimer variants reveals one of the missing pieces to understand how pilus components (VirB2-VirB5) are targeted to form T-pili. Current understanding of T4S system assembly implies that VirB8 first interacts with VirB1 (Höppner et al., 2005; D. Ward et al., 2002), followed by interactions with other VirB proteins to facilitate assembly. VirB4 stabilizes VirB3 and VirB8, which dissociates and interacts with VirB5 to target VirB2-VirB5 complexes to the higher molecular mass complex, presumably via its interaction with VirB3 (Shamaei-Tousi, Cahill, & Frankel, 2004) (Fig. 3.11). Here, we also found that VirB6 levels were reduced in the absence of VirB8, which is consistent with a VirB6-VirB8 interaction. VirB6 co-localization with VirB8 was previously reported using immunofluorescence microscopy (Judd et al., 2005a). The transfer immunoprecipitation assay revealed a T-DNA transfer step dependent on VirB6 and VirB8, which also supports the notion that these two proteins interact (Cascales & Christie, 2004b). The fact that VirB6 is known to stabilize VirB3 and VirB5 in the cells (Hapfelmeier et al., 2000) can also be understood in this context and we here propose that VirB8, in conjunction with VirB6, orients the VirB2-VirB5 complexes to VirB3. Both the association of VirB8 (defective variants VirB8$^{V97A/R}$) as well as its dissociation (VirB8^{V97C}) were necessary for full complementation. These observations led to the proposed model of a VirB8 monomer-dimer cycle necessary for T-pilus assembly. The proposed mechanism is

strikingly similar to that of Nuclear Transport Factor 2 (NTF2) with which VirB8 shares structural similarity (Terradot et al., 2005). NTF2 functions as a monomer and dimer to shuttle RanGDP to and from the nucleus and the dimer interface is involved in interaction with RanGDP (Chaillan-Huntington et al., 2001). Future studies will involve the identification of VirB8 domain(s) necessary for interaction(s) with VirB1, VirB5, and VirB6 to unravel additional details of the mechanistic contribution of this T4S assembly factor. Similarly, it will be important to track the interactions of the VirB2-VirB5 complex with components of the T4S core complex in order to understand how the pilus structure assembles on the surface of *Agrobacterium*. This work constitutes an important step forward towards understanding the protein-protein interactions guiding the assembly of T4S complexes and constitutes a prerequisite for mechanistic understanding of T-pilus assembly.

Table 3.1. Bacterial strains and plasmids.

Strains	Genotype or description	Source o reference
E. coli JM109	*endA1 gyr96 thi hsdR71 supE44 recA1 relA1* (*Δlac-proAB*) (F' *traD36 proAB*$^+$ *lacI*^{q} *lacZ*ΔM15)	(Yanisch-Perron e al., 1985)
A. tumefaciens C58	Wild type, pTiC58	(van Larebeke et al 1974)
A. tumefaciens CB8	pTiC58 carrying an in-frame deletion of *virB8*	(Aly & Baron, 2007)
A. tumefaciens A348	Wild type, pTiA6NC	(van Larebeke et al 1974)
A. tumefaciens PC1008	pTiA6NC carrying an in-frame deletion of *virB8*	(Berger & Christie, 1994)
A. tumefaciens UIA143 pTiA6	A348, ery^r, *recA ery140*	(Bohne, Yim, & Binns, 1998)
E. coli BTH101	F$^-$ *cya-99, araD139, galE15, galK16, rpsL1 (Str^r), hsdR2, mcrA1, mcrB1*	(G. Karimova Ullmann, & Ladant, 2000)
E. coli BL21star (DE3)	F$^-$ *ompT hsdS*$_B$ (*r*$_B^-$ *m*$_B^-$) *gal dcm rne131* (λDE3)	Invitroger
Plasmids		
pLS1	car^r, IncQ plasmid for VirB/D4-mediated conjugative transfer experiments	(Stahl e al., 1998)
pTrcB7B8	strp^r&spc^r, pTrc200 carrying *virB7-virB8* genes from *A. tumefaciens* C58	this work
pT7-7StrepIIB7B8	car^r, pT7-7StrepII carrying *virB7-virB8* genes from *A. tumefaciens* C58	this work
pTrcB7B8^{Q93D}	pTrc200B7B8 modified to encode VirB8 with amino acid change Q93->D	this work
pTrcB7B8^{Q93E}	pTrc200B7B8 modified to encode VirB8 with amino acid	this work

	change Q93->E	
pTrcB7B8^{E94K}	pTrc200B7B8 modified to encode VirB8 with amino acid change E94->K	this work
pTrcB7B8^{E94Q}	pTrc200B7B8 modified to encode VirB8 with amino acid change E94->Q	this work
pTrcB7B8^{Q93DE94K}	pTrc200B7B8 modified to encode VirB8 with two amino acid changes Q93-> D & E94->K	this work
pTrcB7B8^{Q93EE94Q}	pTrc200B7B8 modified to encode VirB8 with two amino acid changes Q93-> E & E94->Q	this work
pTrcB7B8^{Q93CE94C}	pTrc200B7B8 modified to encode VirB8 with two amino acid changes Q93->C & E94->C	this work
pTrcB7B8^{V97A}	pTrc200B7B8 modified to encode VirB8 with amino acid change V97->A	this work
pTrcB7B8^{V97R}	pTrc200B7B8 modified to encode VirB8 with amino acid change V97->R	this work
pTrcB7B8^{V97C}	pTrc200B7B8 modified to encode VirB8 with amino acid change V97->C	this work
pTrcB7B8^{V97T}	pTrc200B7B8 modified to encode VirB8 with amino acid change V97->T	this work
pTrcB7B8^{A100V}	pTrc200 modified to encode VirB8 with amino acid change A100->V	this work
pTrcB7B8^{A100R}	pTrc200B7B8 modified to encode VirB8 with amino acid change A100->R	this work
pT7-7StrepIIVirB8ap	pT7-7StrepII carrying 495 bp *Acc651/PstI* virB8 fragment from *A. tumefaciens* C58 (encoding 164 amino acid periplasmic domain)	this work
pT7-7StrepIIVirB8ap^{V97A}	pT7-7StrepIIVirB8ap modified to encode VirB8 with amino acid change V97->A	this work
pT7-7StrepIIVirB8ap^{V97R}	pT7-7StrepIIVirB8ap modified to encode VirB8 with amino acid change V97->R	this work
pT7-7StrepIIVirB8ap^{V97C}	pT7-7StrepIIVirB8ap modified to encode VirB8 with amino acid change V97->C	this work
pT7-7StrepIIVirB8ap^{V97T}	pT7-7StrepIIVirB8ap modified to encode VirB8 with amino acid change V97->T	this work
pT7-7StrepIIVirB8sp	pT7-7StrepII carrying 492 bp *Acc*65I/*Pst*I *virB8* fragment from *B. suis* (encoding 163 amino acid periplasmic domain)	(Terradot et al., 2005)
pT7-7StrepIIVirB8sp^{M102R}	pT7-7StrepIIVirB8sp carrying modified to encode VirB8 with amino acid change M102 –>R	(Paschos et al., 2006)
pT7-7StrepIIVirB8sp^{Y105R}	pT7-7StrepIIVirB8sp carrying modified to encode VirB8 with amino acid change Y105 –>R	(Paschos et al., 2006)
pT7-	pT7-7StrepIIVirB8sp carrying modified to encode VirB8	(Paschos

7StrepIIVirB8sp^{E214R}	with amino acid change E214 –>R	et al. 2006)
pUT18CB8s	pUT18C carrying 720bp *XbaI/KpnI* VirB8s from *B. suis*	This work
pKT25B8s	pKT25 carrying 720bp *XbaI/KpnI* VirB8s from *B. suis*	This work
pKT25B8s^{M102R}	pKT25B8s modified to encode VirB8s with amino acid change M102->R	This work
pUT18CB8s^{M102R}	pUT18CB8s modified to encode VirB8s with amino acid change M102->R	This work
pKT25B8s^{Y105R}	pKT25B8s modified to encode VirB8s with amino acid change Y105->R	This work
pUT18CB8s^{Y105R}	pUT18CB8s modified to encode VirB8s with amino acid change Y105->R	This work
pKT25B8s^{E214R}	pKT25B8s modified to encode VirB8s with amino acid change E214->R	This work
pUT18CB8s^{E214R}	pUT18CB8s modified to encode VirB8s with amino acid change E214->R	This work
pKT25B8sN	pKT25 carrying 228bp *XbaI/KpnI* VirB8s N-terminus from *B. suis*	This work
pUT18CB8sN	pUT18C carrying 228bp *XbaI/KpnI* VirB8s N-terminus from *B. suis*	This work
pKT25B10s	pKT25 carrying 1176bp *XbaI/KpnI* VirB10s from *B. suis*	This work
pUT18CB10s	pUT18C carrying 1176bp *XbaI/KpnI* VirB10s from *B. suis*	This work

Table 3.2. Oligonucleotide sequences.

Name	Sequence	Constructed plasmid
PCR primers where the underlined sequence corresponds to the restriction enzyme recognition site		
B7B8-5	5'CGCGTGAATTCATGAAATATTGCCTG-3'	pTrcB7B8
B7B8-3	5'CGCGTGGATCCTCATGGTTCGCTGTGGCC-3'	
5B8s	5'-CTAGTCTAGACGGGATGTTTGGACGCAAACAATC TCCA-3'	pKT25B8s/pUT18CB8s
3B8s	5'-CGGGGTACCTCATTGCACCACTCCCATTTCTG G-3'	
3B8Ns	5'-CGGGGTACCTCACACCAGGTAGGGCACATGTTG CTT-3'	pKT25B8sN/pUT18CB 8sN
5B10s	5'-CTAGTCTAGACGGGATGACACAGGAAAACATTCC GGTG-3'	pKT25B10s/pUT18CB 10s
3B10s	5'-CGGGGTACCTCACTTCGGTTGGACATCATACAC	
Inverse PCR primers for site directed mutagenesis in VirB8 encoding gene		
B8Q93D-5	5'GTCTCCCGATTGCCTGCAACTGATGAGGAGGC CGTCGTT-3'	pTrcB7B8^{Q93D}

B8Q93D-3	5'CTCCTCATCAGTTGCAGGCAATCGGGAGACGG ACACCTC-3'	
B8Q93E-5	5'GTCTCCCGATTGCCTGCAACTGAGGAGGAGGC CGTCGTT-3'	pTrcB7B8^{Q93E}
B8Q93E-3	5'CTCCTCCTCAGTTGCAGGCAATCGGGAGACGG ACACCTC-3'	
B8E94K-5	5'GTCTCCCGATTGCCTGCAACTCAAAAAGAGGC CGTCGTT-3'	pTrcB7B8^{E94K}
B8E94K-3	5'CTCTTTTTGAGTTGCAGGCAATCGGGAGACGG ACACCTC-3'	
B8E94Q-5	5'GTCTCCCGATTGCCTGCAACTCAACAAGAGGC CGTCGTT-3'	pTrcB7B8^{E94Q}
B8E94Q-3	5'CTCTTGTTGAGTTGCAGGCAATCGGGAGACGG ACACCTC-3'	
B8Q93DE94 K-5	5'GTCTCCGCATTGCCTGCAACTGATAAAGAGGC CGTCGTT-3'	pTrcB7B8^{Q93DE94K}
B8Q93DE94 K-3	5'CTCTTTATCAGTTGCAGGCAATCGGGAGACGG ACACCTC-3'	
B8Q93EE94 Q-5	5'TCCCGATTGCCTGCAACTGAGCAAGAGGCCGT CGTTAAC-3'	pTrcB7B8^{Q93EE94Q}
B8Q93EE94 Q-3	5'GGCCTCTTGCTCAGTTGCAGGCAATCGGGAGA CGGACAC-3'	
B8Q93CE94 C-5	5'GTCTCCCGATTGCCTGCAACTTGTTGTGAGGCC GTCGTT-3'	pTrcB7B8^{Q93CE94C}
B8Q93CE94 C-3	5'CTCACAACAAGTTGCAGGCAATCGGGAGACGG ACACCTC-3'	
B8V97A-5	5'GCAACTCAAGAGGAGGCCGCTGTTAACGCTTC ATTGTGG-3'	pTrcB7B8^{V97A}
B8V97A-3	5'AGCGTTAACAGCGGCCTCCTCTTGAGTTGCAG GCAATCG-3'	
B8V97R-5	5'GCAACTCAAGAGGAGGCCCGCGTTAACGCTTC ATTGTGG-3'	pTrcB7B8^{V97R}
B8V97R-3	5'AGCGTTAACGCGGGCCTCCTCTTGAGCTGCAG GCAATCG-3'	
B8V97C-5	5'CGATTGCCTGCAACTCAAGAGGAGGCCTGTGT TAACGCC-3'	pTrcB7B8^{V97C}
B8V97C-3	5'ACAGGCCTCCTCTTGAGTTGCAGGCAATCGGG AGACGGA-3'	
B8V97T-5	5'CCTGCAACTCAAGAGGAGGCCACCGTTAACGC CTCACTG-3'	pTrcB7B8^{V97T}
B8V97T-3	5'GTTAACGGTGGCCTCCTCTTGAGTTGCAGGCA ATCGGGA-3'	

B8A100V-5	5'GAGGAGGCCGTCGTTAACGTTTCACTGTGGGA GTATGTT-3'	pTrcB7B8^{A100V}
B8A100V-3	5'CCACAGTGAAACGTTAACGACGGCCTCCTCTT GAGTTGC-3'	
B8A100R-5	5'GAGGAGGCCGTCGTTAACCGCTCATTGTGGGA GTACGTT-3'	pTrcB7B8^{A100R}
B8A100R-3	5'CCACAATGAGCGGTTAACGACGGCCTCCTCTT GAGTTGC-3'	

Table 3.3: Tumor formation and conjugative transfer of pLS1 by *A. tumefaciens* wild type and *virB8* deletion strains expressing different VirB8 variants where wildtype strain is set to 100%.

Strains	**TC[b]/ Donors (%)[a]**	**SD[c]**	**Tumor formation[d]**
A. tumefaciens wt	449	155.1	+++
Δ*virB8*	0	0	-
Δ*virB8*-VirB8wt	100	0	+++
Δ*virB8*-Q93D	4.83	0.25	+
Δ*virB8*-E94K	26.4	9.23	+++
Δ*virB8*-Q93DE94K	1.16	0.78	+
Δ*virB8*-Q93E	213.5	76.8	+++
Δ*virB8*-E94Q	121.7	42.9	+++
Δ*virB8*-Q93EE94Q	148.7	48.6	+
Δ*virB8*-Q93CE94C	0.024	0.023	-
Δ*virB8*-V97A	0	0	-
Δ*virB8*-V97R	0	0	-
Δ*virB8*-V97C	2.66	1.5	+
Δ*virB8*-V97T	1.71	0.27	+
Δ*virB8*-A100V	0	0	-
Δ*virB8*-A100R	0	0	-

[a]Ratio of donors (carrying pLS1) to recipients mixed for conjugation was 5 to 1 (Bohne et al., 1998; Höppner et al., 2004).
[b]TC = transconjugants
[c]SD= standard deviation, average from three independent trails
[d]Results from three replicates

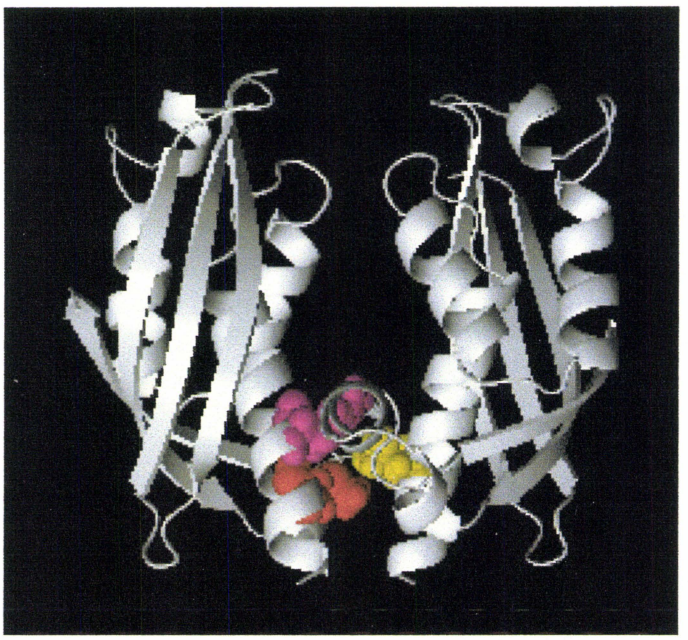

Figure 3.1 Ribbon diagram of the VirB8sp dimer. The residues indicated (M102, red; Y105, yellow; and E214, purple) are important for self-association. The VirB8sp model was generated based on the data base file (2BHM.pdb) by MacPymol (pymol.sourceforge.net).

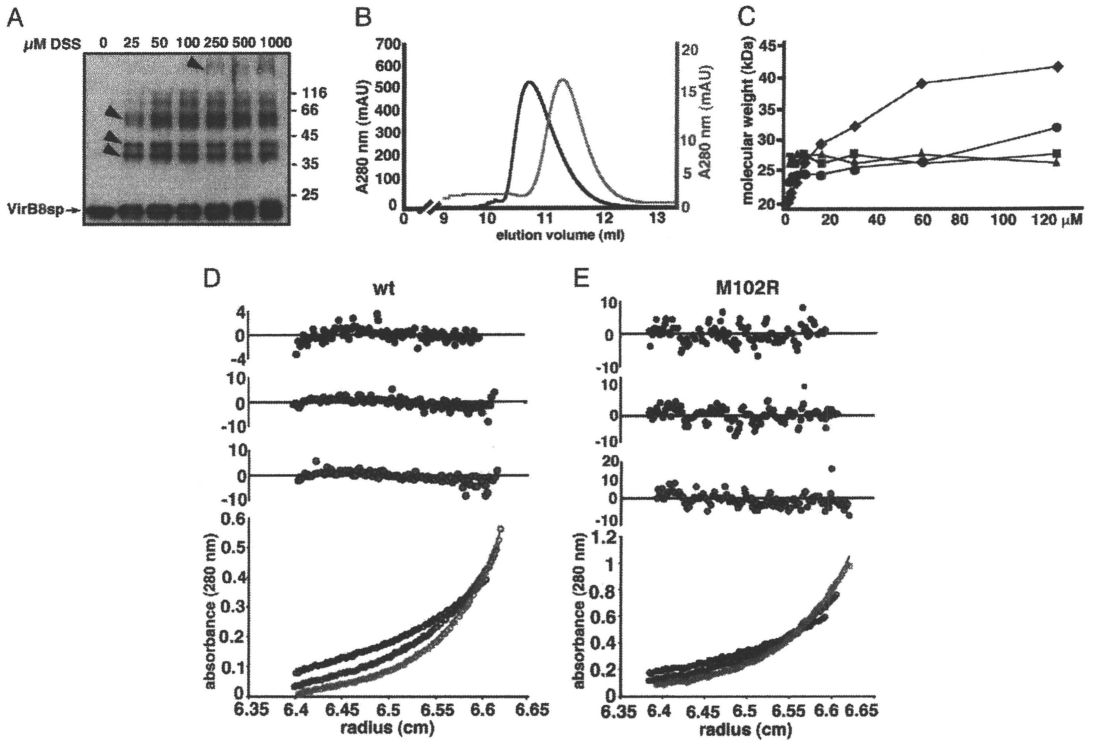

Figure 3.2 Crosslinking, gel filtration, and analytical ultracentrifugation to assess dimer formation of VirB8sp (Paschos et al., 2006). **A.** StrepIIVirB8sp was incubated in the presence of increasing amounts of DSS before SDS/PAGE and Western blotting with VirB8sp-specific antisera. Arrowheads indicate the formation of higher molecular mass complexes, and molecular masses of reference proteins are shown on the right (in kDa). **B**. Chromatogram showing elution of different concentrations of VirB8sp from a Superdex S75 column, 128 μM (black line), and 2 μM (gray line). The corresponding absorbance scales are indicated (mAU, milliabsorbance units at 280 nm). **C**. Plot of the calculated molecular masses of StrepIIVirB8sp (rhombus), M102R (triangle), Y105R (square), and E214R (circle) obtained by size-exclusion chromatography as a function of the applied concentration. **D** and **E**. Sedimentation equilibrium analysis of StrepIIVirB8sp and M102R, respectively. The lower graphs show a representative fit of the experimental data to a monomer/dimer model in case of StrepIIVirB8sp and to a single species (= monomer) model in case of M102R. The upper graphs show the residuals of the fit. The representative fits shown here were taken from the data obtained for proteins at concentration of A_{280} 0.3 and rotor speeds of 20,000, 24,000, and 28,000 rpm in a Beckman Coulter XL-A analytical ultracentrifuge (Paschos et al., 2006).

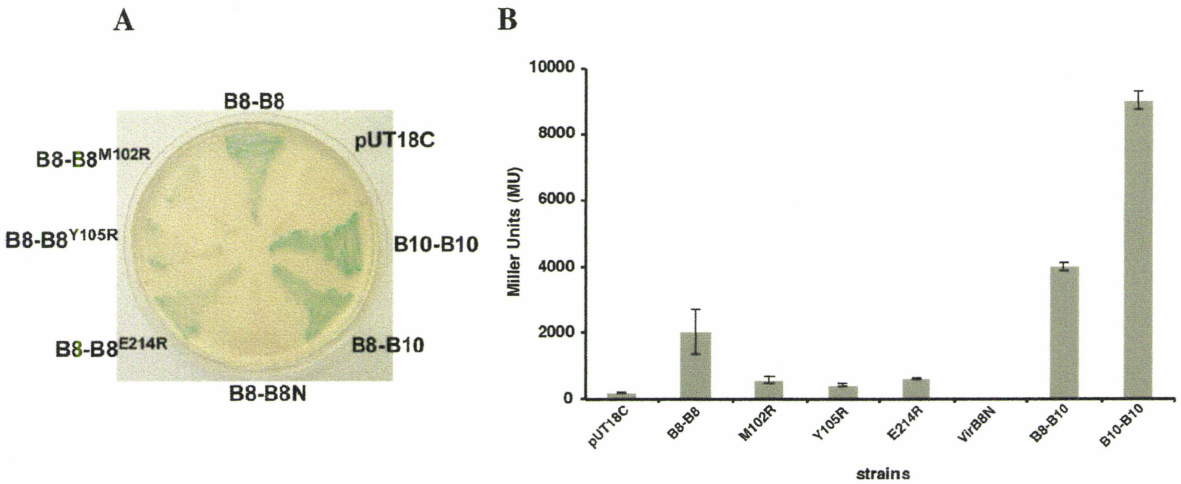

Figure 3.3 Use of the bacterial two-hybrid system to monitor interactions of VirB8 and VirB10. **A.** Screening of VirB8s and variants' self-association using LB-X-Gal agar plates. **B.** Liquid cultures of strains carrying various T18 and T25 constructs were tested by using ONPG (*o*-nitrophenol-β-galactoside) as substrate. VirB8 and VirB10 were expressed as fusions to the enzymatically inactive T18 and T25 domains of adenyl cyclase. The β-galactoside levels were determined to measure protein-protein interactions of VirB8, VirB10 and of VirB8 dimer site variants (M102R, Y105R, and E214R) as compared to a strain expressing the T18 and T25-VirB8 fusion (C). The results shown are from four independent assays and the error bars represent standard deviation.

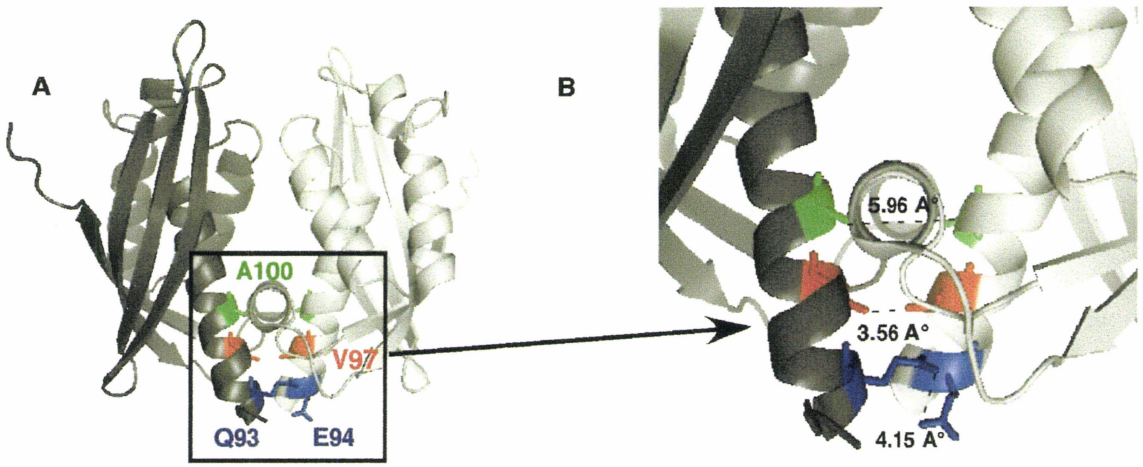

Figure 3.4 Ribbon diagram of the periplasmic domain of *Agrobacterium* VirB8. The residues involved in dimerization are highlighted and images were generated with MacPyMOL (http://www.pymol.org) with structural information from the Protein Data Bank (http://www.pdb.org) file PDB 2CC3. **A**. Residues postulated to be involved in dimerization in *Agrobacterium* VirB8 that were changed in this work. VirB8^{Q93} and VirB8^{E94} (postulated to form a hydrogen bond) are shown in blue and hydrophobic residues VirB8^{V97} and VirB8^{A100} are shown in red and green, respectively. **B.** Distance measurement of atoms that are in close proximity at the dimer interface of *Agrobacterium* VirB8.

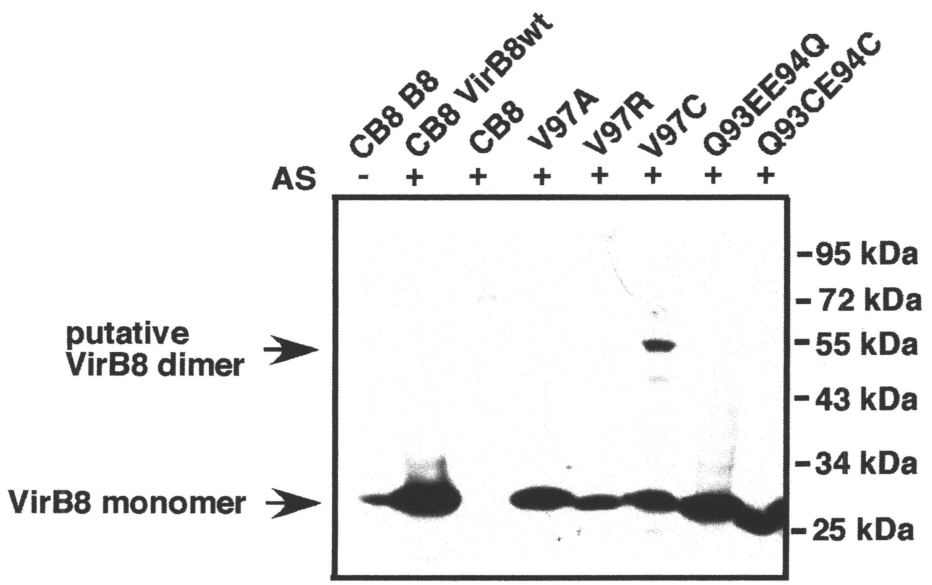

Figure 3.5 Analysis of the accumulation in the cell and dimerization of VirB8 variants. A *virB8* deletion strain (CB8) was complemented with *A. tumefaciens* VirB8 and its variants with changes at the dimer interface. The strains were cultivated under virulence gene-inducing (+AS) or non-inducing conditions (-AS) in the presence of ITPG for expression of the plasmid-encoded genes. The cell lysates were separated by SDS-PAGE under non-reducing conditions. Western blotting was performed using VirB8-specific antiserum and signals corresponding to VirB8 monomer (~ 27 kDa) and dimer (~ 54 kDa) are shown by arrows. The molecular masses of reference proteins are shown on the right in kDa.

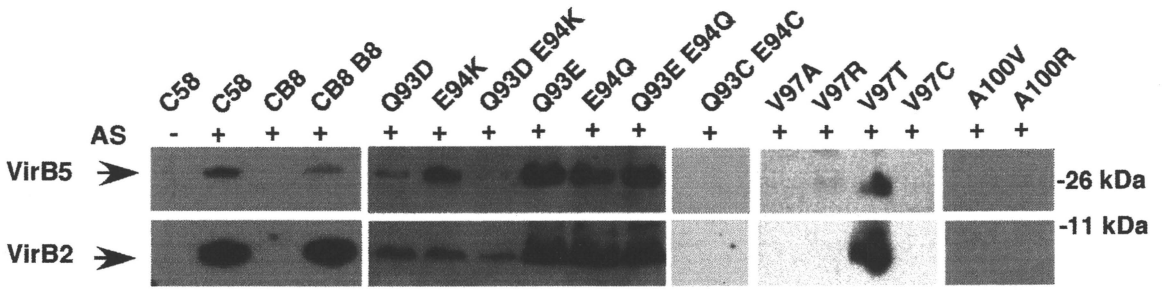

Figure 3.6 Analysis of T-pilus formation. The *virB8* deletion strain (CB1008) was complemented with *A. tumefaciens* VirB8 and its variants with changes at the dimer interface. The strains were cultivated under virulence gene-inducing (+AS) or non-inducing conditions (-AS) in the presence of ITPG for expression of the plasmid-encoded genes. Examination of pilus formation was followed by ultracentrifugation to sediment the pili, SDS-PAGE and Western blotting to detect the pilus components VirB2 and VirB5. Molecular masses of reference proteins are shown on the right in kDa. Representative blots are shown of independent experiments conducted at least three times.

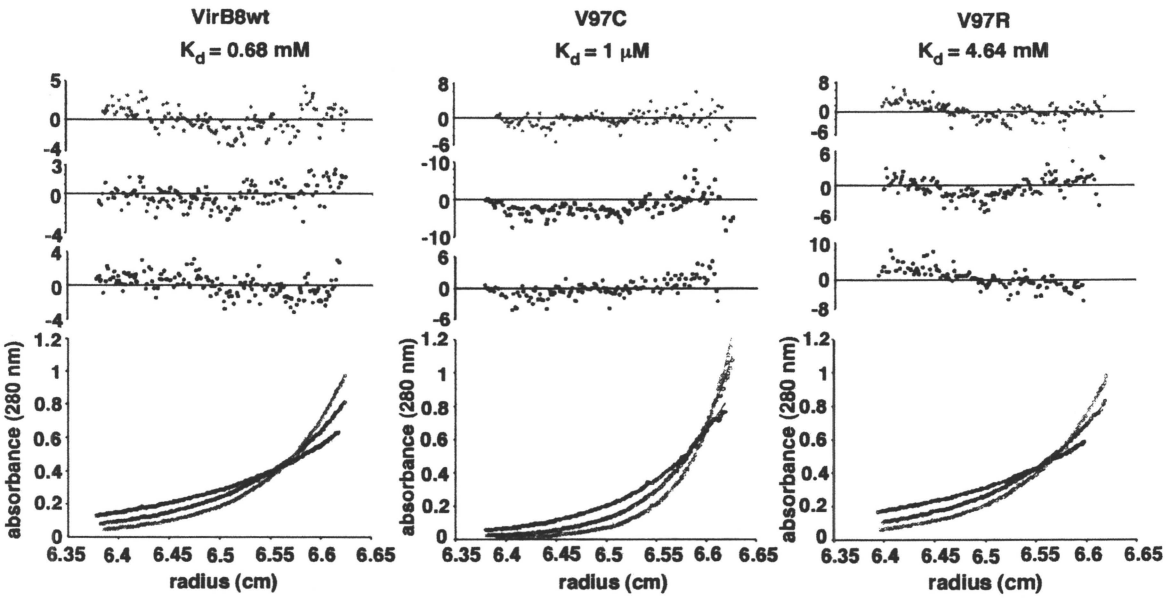

Figure 3.7 Analysis of self-association of VirB8 and variants by analytical ultracentrifugation. Sedimentation equilibrium analysis of StrepIIVirB8ap (wt), StrepIIVirB8sp^{V97C}, and StrepIIVirB8ap^{V97R} were performed using a Beckman Coulter XL-A analytical ultracentrifuge. The representative fits of the experimental data to monomer/dimer equilibrium are shown in the lower graphs with the upper graphs displaying the residuals of the fit. The fits shown here are representative from data obtained for proteins at concentration of A_{280} 0.3 and at speeds 20, 24, and 28 krpm.

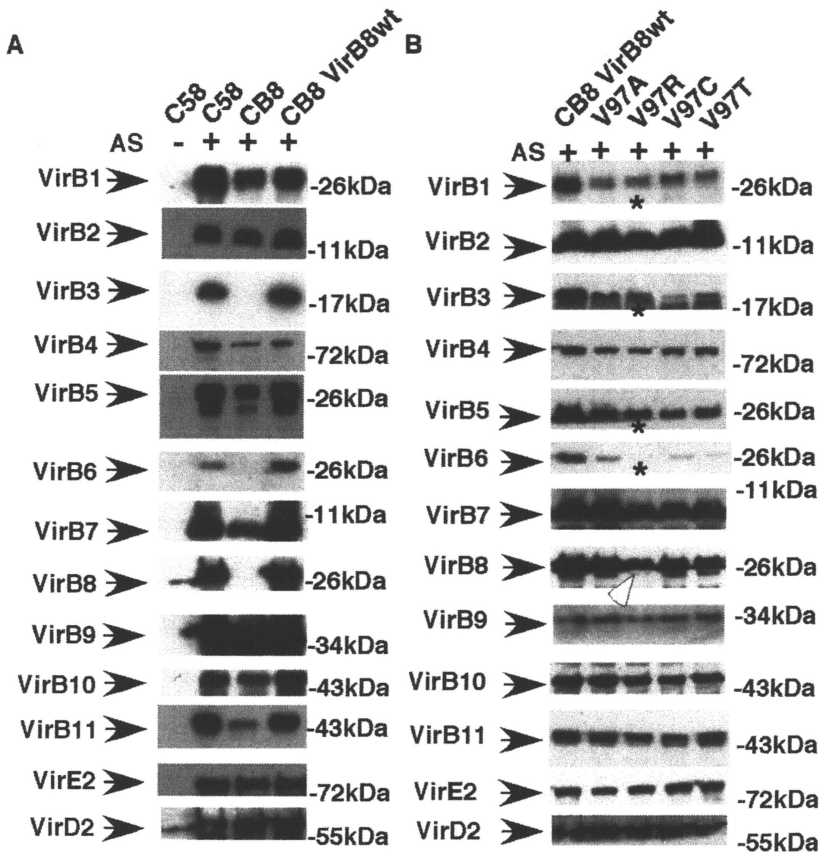

Figure 3.8 Stabilization of VirB proteins in *A. tumefaciens* strains by VirB8 and its V97 variants. Wild type C58, CB1008 and its complemented variants were grown on AB minimal medium with and without virulence inducer (AS) and in presence of IPTG. Cell lysates were separated by SDS-PAGE, followed by Western blotting using specific antisera. **A**. Effects of the deletion of *virB8* and restoration in trans. **B**. Stabilization by VirB8^{V97} variants, the protein levels of V97R are reduced correlating with reduced amounts of many VirB proteins as indicated by an arrow. VirB1, VirB3, VirB5 and VirB6 levels are not restored to wild type levels (indicated by stars) by any V97 variant. Molecular masses of reference proteins are shown on the right in kDa.

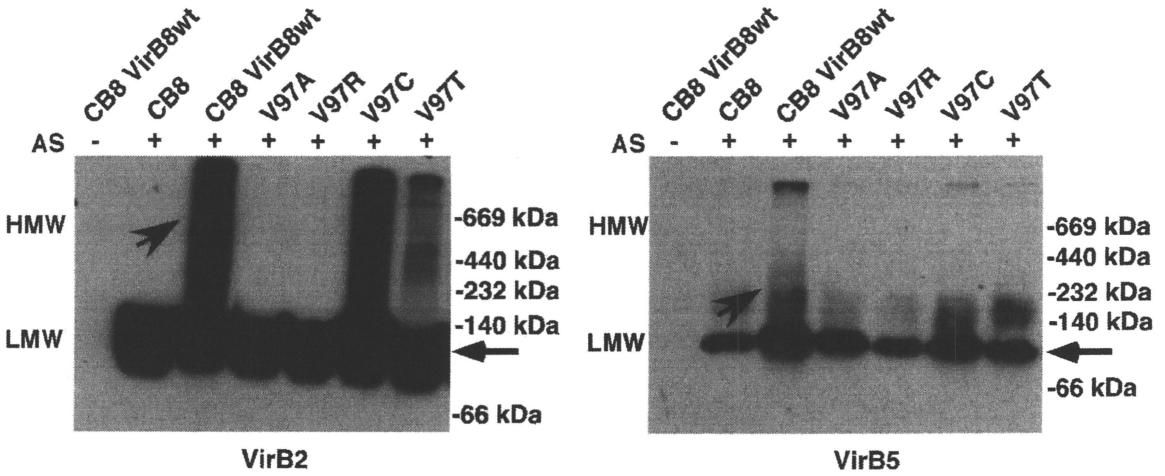

Figure 3.9 Separation of DDM-extracted membrane proteins from *Agrobacterium* using blue native PAGE. CB1008 and complemented variants were cultivated with and without virulence inducer (AS) in liquid medium, followed by the isolation of membranes and extraction with the mild detergent DDM. Samples were mixed with 5% Coomassie Blue G-250 and electrophoresed on a 15% blue native acrylamide gel, followed by Western blotting with VirB specific antisera. VirB2 and VirB5 co-fractionate in the low molecular weight (LMW) region of about 100 kDa as indicated by the arrow found to the right of the western blots, however VirB2 and to lesser extent VirB5 also co-fractionates in the high molecular weight (HMW) complexes as indicated by the arrow on the western blot. Molecular masses of reference proteins are shown on the right in kDa.

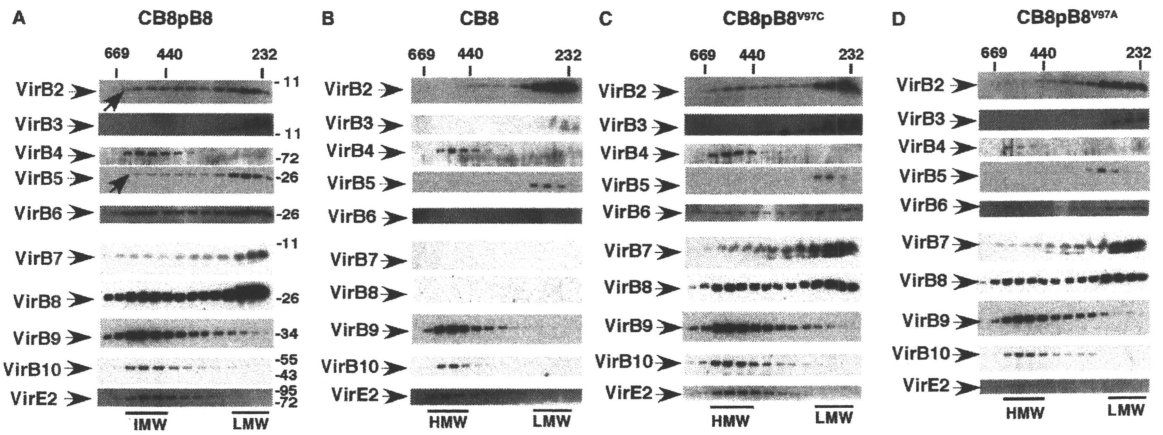

Figure 3.10 Separation of DDM-extracted membrane proteins from *Agrobacterium* using gel filtration. CB1008 expressing VirB8 **(A)**, CB1008 **(B)**, CB1008 expressing VirB8^{V97C} **(C)** and VirB8 expressing VirB8^{V97A} **(D)** were cultivated in virulence gene-inducing liquid medium, followed by the isolation of membranes and extraction with the mild detergent DDM. Samples were subjected to gel filtration chromatography and proteins in the eluted fractions were detected by SDS-PAGE and Western blotting with VirB specific antisera. LMW indicates low molecular weight fractions and HMW indicates high molecular weight fractions, VirB2 and VirB5 co-fractionating with HMW fractions are indicated by arrows. Molecular masses of reference proteins are shown on the top in kDa.

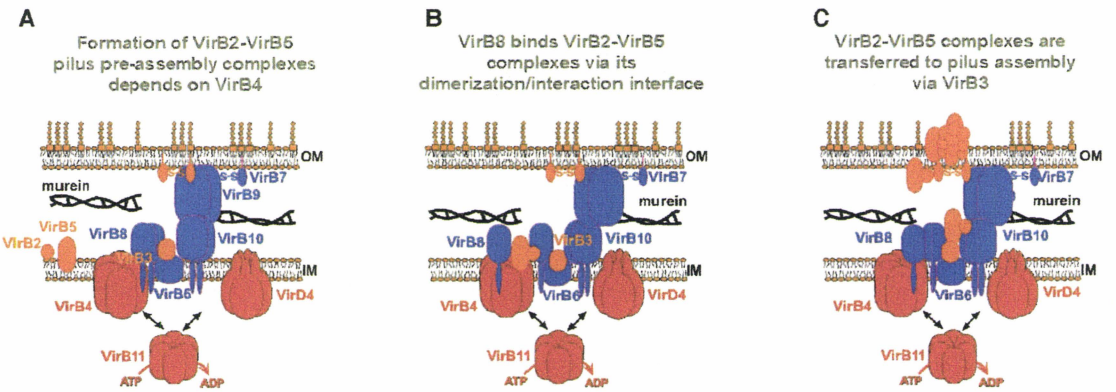

Figure 3.11 Model showing the contribution of VirB8 dimerization towards T-pilus assembly. **A**. VirB4 stabilizes VirB8 and mediates the formation of VirB2-VirB5 complexes. **B**. VirB8 dissociates and binds to VirB5-VirB2 complexes via its dimerization interface. **C.** VirB2-VirB5 complexes are then transferred to the outer membrane high molecular mass complex, presumably via the interaction of VirB5 with VirB3, followed by T-pilus assembly.

CHAPTER FOUR: Quantitative analysis of VirB8-VirB9-VirB10 interactions provides a dynamic model of type IV secretion system core complex assembly

Preface:

The work in this chapter involves understanding the complex formation between core complex proteins VirB8, VirB9 and VirB10 from *B. suis*. This work is essentially a manuscript that is published (D. Sivanesan, M. A. Hancock, A. M. V. Giraldo and C. Baron (2010) Biochemistry. 49:4483-93). Dr. Mark Hancock from Sheldon Biotechnology Institue at McGill University conducted the SPR experiments with the proteins provided by me. Dr. Hancock and I planned the SPR experiments and Dr. Mark Hancock analyzed the results. Dr. A. M. V Giraldo helped with purification of VirB9 and VirB10 proteins for experiments that were requested during review of the manuscript.

CHAPTER FOUR: Quantitative analysis of VirB8-VirB9-VirB10 interactions provides a dynamic model of Type IV secretion system core complex assembly

Abstract

Type IV secretion systems are multi-protein complexes that translocate macromolecules across the bacterial cell envelope. The type IV secretion system in *Brucella* species encodes 12 VirB proteins that permit this pathogen to translocate effectors into mammalian cells, where they contribute to its survival inside the host. The "core" complex proteins are conserved in all type IV secretion systems and they are believed to form the channel for substrate translocation. We have investigated the *in vitro* interactions between the soluble periplasmic domains of three of these VirB components, VirB8, VirB9, and VirB10 using enzyme-linked immunosorbent assays, circular dichroism, and surface plasmon resonance techniques. The *in vitro* experiments helped quantify the self-association and binary interactions of VirB8, VirB9, and of VirB10. Individually, distinct binding properties were revealed that may explain their biological functions and, collectively, we provide direct evidence for VirB8-VirB9-VirB10 ternary complex formation *in vitro*. To assess the dynamics of these interactions in a simplified *in vivo* model of complex assembly, the bacterial two-hybrid system was applied to study interactions between the full-length proteins. This approach demonstrated that VirB9 stimulates the self-association of VirB8, but that it inhibits the VirB10-VirB10 as well as the VirB8-VirB10 interaction. Analysis of a dimerization site variant of VirB8 ($VirB8^{M102R}$) suggested that the interactions with VirB9 and VirB10 are independent of

its self-association, which stabilizes VirB8 in this model assay. We propose a dynamic model for secretion system assembly in which VirB8 plays a role as assembly factor that is not closely associated with the functional core complex comprising VirB9 and VirB10.

4. 1 Introduction

Type IV secretion systems (T4SS) are essential virulence factors in many Gram-negative pathogens (Baron, 2005; Baron et al., 2002; Cascales & Christie, 2003; P.J. Christie, 2004; Llosa & O'Callaghan, 2004). The association between 8-12 VirB proteins generates a macromolecular complex that spans the inner and outer membrane of Gram-negative bacteria, and this complex mediates substrate translocation across the cell envelope (Baron, 2005). T4SS serve different functions that are specifically adapted to the needs of individual organisms. In the well-studied plant pathogen *Agrobacterium tumefaciens*, two T4SS serve as conjugation machineries that transfer plasmid DNA between bacterial cells, and the third one transfers the tumor inducing DNA (T-DNA) into plant cells (Baron & Zambryski, 1996). In *Brucella* species, the causal agents of brucellosis in humans and animals, the T4SS transfers effector proteins to evade the host immune system and facilitate replication in mammalian cells (de Jong, Sun, den Hartigh, van Dijl, & Tsolis, 2008a; O´Callaghan et al., 1999; Roux et al., 2007). Regardless of the functional differences between the two pathogens *A. tumefaciens* and *Brucella*, the *virB* operon structures are similar and the gene products have significant sequence similarity (O'Callaghan et al., 1999). However, the T4SS of *Brucella* does not appear to contain a homolog of VirD4, a coupling protein that targets T-DNA to the *Agrobacterium* VirB components (Atmakuri, Ding, & Christie, 2003; Guo, Jin, Sun, Hew, & Pan, 2007), but the operon encodes an additional VirB component, the VirB12 protein. It was shown that VirB2-VirB11 are essential for virulence in the *A. tumefaciens* model, whereas VirB12 is not essential for *Brucella* virulence (A. B. den Hartigh et al., 2008; A.B. den Hartigh et

al., 2004; Sun, Garcia-Rolan, den Hartigh, Sondervan, & Tsolis, 2005). Most T4SS comprise a VirB1 homolog, a lytic transglycosylase that is believed to facilitate complex assembly by degrading the peptidoglycan in the periplasm (Zahrl et al., 2005b; Zupan et al., 2007). The T4SS proteins are grouped into three categories: energizers (VirB4, VirB11 and VirD4) that predominately localize in the cytoplasm but also associate with the inner membrane; core components (VirB6-VirB10) that are believed to form a conduit from the inner to the outer membrane; pilus assembly components (VirB2, VirB3 and VirB5) that mediate the assembly of the extracellular pilus comprised of VirB2 and VirB5 (Atmakuri et al., 2003; Baron, 2005; P.J. Christie et al., 2005; Fronzes, Schafer et al., 2009).

A major challenge in the T4SS field is to understand in which sequence VirB proteins assemble into a functional complex in the membranes of Gram-negative bacteria. Working with *Brucella* species requires level three-biohazard containment, which constitutes a major constraint that prevents extensive biochemical experimentation (e.g. large-scale growth, extraction and protein analysis) of the T4SS from this organism. To circumvent these constraints, we previously expressed the *B. suis* VirB proteins in the heterologous host *A. tumefaciens* and showed via cross-linking and immunofluorescence analysis that the core complex structure was qualitatively similar to T4SS from other bacteria (Carle et al., 2006). In addition, different approaches such as detergent extraction of the membrane proteins, yeast-two hybrid analysis, cross-linking, and pull down studies in the model organism *A. tumefaciens* provided a working model of T4SS assembly (Das & Xie, 2000; Krall et al., 2002; D. Ward et al., 2002; Yuan et al., 2005). These studies

provided mostly qualitative and static insights into core complex assembly, and quantitative analyses of protein interaction are required to gain insights into the dynamics and sequence of complex assembly (Vetsch et al., 2006; Vitagliano, Ruggiero, Pedone, & Berisio, 2007).

To quantitatively analyze T4SS assembly, we here characterize complex formation between *B. suis* VirB8, VirB9 and VirB10. VirB8 and VirB10 are bitopic inner membrane proteins. The N-termini comprise short cytoplasmic domains, followed by a single transmembrane region and a large C-terminal periplasmic domain that determines the key protein functions (Das & Xie, 2000). Recently, it was identified that VirB10 inserts into the outer membrane as well as inner membrane (Chandran et al., 2009). VirB9 is a periplasmic protein that contains a signal sequence and it localizes in the outer membrane where it forms a complex with the small lipoprotein VirB7 (Anderson, Vogel Hertzel, & Das, 1996; Baron et al., 1997; Beijersbergen, Smith, & Hooykaas, 1994; Das, Anderson, & Xie, 1997; A. Das & Y.-H. Xie, 1998; Fernandez, Dang et al., 1996; Fernandez, Spudich et al., 1996; S.J. Jakubowski et al., 2003). All three proteins are essential for T4SS assembly and function (Beaupré, Bohne, Dale, & Binns, 1997; Berger & Christie, 1994; Cascales & Christie, 2004a; S.J. Jakubowski et al., 2005; Kumar & Das, 2001; Kumar et al., 2000; Liu & Binns, 2003; Paschos et al., 2006; J. E. Ward, Dale, Nester, & Binns, 1990) and binary interactions between VirB8, VirB9, and VirB10 were previously reported (Das & Xie, 2000; Ding et al., 2002; Judd et al., 2005a; Kumar et al., 2000; Paschos et al., 2006; D. Ward et al., 2002). Despite the finding that VirB8 did not co-immunoprecipitate with VirB9 and VirB10 from *A.*

tumefaciens (S.J. Jakubowski et al., 2003) and that it was not part of the VirB7-VirB9-VirB10 core complex recently described by cryo-EM and crystallographic analysis (Chandran et al., 2009; Fronzes, Schafer et al., 2009), the fact that it interacts with many proteins *in vitro* and in the yeast two-hybrid system suggest that VirB8, VirB9 and VirB10 form at least a transient complex.

In this report, we provide qualitative and quantitative results that provide novel insights into T4SS core complex assembly, notably into the role of VirB8. Using ELISA (enzyme linked immunosorbent assay), CD (circular dichroism) spectroscopy, SPR (surface plasmon resonance), and BTH (bacterial two-hybrid) assays, we assessed self-associations and binary interactions between VirB8, VirB9 and VirB10. Furthermore, we provide direct evidence for the formation of a ternary complex of VirB8, VirB9 and VirB10 leading to a dynamic model for their assembly into the core complex.

4.2 Materials and Methods

4.2.1 Growth of bacterial strains and construction of plasmids

All *E. coli* strains were grown in LB medium (1% tryptone, 0.5% yeast extract, 1% NaCl) at 37°C unless otherwise stated in subsequent procedures. The strains and plasmids used in this study are listed in Table 4.1. For propagation of pT7-7StrepII and pUT18C constructs, carbenicillin was added to the media at 100 μg/mL, whereas for the propagation of pKT25 constructs, 50 μg/mL of kanamycin was added. All cloning experiments were conducted according to standard procedures (Maniatis et al., 1982). The bicistronic plasmids for the bacterial two hybrid assays were constructed by first eliminating the single *Hind*III restriction site in the gene encoding the T18 fragment of adenylate cyclase in pUT18CB8. To this end, we created a silent mutation using inverse PCR with 5HIN and 3HIN primers to produce the construct pUT18CB8HIN and this permitted the cloning of Shine-Dalgarno (SD) and *virB* genes downstream of the first *virB* gene. The primers used for PCR reactions are listed in Table 4.2. For cloning of the genes downstream to the pUT18-encoded *virB8* gene, two oligonucleotides (5LNH and 3LNH) carrying unique restriction sites (*Nco*I & *Hind*III) and a SD sequence to ensure gene expression were synthesized. The annealed oligonucleotides were cloned into the *Kpn*I and *EcoR*I restriction sites downstream of *virB8* in pUT18CB8HIN to create pUT18CB8+SD. Next, the *virB9* and *virB10* fragments were PCR amplified from a template containing the *virB* operon of *B. suis* (pTrc200B1+3-12) (Carle et al., 2006) using primers listed in Table 4.2 and were sub-cloned into pUT18CB8+SD to create pUT18CB8+B9 and pUT18CB8+B10. Finally, the SD sequence along with the *virB9*

and *virB10* genes from pUT18CB8+B9 and pUT18CB8+B10 were subcloned into pUT18CB10 to create pUT18CB10+B9 and pUT18CB10+B10. The variant VirB8^{M102R} was subcloned into pKT25 and pUT18C to create pKT25B8^{M102R} and pUT18CB8^{M102R}, respectively, by using PCR primers that are described elsewhere (Paschos et al., 2009) and chapter 3 (Table 3.2). The pUT18CB8^{M102R} construct was used to subclone the SD sequence along with the *virB9* gene from pUT18CB8+B9 to create pUT18CB8^{M102R}+B9.

4.2.2 Over-production and purification of proteins

Derivates of plasmid pT7-7StrepII expressing the periplasmic portions of VirB8, VirB9, and VirB10 were electroporated into *E. coli* BL21star (λDE3) for over-production and purification. The BL21star (λDE3) cells expressing the *virB* genes were grown at 37°C under aerobic conditions to an optical density (A_{600}) of 0.4-0.8, induced for T7 expression by addition of 0.5 mM IPTG and they were further cultivated for 16 h at 26°C. The cells were then harvested, lysed in a French press and purified using Strep-tactin sepharose affinity chromatography as described previously (Yuan et al., 2005). In case of StrepIIVirB8 and StrepIIVirB8^{M102R}, the eluted proteins were subsequently purified using size exclusion chromatography (Superdex 75, Amersham Biosciences) at a flow rate of 0.5 ml/min in buffer A (100 mM Tris-HCl, pH 8; 150 mM NaCl; 1 mM EDTA). StrepIIVirB9 and strepIIVirB10 proteins eluted from the Strep-tactin affinity column were further purified using ion exchange chromatography at a flow rate of 1 ml/min. For VirB9, the affinity-purified fractions were first dialyzed into 20 mM Tris-HCl (pH 6.8) for 12 h at 4°C, followed by CM Sepharose fast flow cation exchanger chromatography. The column was washed with buffer B (20 mM Tris-HCl, pH 6.8),

followed by elution with buffer C (buffer B with 1 M NaCl). For VirB10, the affinity purified fractions were first dialyzed into 20 mM Tris-HCl (pH 8) for 12 h at 4°C, followed by Q-Sepharose fast flow anion exchange chromatography using buffers B and C at pH 8. After elution, the purified proteins were dialyzed extensively against HBS (10 mM Hepes, pH 7.5; 150 mM NaCl; 3 mM EDTA) at 4°C and the final concentrations were determined by Bradford Assay using the Bio-Rad protein reagent (Bio-Rad, CA, U.S.A) with BSA as standard. The molecular weight and purity of the proteins were verified by SDS-PAGE followed by Coomassie Blue and silver staining.

4.2.3 Enzyme-linked immunosorbent assay

For ELISA assays, 50 µL of strepIIVirB8, strepIIVirB10 and BSA (10 µg/mL each in 100 mM sodium carbonate buffer, pH 9.6) were coated to microtitre wells of Immuno 96 Microwell™ plates (NUNC™, NY, U.S.A) for 12 h at 4 °C. Multi-well plates were then washed with HBS-EP (10 mM Hepes, pH 7.5; 150 mM NaCl; 3 mM EDTA; 0.005% Tween 20) to remove non-coated protein and then blocked with 3% skim milk solution (200 µL/well in HBS-EP) to inhibit nonspecific binding. For dose response experiments, strepIIVirB9 and strepIIVirB10 (0, 25, 50 and 100 pmol in 3% skim milk solution) were added to the wells (100 µL final volume) and incubated for 2 h at room temperature. Next, the wells were washed twice (200 µL each) with HBS-EP, followed by the addition of VirB9 or VirB10-specific antisera (1:10,000 dilution; 100 µL/well) for 2 h at room temperature. The wells were then washed twice and incubated with HRP-conjugated goat anti rabbit IgG (1:3000 dilution; 100 µL/well) for 2 h at room temperature. The binding of antibody corresponding to bound protein was determined by

colour development using 100 μL of chromogenic solution (Research & Development Systems, Minneapolis, MN, U.S.A), the reaction was stopped by the addition of 50 μL of 0.5 M H_2SO_4 and colour development was measured at 450 nm. The A_{540} value was subtracted in order to correct for the plate background according to supplier's description (Research & Development Systems). For dissociation experiments, 150 mM to 1 M NaCl was included in sample incubations. In all experiments, controls were used such as incubating the test proteins alone in the microtitre wells to account for background protein attachment, and the primary antisera were tested for cross-reactivity to the bound protein in the wells.

4.2.4 Circular dichroism spectroscopy

For CD assays, purified strepII-tagged VirB8, VirB9 and VirB10 were dialyzed into 10 mM sodium phosphate buffer (pH 7.5) containing 100 mM NaCl and 1 mM EDTA at 4°C for 12 h. Far UV wavelength scans (260 nm to 195 nm) of 1,250 pmol of each protein alone and in combinations were conducted using an AVIV spectropolarimeter with temperature control at 25°C in a 1 mm path length cell, a time constant of 1 sec and a bandwidth of 1 nm. Melting curves of the purified proteins alone and of mixtures were recorded from 25°C to 95°C (measurements at 222 nm at every step of 5°C). The spectra obtained from the far UV CD measurements and the temperature scans were corrected by subtracting the signal obtained from parallel measurements with buffer alone. The measured ellipticity of the protein was converted to the mean residue ellipticity (deg. cm^2/dmole) using the molar extinction coefficients of strepIIVirB8 (37,820 cm^{-1} M^{-1}), strepIIVirB9 (37,820 cm^{-1} M^{-1}) and strepIIVirB10 (28,010 cm^{-1} M^{-1}),

the total number of residues and the concentration of the sample for analysis of secondary structure content. Averages of the mean residue ellipticities (MRE) from the individual proteins were used for conversion of the ellipticity from protein mixtures for analysis of secondary structure content. The quantification of secondary structures was performed by taking the average that was calculated by the programs SELCON, and CONTINILL, which were downloaded from the software package CDPro available at http://lamar.colostate.edu/~sreeram/CDPro (Taneva, 2003). The quantification was performed as described (Sreerama & Woody, 2000).

4.2.5 Surface plasmon resonance

For SPR assays, the interactions between the purified strepII-tagged periplasmic domains of VirB8 (~20 kDa), VirB8^{M102R} (~20 kDa), VirB9 (~31 kDa), and VirB10 (~48 kDa) were examined using a BIACORE 3000 system (GE Healthcare Bio-Sciences AB, Upsala, Sweden; BIAcontrol v4.1 operating software). Experiments were performed on research-grade CM4 sensor chips (Biacore) at 25°C using filtered (0.2 μm) and degassed ELISA buffer (HBS-EP; 10 mM Hepes pH 7.4, 150 mM NaCl, 3 mM EDTA, 0.005% (v/v) Tween 20). Immobilized VirB surfaces (10 μg/mL in 10 mM sodium acetate pH 4.0; ~900 resonance units (RU) final) were prepared using the Biacore Amine Coupling Kit as recommended by the manufacturer; corresponding reference surfaces were prepared in the absence of VirB proteins. Protein-grade detergents (Tween 20 and Empigen) were from Anatrace (Maumee, OH, USA), fatty acid-free bovine serum albumin (BSA) was purchased from Millipore (Billerica, MA, USA), ImmunoPure Gentle Ag/Ab Elution Buffer was from Pierce (Rockford, IL, USA), and all other

chemicals were reagent grade quality. To assess binding specificity and kinetics, equilibrium analyses were performed in which VirB proteins were titrated (0 – 25 μM VirB8; 0 – 5 μM VirB9; 0 – 5 μM VirB10; 0 – 25 μM BSA as negative control) over VirB immobilized and reference surfaces at 5 μL/min using the 'KINJECT' mode (10 – 20 min association, 10 – 20 min dissociation). For each titration series, a buffer blank was injected first, the highest analyte concentration second, and serial dilutions followed (from the lowest to the highest concentration). Comparing binding responses between the duplicated injections of the highest analyte injections verified consistent immobilized VirB surface activity throughout each assay. To determine if a single-point mutation (M102R) affects VirB8 self-association, wild type and variant VirB8 (0 – 50 μM) were also titrated over immobilized VirB8 and VirB8^{M102R} surfaces as described above (including 0-50 μM BSA as a negative control). In all cases, the surfaces were regenerated between sample injections at 50 μL/min using two 30 sec pulses of solution I (Pierce Gentle Elution containing 0.05% (v/v) Empigen) and solution II (HBS-EP containing 0.5 M NaCl; 50 mM EDTA; 5 mM NaOH; 0.05% (v/v) Tween 20; and 0.05% (v/v) Empigen), followed by the 'EXTRACLEAN' and 'RINSE' procedures. Due to the equilibrium style of analysis, binding responses were independent of mass transport limitations and all double-referenced data (Myszka, 1999) presented are representative of duplicate injections acquired from three independent trials. To predict overall equilibrium dissociation constants (K_D), steady-state binding responses (Req) were averaged near the end of the association phase, plotted as a function of VirB

concentration (C), and then subjected to non-linear regression analysis ("Steady state affinity" model; BIAevaluation v4.1 software).

To assess complex formation, multi-component analyses were performed in which fixed concentrations of VirB8, VirB9, and VirB10 (5 μM each) were flowed over immobilized VirB8 at 10 μL/min using the 'QUICKINJECT' mode (5 min association). After each sequential addition, the amount of VirB protein bound in a stable fashion was verified using two 30 sec pulses of NaCl (0.5 M in HBS-EP) that removed transiently bound proteins. At the end of each multi-component series, the immobilized VirB8 surface was regenerated at 50 μL/min using two 30 sec pulses of solution III (Pierce Gentle Elution containing 0.1% (v/v) Empigen) and solution IV (HBS-EP containing 1 M NaCl; 50 mM EDTA; 10 mM NaOH, 0.1% (v/v) Tween 20; and 0.1% (v/v) Empigen), followed by 'EXTRACLEAN' and 'RINSE' procedures. Double-referenced data (Myszka, 1999) are representative of duplicate injections acquired from three independent trials.

4.2.6 Bacterial two hybrid assay

To test for VirB8, VirB9 and VirB10 interactions in vivo, the bacterial two-hybrid system interaction assay based on re-constitution of the AC active site was used (Bourg, Sube, O'Callaghan, & Patey, 2009; G. Karimova, Josette Pidoux, Agnes Ullmann and Daniel Ladant, 1998). The genes encoding full length VirB8, VirB8^{M102R}, and VirB10 were fused to the T18 and T25 fragments (encoding the catalytic domain of Bordetella pertussis AC) and bicistronic constructs co-expressing VirB9 and VirB10 were tested (Paschos et al., 2009). Briefly, E. coli strain BTH101 was co-transformed with vectors

expressing recombinant T25 and T18 fusions to VirB proteins and T25 and T18 domains alone as negative controls, cultivated in liquid LB medium with kanamycin (50 μg/mL), carbenicillin (100 μg/mL) and 1 mM IPTG for 16 h at 26 °C. The interactions were detected by determining the VirB interaction-mediated functional complementation of the two CyaA fragments that led to the production of cAMP, which triggered the β-galactosidase production in BTH101 strain and quantified using ONPG as a substrate (Cowie, 2006). The levels of VirB proteins expressed in the BTH101 strain were assessed by electrophoresis of cell lysates on 10% SDS-PAGE standardized according to OD_{600}, followed by Western blotting using specific VirB antisera.

4.3 Results

4.3.1 Qualitative analysis of interactions between VirB8, VirB9, and VirB10

To initiate the *in vitro* analysis of interactions between VirB8, VirB9, and VirB10, the periplasmic portions of the *B. suis* proteins, known to comprise the main functional domains, were overproduced and purified. We used strep-tactin affinity chromatography to isolate the three VirB proteins from *E. coli* lysates, followed by additional size exclusion (VirB8, VirB8^{M102R}) or ion exchange (VirB9, VirB10) chromatography. SDS-PAGE analysis (Figure 4.1A) demonstrated that all of the VirB preparations were purified to homogeneity (>95%) and migrated at the anticipated molecular weights.

The purified strepII-tagged periplasmic domains of VirB proteins and BSA (negative control) were then coated to wells of NUNC microtitre plates to test for the binding of VirB8, VirB9 and VirB10 using ELISA based detection. We observed binding of VirB9 and VirB10 to immobilized VirB8, and of VirB9 to immobilized VirB10 (Figure 4.1B), with little or no non-specific binding of the VirB proteins to immobilized BSA under identical conditions. Due to cross-reactivity of the VirB8 antiserum towards VirB9 and VirB10, we could not conduct reciprocal experiments with VirB8 binding to immobilized VirB9 and VirB10. Our ELISA results are consistent with interactions previously reported in case of the homologous T4SS proteins from *A. tumefaciens* (Das & Xie, 2000; Ding et al., 2002; Paschos et al., 2006; D. Ward et al., 2002).

4.3.2 Conformational changes upon VirB8-VirB9-VirB10 complex formation

Next, to assess the formation of VirB protein complexes, CD spectroscopy measurements of strepII-tagged periplasmic domains of VirB8, VirB9, and VirB10 were

performed, measuring individual proteins and combinations. In comparison to the scans of individual proteins (Figure 4.2A-C), combining VirB8 and VirB9 led to a decrease in ellipticity of the spectrum as compared to the calculated addition of the VirB8 and VirB9 spectra (data not shown) suggesting that there is a conformational change upon interaction. In contrast, combining VirB8-VirB10 and VirB9-VirB10 led to an increase in ellipticity and this also indicates conformational changes (data not shown). These observations suggest that structural changes occur when VirB8, VirB9, and VirB10 interact in a pair wise fashion. When all three proteins were mixed and a wavelength scan was performed, we noticed a large increase in ellipticity, which is notably different from the theoretical sum of the spectra of the three individual proteins (Figure 4.2D). These findings indicate that upon interaction, conformational changes occur. It is difficult to assess the secondary structure content from the CD scans, and therefore programs from the CDpro collected were used to predict the secondary structure purely from CD scans and therefore programs from the CDpro were used to predict the secondary structures of VirB8, VirB9, and VirB10, as well as the VirB8-VirB9-VirB10 complex. VirB8 was predicted to have slightly higher percentage of beta strands (29.8%) than helices (22.2%) (Table 4.3), which is consistent with the X-ray structure (Bailey et al., 2006; Terradot et al., 2005). Most of VirB9 is predicted to be unordered (43.3%) and VirB10 is predicted to contain 41.3% beta strands (Table 4.3), which is consistent with the X-ray structure of the VirB10 homolog from *Helicobacter pylori* (ComB10) (Chandran et al., 2009; Terradot et al., 2005). Interestingly, the VirB8-VirB9-VirB10 mixture is predicted to contain more alpha helix content (49.9%) suggesting that upon

complex formation, there is a large increase in overall alpha helix content indicating that conformational changes occur (Table 4.3).

Subsequently, we used scanning CD measurements of the thermal stability of the VirB proteins individually and in combinations to assess whether complex formation impacts their stability. This approach is commonly used to analyze protein complexes of unknown structure (Greenfield & Fowler, 2002; Nanao et al., 2003; Quinaud et al., 2005). The unfolding of VirB helical content was monitored at 222 nm as in previous work (Greenfield & Fowler, 2002; Nanao et al., 2003; Quinaud et al., 2005). Our analysis showed that VirB8 unfolds in a co-operative manner (Figure 4.3A). In contrast, VirB9's ellipticity increased beginning at 35°C and the apparent α-helical content continued to increase with temperature. Finally, VirB10 unfolded in a non-cooperative manner with increasing temperature and apparently a low amount of helices was lost (Figure 4.3A). Next, proteins were analyzed in pair-wise combinations to determine whether there are conformational changes upon interaction. The analysis of VirB9-VirB10 did not yield interpretable results and therefore it was omitted from the analysis (data not shown). In the case of VirB8-VirB9 (Figure 4.3B), VirB8-VirB10 (Figure 4.3C), and VirB8-VirB9-VirB10 (Figure 4.3D), however, we observed clear transitions in their thermal denaturation curves. Therefore, the thermal denaturation studies indicate that upon interaction, conformational changes occur and were stabilized.

4.3.3 Quantitative analysis of interactions between VirB8, VirB9 and VirB10

To quantitatively characterize the interactions, we then analyzed the VirB protein interactions using label-free, real-time SPR. In a typical experiment, one protein is

immobilized to the sensor chip surface and the binding partner(s) is then flowed overtop in solution. Association and dissociation events are monitored by changes in molecular mass accumulation at the solid-liquid interface, commonly plotted as binding response (resonance units, RU) as a function of time (De Crescenzo, Boucher, Durocher, & Jolicoeur, 2008). For our analyses, purified strepII-tagged periplasmic domains of VirB8, VirB9 and VirB10 were immobilized to the sensor chips via amine group coupling. Dose-dependant binding of VirB8 to immobilized VirB8 was detected and this interaction was characterized by rapid association and rapid dissociation kinetics (Figure 4.4A). The micromolar VirB8-VirB8 affinity predicted by SPR (K_D = 26 +/- 5 μM) correlated well with our VirB8 self-association analysis (K_D = 116 +/- 7.5 μM) previously quantified using AUC (Paschos et al., 2006). While VirB8 binding to immobilized VirB9 and VirB10 surfaces yielded low signal responses (Figure 4.4A), reciprocal titrations of VirB9 and VirB10 binding to immobilized VirB8 (Figure 4.4B, 4.4C) showed mid-nanomolar affinities (K_D = 418 +/- 63 nM and K_D = 218 +/- 20 nM, respectively). Similarly, VirB9 and VirB10 binding to immobilized VirB9 (K_D = 374 +/- 63 nM and K_D = 216 +/- 32 nM, respectively) and to immobilized VirB10 (K_D = 443 +/- 59 nM and K_D = 236 +/- 38 nM, respectively) exhibited similar mid-nanomolar binding affinities (Figure 4.4B and Figure 4.4C). Regardless of the immobilized VirB surface, the micromolar affinity seen in case of the VirB8-VirB8 interaction (rapid-on/rapid-off kinetics; Figure 4.4A) were distinctly different from the nanomolar binding observed with VirB9 (fast-on/fast-off kinetics; Figure 4.4B) and VirB10 (fast-on/slow-off kinetics; Figure 4.4C & Table 4.4). VirB10 had the overall highest affinity for its interaction

partners followed by VirB9 and VirB8. These results demonstrate that the three VirB proteins have distinct binding properties (i.e. kinetics and affinities) that may be required for their biological functions. There was little or no non-specific binding of BSA to the immobilized SPR surfaces indicating that the VirB proteins only interact with specific binding partners (data not shown).

To further validate the specificity of our SPR results, we also characterized the binding of a VirB8 variant (M102R) previously shown to exhibit reduced dimerization by analytical gel filtration and AUC (Paschos et al., 2009; Paschos et al., 2006). VirB8 and VirB8^{M102R} were immobilized and then titrated over a higher concentration series (up to 50 mM) as interactions were expected to be weaker. Wild type VirB8 interacted strongly with itself, yielding a low micromolar K_D (23+/- 3 μM; Figure 4.5A) that correlated well with the earlier titration series (K_D = 26+/- 5 μM; Figure 4.4A). When VirB8 was titrated over VirB8^{M102R} (K_D > 1 mM; Figure 4.5B) or VirB8^{M102R} was titrated over itself (K_D > 1 mM; Figure 4.5C), very low binding responses were observed compared to the wild type VirB8-VirB8 interaction. These observations are consistent with the previous finding that VirB8^{M102R} is a dimer site variant and here validates the specificity of the binding interactions tested by SPR.

4.3.4 Ternary complex formation between VirB8, VirB9, and VirB10

We next performed multicomponent SPR analyses to test whether VirB8, VirB9 and VirB10 assemble into a ternary complex as predicted by current models of T4SS assembly. All three VirB proteins were injected in variable sequence over the immobilized VirB8 surface. For each series of injections, with intermittent salt washes to

remove loosely bound protein, successive increases in the binding responses demonstrated that stable complexes formed (Figure 4.6). When VirB8 was flowed over immobilized VirB8 followed by VirB9 and VirB10 (Figure 4.6A), the overall magnitude of complex formation (assessed by final level of response; i.e. ~120 RU) was similar to the experiment in which VirB9 was first flowed over VirB8 immobilized surface followed by VirB8 and VirB10 (Figure 4.6B). Similarly, when VirB10 was flowed over immobilized VirB8 followed by VirB9 and VirB8 (Figure 4.6C), the final magnitude of complex formation was unaltered; an additional experiment in which VirB8 was flowed over immobilized VirB8 followed by VirB10 and VirB9 was also unaltered (data not shown). Thus, ternary complexes formed independently of the order of injection over VirB8-immobilized surface suggesting that VirB8, VirB9, and VirB10 interact through distinct binding sites. Similar outcomes were observed using immobilized VirB9 and VirB10 surfaces (data not shown), further demonstrating that ternary complexes formed independently of the order of injection. The association and dissociation rates were independent of the order of VirB protein addition and were similar the rates observed upon formation of each respective binary complex (Figure 4.4). Overall, this data provides the first direct evidence that VirB8, VirB9, and VirB10 can form a ternary complex *in vitro*.

4.3.5 Bacterial two-hybrid assay detects dynamic associations between VirB8, VirB9, and VirB10

To complement the *in vitro* analyses with a more physiologically relevant assay, we applied the BTH system that is based on the reconstitution of the enzymatic activity

of AC by interacting proteins fused to its two domains. Full-length versions of VirB8 and VirB10 were expressed in *E. coli* as fusions to the cytoplasmic T18 and T25 domains of AC and their interaction was shown to restore cAMP production and ultimately ß-galactosidase activity as readout (Bourg et al., 2009). We here tested more complex interactions among core complex components. To this end, we generated bicistronic constructs that permitted the simultaneous expression of proteins not fused to the AC domains (Figure 4.7A). When VirB9 was co-expressed in the periplasm with VirB8 fused to the AC domains, we observed strongly increased ß-galactosidase activity (3.8 fold) indicating that VirB9 stimulated VirB8 self-association (Figure 4.7B). In contrast, the co-expression of VirB10 did not affect VirB8 self-association. The co-expression of VirB9 reduced the VirB8-VirB10 interaction to 15% of the control, and similarly, expression of VirB9 reduced the VirB10-VirB10 interaction to 38%. In contrast, expression of VirB10 further increased VirB10 self-association 1.5 fold (Figure 4.7B). These results show that VirB9 modulates the homomeric and heteromeric interactions between VirB8 and VirB10, which suggest a previously not assigned role for this protein in T4SS assembly. The reduced dimerization of the purified VirB8^{M102R} variant was shown by AUC and here by SPR. As expected, fusions of the VirB8^{M102R} variant to AC domains resulted in reduced in ß-galactosidase activity indicating reduced dimerization (Figure 4.7B). However, when this variant was tested in a bicistronic construct co-expressed with VirB9, an increase in ß-galactosidase activity was observed suggesting that binding to VirB9 is not negatively impacted by the change. Similarly, the BTH assay showed that the VirB8^{M102R} variant was not affected in its interaction with VirB10 (Figure 4.7B),

suggesting that this residue and dimerization are not important for VirB9 as well as for VirB10 binding.

In order to assess the levels of VirB8/VirB10 fusion proteins in the BTH101 strain, the cell lysates were separated by SDS-PAGE, followed by Western blotting using VirB-specific antisera. It was interesting to note that levels of VirB8 protein did not change when the β-galactosidase activity increased in the presence of VirB9 (Figure 4.7C). However, VirB8 was not detected in cells that served as negative control when the T18 catalytic fragment was expressed with T25-fused VirB8. In addition, the VirB8 protein level was lower when VirB9 was co-expressed in the presence of T25-fused VirB8 and T18-fused VirB10, and in this case the β-galactosidase activity was reduced (Figure 4.7C). A similar observation was made when VirB9 was expressed in presence of T25VirB10 and T18VirB10 (Figure 4.7C). In addition, the protein level was also reduced when the VirB8 dimer site variant ($VirB8^{M102R}$) was tested using the BTH system. Therefore, the levels of the hybrid proteins were reduced as consequence of reduced interactions, which may leave them more susceptible to degradation by periplasmic proteases. Overall, these results show that the BTH system is well suited to study the dynamic interactions between VirB proteins in a simplified system for T4SS assembly.

4.4 DISCUSSION

T4SS function depends on the formation of a complex between VirB proteins. To advance our understanding of how this machinery assembles, we characterized the interactions between the conserved core complex components VirB8, VirB9, and VirB10. The detection of VirB8-VirB9, VirB8-VirB10, and VirB9-VirB10 interactions by ELISA indicated that the *B. suis* proteins purified were functionally active and corroborated interaction data previously acquired using *A. tumefaciens* homologues.

To study the *B. suis* proteins in greater detail, we used CD spectroscopy to assess whether VirB interactions trigger conformational changes. Both far UV wavelength scans and thermal denaturation were previously utilized to analyze the structural changes that occur when proteins form complexes in solution (Greenfield & Fowler, 2002; Nanao et al., 2003). This approach demonstrated complex formation of three proteins (PscE, PscF, and PscG) involved in needle biogenesis of a type III secretion system (Quinaud et al., 2005). Using CD scans we demonstrated that structural changes occur when VirB8, VirB9, and VirB10 are mixed and this is indicative of dynamic interactions (Figure 4.2). Thermal scans showed that VirB8 unfolds in a co-operative fashion, whereas VirB9 and VirB10 alone are thermodynamically stable, as they did not exhibit a clear Tm. This case is comparable to the PscF needle-like protein that exhibited a curve in thermal scans similar to VirB10. The authors of this study proposed that PscF is present in a lower energetic state and that it aggregated into a structure that could not be changed by heat (Quinaud et al., 2005). However, in the presence of the interaction partners (PscE and PscG), PscF was recruited into complexes that were more stable, indicated by a thermal

denaturation curve of the PscE, PscG and PscF mixture that had a higher Tm than PscE and PscG. Similarly, we propose that VirB8 forms stable binary interactions with VirB9 and VirB10. This further supports the hypothesis that the interaction of VirB8 with VirB9 and VirB10 may lead to the recruitment of the proteins into polar T4SS assembly as proposed previously (Judd et al., 2005a). The action of VirB8 may prevent a biologically non-productive aggregation of VirB9 and VirB10.

To characterize the VirB8, VirB9 and VirB10 interactions in a quantitative fashion, we then utilized SPR. Signal responses for VirB8 flowing over immobilized VirB9 and VirB10 were weak, but VirB9 and VirB10 injected over immobilized VirB8 yielded dose-dependent, saturable binding responses. This effect may be due to the masking of key binding residues for VirB8 by the amine coupling of VirB9 and VirB10 to the sensor chip. In agreement with previous AUC data, the periplasmic VirB8-VirB8 interaction exhibited a micromolar binding affinity constant. The relatively weak VirB8 self-association and the fast-on and fast-off kinetics may be important for rapid dimer formation and dissociation. Physiologically, this suggests that VirB8 may rapidly mediate other VirB protein interactions required for T4SS assembly. In support of this hypothesis, VirB8 was postulated to be a nucleation factor for T4SS assembly (Judd et al., 2005a) and shown to interact with many other VirB proteins (Das & Xie, 2000; Höppner et al., 2005; Paschos et al., 2006; D. Ward et al., 2002; Yuan et al., 2005). Furthermore, rapid association and dissociation of the VirB8 dimers may be necessary for its interaction with other VirB proteins as T4SS assembly factor. Our work suggests that such an interaction occurs with VirB5 to facilitate pilus assembly ((Yuan et al., 2005);

Sivanesan *et al.* 2010, unpublished data). Interestingly, the other periplasmic VirB interaction pairs exhibited mid-nanomolar binding affinities suggesting that they may be primarily structural components. The higher-affinity interactions of VirB9 and VirB10, and the fast-on and slow-off kinetics of VirB10 interactions are in accord with the requirement of stabilizing the core complex once assembled. Next, similar to the FhuA-TonB-FhuD system (Carter DM, 2006), we adopted a multicomponent style of SPR analysis and demonstrated that VirB8, VirB9, and VirB10 form a ternary complex. The multicomponent SPR analysis builds upon recent cryo-EM and crystallographic studies in which VirB8 was not detected nor required for the formation of the VirB7-VirB9-VirB10 T4SS core complex (Chandran et al., 2009; Fronzes, Schafer et al., 2009). All the available data indicate that VirB8 is required for T4SS assembly and correct subcellular localization under natural conditions, but under conditions of artificial overexpression of the components for structural studies, it is apparently not essential. This is consistent with our finding that the affinity of VirB8 is relatively weak, suggesting that it acts in a transient fashion as assembly factor that may only be loosely associated with the final T4SS core complex *in vivo*. VirB8 was cross-linked to the translocated T-DNA substrate in *Agrobacterium*, but this merely indicates its localization and does not necessarily imply that it is an active component of the translocation machinery; the available data are consistent with a primary role as protein assembly factor.

As the final approach to examine the dynamic nature of interactions between *B. suis* VirB8, VirB9, and VirB10, we utilized the BTH system *in vivo*. This assay permits the analysis of full-length proteins in their natural environment, the periplasm of a gram-

negative cell. This experimental approach was previously applied to characterize the VirB8-VirB10 interaction (Bourg et al., 2009; de Paz et al., 2005), VirB8 self-association (Bourg et al., 2009), and VirB8 dimer variants (Paschos et al., 2009). The use of bicistronic constructs demonstrated that VirB9 stabilizes VirB8 dimers, but that VirB10 had no impact on the dimerization of VirB8. This was further supported by the VirB8^{M102R} dimer variant, which was stabilized by VirB9 and this variant was not affected in interaction with VirB10. Therefore, it is reasonable to hypothesize that VirB8 dimers interact with VirB9 and with VirB10 dimers to target these proteins to poles of the bacterial cells. In addition, VirB9 stabilized VirB8 dimers but dissociated VirB8-VirB10 and VirB10-VirB10 dimers, which suggests an important regulatory function for VirB9 in T4SS core complex assembly. It is possible that the affinity between VirB9 and VirB10 *in vivo* is stronger than VirB8-VirB10 and VirB8-VirB9, leading to dissociation of VirB8-VirB10 and VirB8-VirB9 heterodimers. The SPR results, however, did not detect large differences of the affinities between VirB8-VirB9, VirB8-VirB10, VirB9-VirB10 and VirB10-VirB10 complexes, but VirB10 was generally the strongest binding partner. It is possible that the periplasmic-only domains of VirB8 and VirB10 utilized in the *in vitro* SPR experiments do not completely mimic the full-length proteins in the *in vivo* BTH experiments that may adopt alternative conformations in the periplasm. Future studies are also needed to examine whether the transmembrane domains may influence the overall binding affinities.

Several lines of evidence support our proposed model of T4SS core complex assembly. First, VirB8 self-associates as identified in this study and as previously

reported, it exists in a monomer-dimer equilibrium (Paschos et al., 2006). VirB9 localizes in the periplasm, interacts with VirB7 (Baron et al., 1997; Bayliss et al., 2007; Das et al., 1997), and VirB9 and VirB10 form homo-multimers. This step is followed by VirB8 dimer interaction with VirB9 and VirB10 to mediate their co-localization (Judd et al., 2005a) (Figure 4.7B). VirB9 stabilizes VirB8 self-association and the nucleation by VirB8 facilitates the VirB9-VirB10 interaction and presumably the formation of the functional complex observed by cryo-EM and crystallography (Chandran et al., 2009; Fronzes, Schafer et al., 2009). This model is further supported by additional results of the BTH assay, namely the fact that VirB10 stimulates VirB10-VirB10 interaction, a process that could represent unproductive aggregation. VirB9 reduced this interaction as well as the VirB8-VirB10 interaction and this may explain why VirB8 was not co-crystallized with the VirB7-VirB9-VirB10 complex (Chandran et al., 2009; Fronzes, Schafer et al., 2009). This model is also supported by the results of CD spectroscopy experiments that demonstrated that mixtures of VirB proteins (VirB8-VirB9, VirB8-VirB10 and VirB8-VirB9-VirB10) were more stable than the individual proteins. Moreover, accumulation of VirB9 was previously suggested to cause conformational changes of VirB10 and may thereby interfere with VirB10 self-association (Banta, Bohne, Lovejoy, & Dostal, 1998; Beaupré et al., 1997; Zhou & Christie, 1997). Furthermore, an in-frame deletion of the *virB9* gene reduced the stability of VirB4, VirB8, VirB10 and VirB11 in *A. tumefaciens* cells indicating a role of VirB9 in stabilization of VirB8 and of VirB10 (Berger & Christie, 1994). We propose that VirB8 acts as an assembly factor to bring VirB9 and VirB10 to the poles of the bacteria. As next step, VirB9, an intermediate in the complex

as shown by its fast-on/fast-off kinetics interacts with VirB10, inducing conformational changes that reduce unproductive aggregation and dissociate VirB10 from VirB8. VirB10 displays fast-on and slow-off kinetics and the highest binding affinities, which suggests that the VirB10 interaction with VirB9 occurs later in the sequence of interactions. In contrast, VirB8 interactions (fast-on/fast-off) with VirB9 and VirB10 suggest a transient role as a scaffolding protein in T4SS assembly that may only be loosely attached to the final complex (Chandran et al., 2009; Fronzes, Schafer et al., 2009).

In summary, the results presented here validate previously described VirB8, VirB9, and VirB10 interactions, but they also provide novel quantitative (i.e. real-time binding kinetics and affinity), structural (i.e. ternary complex formation), *in vivo* (i.e. BTH assay), and dynamic (i.e. proposed assembly model) insights into T4SS core complex assembly. Future work will identify the VirB protein domains and residues that are specifically required for complex formation. Importantly, following the approaches developed here, other VirB proteins could be added to determine their influence on VirB8-VirB9-VirB10 complex formation. For instance, the effects of VirB7 on VirB8-VirB9-VirB10 interactions will be tested in future. VirB7 stabilizes VirB9 and interacts via a covalent bond in *A. tumefaciens* T4SS (Baron et al., 1997; Fernandez, Dang et al., 1996; Fernandez, Spudich et al., 1996), and its interaction with VirB9 may influence VirB9 interaction with VirB8 and VirB10. The influence of the cytoplasmic and transmembrane domains of VirB8 and VirB10 proteins on binding affinities should also be assessed using purified full-length proteins. Overall, the present study builds upon

previous literature and proposes a defined sequence of binding interactions that ultimately leads to the assembly of the core T4SS complex. The proposed model will help to define potential targets for the development of new antimicrobials.

Table 4.1. Bacterial strains and plasmids used.

Strains	Genotype or description	Source or reference
E. coli JM109	*endA1 gyr96 thi hsdR71 supE44 recA1 relA1* (*Δlac-proAB*) (F' *traD36 proAB*$^{+}$ *lacI*^{q} *lacZ*ΔM15)	(Yanisch-Perron et al., 1985)
E. coli BTH101	F^{-} *cya-99, araD139, galE15, galK16, rpsL1 (Str*^{r}*), hsdR2, mcrA1, mcrB1*	(G. Karimova et al., 2000)
E. coli BL21star (DE3)	F^{-} *ompT hsdS*$_{B}$ (*r*$_{B}^{-}$ *m*$_{B}^{-}$) *gal dcm rne131* (λDE3)	Invitrogen
Plasmids		
pT7-7StrepIIVirB8sp	pT7-7StrepII carrying 492 bp *Acc65*I/*Pst*I *virB8* fragment from *B. suis* (encoding 163 amino acid periplasmic domain)	(Terradot et al., 2005)
pT7-7StrepIIVirB8sp^{M102R}	pT7-7StrepII carrying 492 bp *Acc65*I/*Pst*I *virB8* fragment from *B. suis* (encoding 163 amino acid periplasmic domain) with an amino acid chage at 102 position from M->R	(Paschos et al., 2006)
pT7-7StrepIIVirB9sp	pT7-7StrepII carrying 813 bp *Acc65*I/*Pst*I *virB9* fragment from *B. suis* (encoding 271 amino acid periplasmic domain)	(Yuan et al., 2005)
pT7-7StrepIIVirB10sp	pT7-7StrepII carrying 1020 bp *Acc*65I/*Pst*I *virB10* fragment from *B. suis* (encoding 339 amino acid periplasmic domain)	(Yuan et al., 2005)
pKT25	kan^{r}, pSU40 derivative encodes T25 fragment (amino acids 1-224 of CyaA)	(G. Karimova et al., 2000)
pUT18C	car^{r}, pUC19 derivative encodes T18 fragment (amino acids 225-399 of CyaA)	(G. Karimova et al., 2000)
pUT18CB8	car^{r} , pUT18C harboring 720 bp *Xba*I/*Kpn*I *virB8* fragment from *B. suis* (encoding full-length VirB8)	(Paschos et al., 2009), chapter 3
pUT18CB8^{M102R}	car^{r} , pUT18CB8 harboring 720 bp *Xba*I/*Kpn*I *virB8* fragment determining an amino acid change in VirB8 (M102-> R)	(139), chapter 3
pKT25B8	kan^{r}, pKT25 harboring 720 bp *Xba*I/*Kpn*I *virB8* fragment from *B. suis* (encoding full-length VirB8)	(Paschos et al., 2009), chapter 3

pKT25B8^{M102R}	kan^r , pKT25B8 harboring 720 bp *XbaI/KpnI virB8* fragment determining an amino acid change in VirB8 (M102-> R)	(139), chapter 3
pUT18CB8HIN	car^r, pUT18CB8 in which a silent mutation eliminated the *Hind*III site in the *cyaA* gene fragment	this work
pUT18CB8+SD	car^r, pUT18CB8 carrying a Shine Dalgarno sequence downstream of *virB8*	this work
pKT25B10	kan^r, pKT25 harboring 1176 bp *XbaI/KpnI virB10* fragment from *B. suis* (encoding full-length VirB10)	(Paschos et al., 2009)
pUT18CB10	car^r, pUT18C harboring 1176 bp *XbaI/KpnI virB10* fragment from *B. suis* (encoding full-length VirB10)	(Paschos et al., 2009)
pUT18CB8+B9	car^r, pUT18CB8+SD harboring 870 bp *NcoI/Hind*III *virB9* fragment from *B. suis* (encoding full-length VirB9)	this work
pUT18CB8^{M102R}+B9	car^r, pUT18CB8+B9 harboring 720 bp *XbaI/KpnI virB8* fragment determining an amino acid change in VirB8 (M102-> R)	this work
pUT18CB8+B10	car^r, pUT18CB8+SD harboring 1176 bp *NcoI/Hind*III *virB10* fragment from *B. suis* (encoding full-length VirB10)	this work
pUT18CB10+B9	car^r, pUT18CB10+SD harboring 870 bp *NcoI/Hind*III *virB9* fragment from *B. suis* (encoding full-length VirB9)	this work
pUT18CB10+B10	car^r, pUT18CB10+SD harboring 1176bp *NcoI/Hind*III *virB10* fragment from *B. suis* (encoding full-length VirB10)	this work

Table 4.2. Oligonucleotide sequences.

Name	Sequence	Constructed plasmid
Inverse PCR primers		
5HIN	5'-ACGCCATCCGTAGCCGCCAGCGAGGCCACGG GCGGCCTG-3'	pUT18CB8HIN
3HIN	5'-CGTGGCCTCGCTGGCGGCTACGGATGGCGTA ATCATGGT-3'	
5' phosphorylated oligonucleotides		
5LNH	5'-CGAAGGAGATATATATCCATGGCCCGGGAAG CTTGAGCTCG-3'	pUT18CB8+SD
3LNH	5'-AATTCGAGCTCAAGCTTCCCGGGCCATGGATA TATATCTCCTTCGGTAC-3'	
PCR primers		
5BB9	5'-CATGCCATGGCAAAAAGATTCCTGCTTGCGTG C-3'	pUT18CB8+B9/ pUT18CB10+B9
3BB9	5'-CCCAAGCTTTCATTGCAGGTTCTCCCCGGGCG A-3'	
5BB10	5'CATGCCATGGCAACACAGGAAAACATTCCGGT	pUT18CB8+B10/

	GCAG-3'	pUT18CB10+B10
3BB10	5'-CCCAAGCTTTCACTTCGGTTGGACATCATACA C-3'	

* The underlined sequence represents the restriction site of the enzyme used for cloning.

Table 4.3. Predicted secondary structure of VirB8, VirB9, VirB10, and VirB8-VirB9-VirB10 from CD scans were calculated using SELCON and CONTINILL programs from the CDpro software package.

	% helix	% beta strand	% turn	% unordered
VirB8	22.2	29.8	19.8	28.2
VirB9	11.9	18.7	27.7	43.3
VirB10	5.8	41.3	18.7	29.4
VirB8+VirB9+VirB10	49.9	1.2	16.8	32.0

Table 4.4. Apparent equilibrium dissociation constants determined for VirB protein interactions.

Equilibrium SPR Analysis	K_D
VirB8 -> VirB8	26 +/- 5 μM
VirB8 -> VirB9	> 84 μM
VirB8 -> VirB10	> 84 μM
VirB9 -> VirB8	418 +/- 63 nM
VirB9 -> VirB9	374 +/- 63 nM
VirB9 -> VirB10	443 +/- 59 nM
VirB10 -> VirB8	218 +/- 20 nM
VirB10 -> VirB9	216 +/- 32 nM
VirB10 -> VirB10	236 +/- 38 nM
$VirB8^{M102R}$ -> VirB8	> 1 mM
$VirB8^{M102R}$ -> $VirB8^{M102R}$	> 1 mM

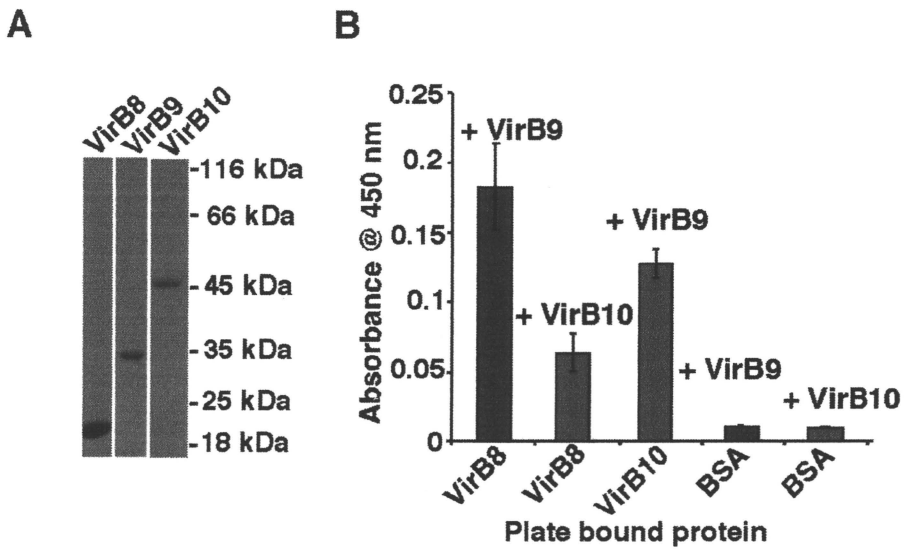

Figure 4.1. Qualitative analysis of VirB protein interactions using antibody-based ELISA. A, Representative SDS-PAGE (10% polyacrylamide) of soluble, periplasmic forms of strepIIVirB8, strepIIVirB9, and strepIIVirB10 purified to apparent homogeneity, similar for VirB8^{M102R} (not shown). B, ELISA results depicting the binding of 50 pmol of VirB proteins (VirB9 or VirB10) to immobilized partners (VirB8, VirB10, or BSA), as detected using VirB protein-specific antisera, followed by secondary HRP-conjugated goat anti rabbit IgG. Colour development was measured after addition of chromogenic solution containing HRP substrate, followed by addition of sulphuric acid to stop the reaction and measurement of absorbance at 450 nm. The results from three independent experiments are shown and bars represent the standard deviation.

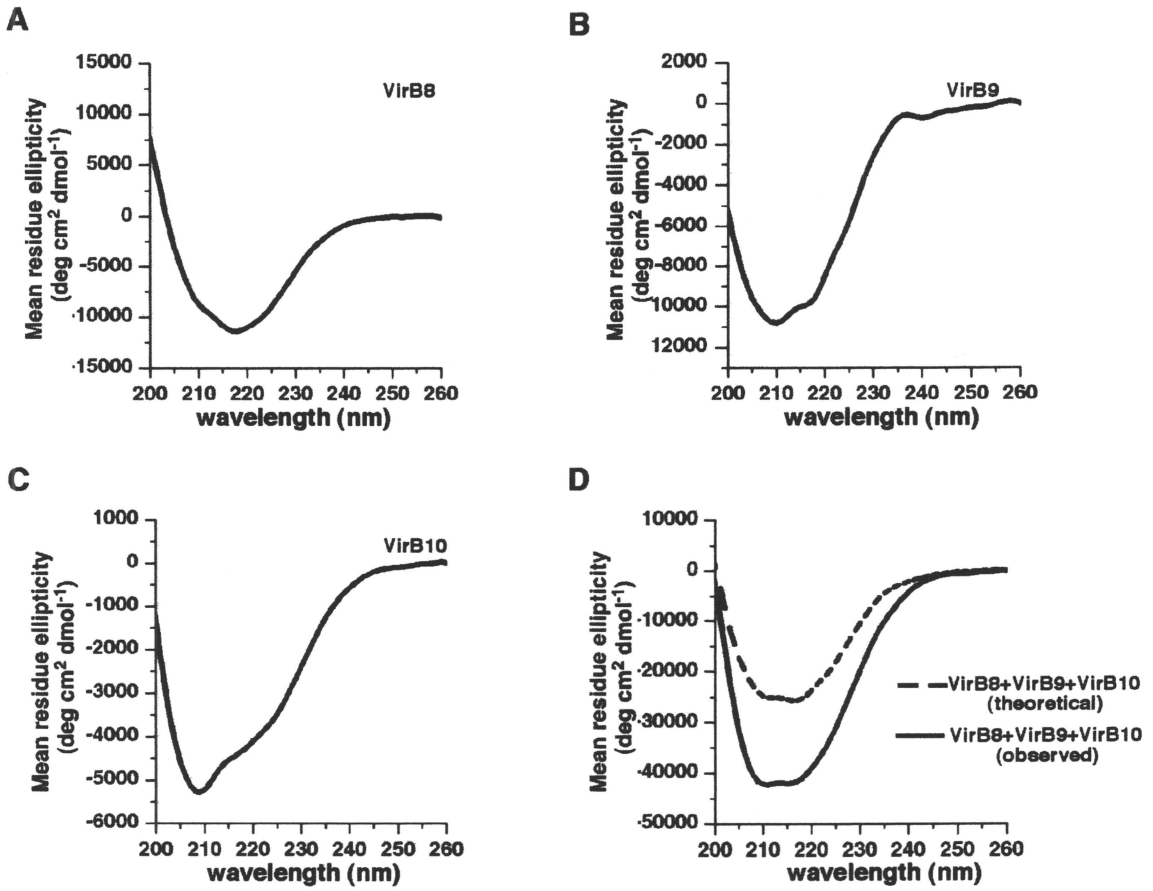

Figure 4.2. Analysis of interactions between VirB proteins using far UV circular dichroism. Characterization of the structures of purified periplasmic domains of VirB8, VirB9 and VirB10 alone and in mixtures by CD spectroscopy. Spectra for 1,250 pmol VirB8 (A), VirB9 (B), and VirB10 (C) respectively, were acquired alone and in combinations at 25°C. D, The solid black line represents the result obtained after analysis of an equimolar mixture of VirB8, VirB9, and VirB10, whereas the dashed line represents the theoretical result representing the addition of the spectra of the three individual proteins.

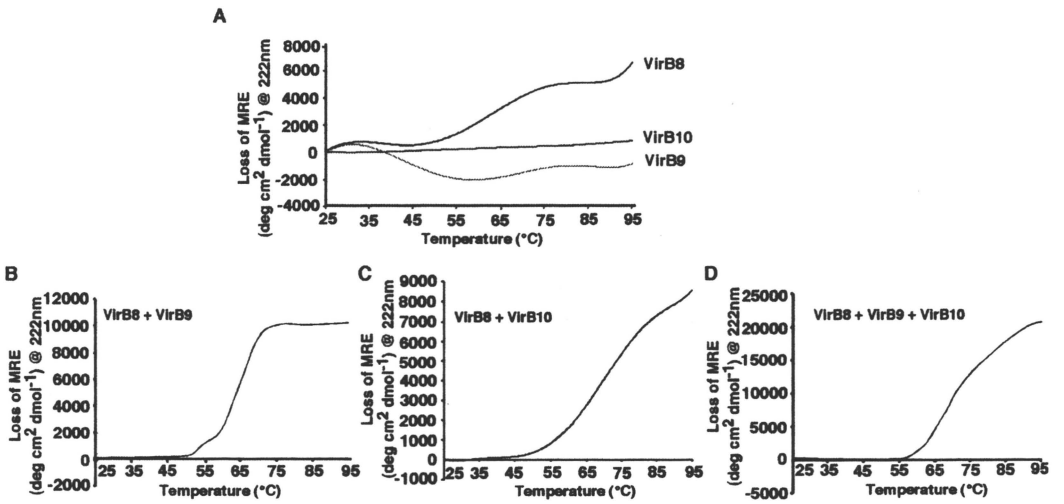

Figure 4.3. Stability of VirB proteins and complexes assessed by thermal denaturation and CD spectroscopy. A, Analysis of change in mean residue ellipticity (MRE) at 222 nm of VirB8, VirB9, and VirB10 as function of temperature (25°C to 95°C). B, Change in MRE at 222 nm of equimolar mixture (1,250 pmol) of VirB8 and VirB9 as a function of temperature. C, Analysis of equimolar mixture of VirB8 and VirB10. D, Analysis of equimolar mixture of VirB8, VirB9, and VirB10.

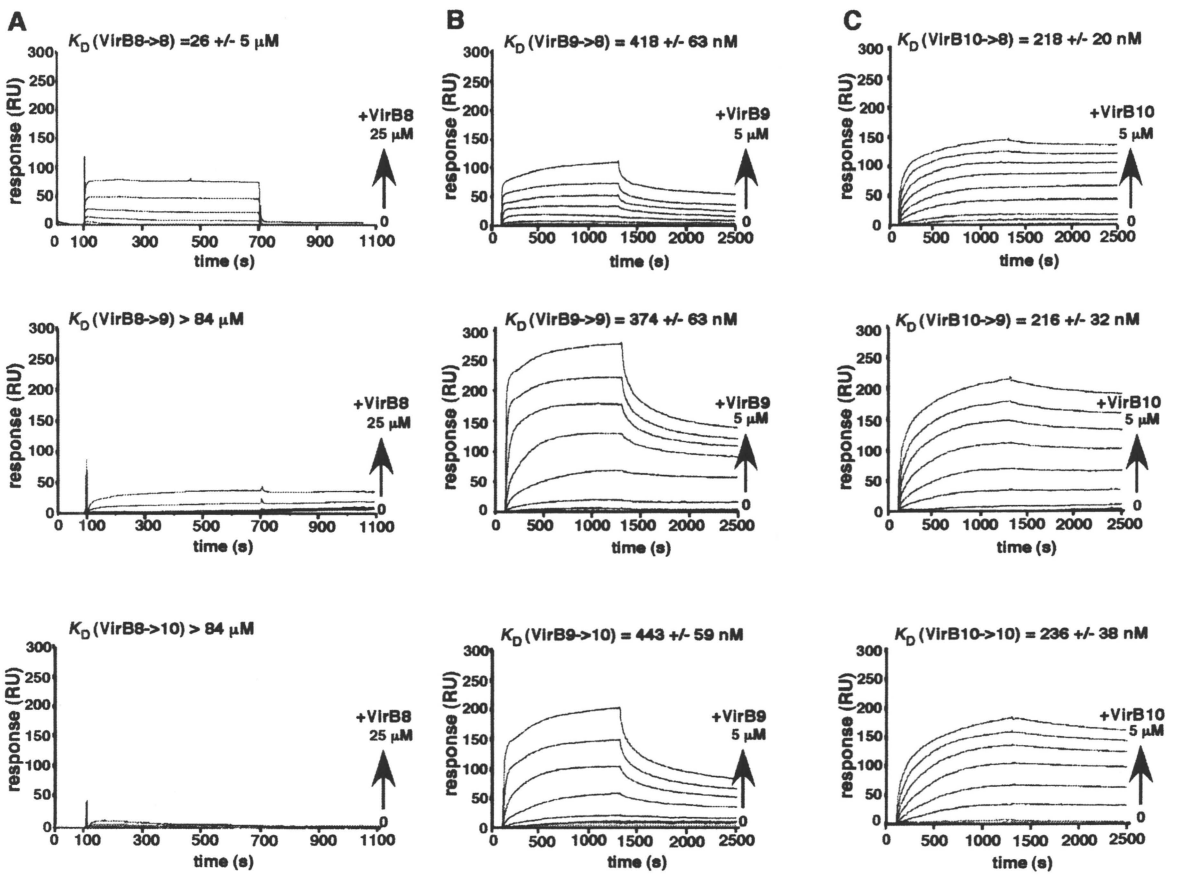

Figure 4.4. Quantitative analysis of VirB protein interactions using label-free, real-time SPR. Purified periplasmic VirB domains were amine coupled to CM4 sensor chips to final surface densities of 900 RU each. A, VirB8 was flowed over VirB8, VirB9 and VirB10 immobilized surfaces; B, VirB9 was flowed over VirB8, VirB9 and VirB10 immobilized surfaces; C, VirB10 was flowed over VirB8, VirB9 and VirB10 immobilized surfaces. Each VirB protein was titrated using a 2-fold dilution series and the binding was monitored as a function of RU over time (sec): VirB8, 0 – 25 μM, 10 min association + 10 min dissociation; VirB9, 0 – 5 μM, 20 min association + 20 min dissociation; VirB10, 0 – 5 μM, 20 min association + 20 min dissociation. Apparent equilibrium dissociation constants (K_D) were determined by plotting steady-state binding responses (Req) as a function of VirB concentration (C); resultant binding isotherms were fitted to a "steady-state affinity" model using BIAevaluation software (v4.1). The results represent the average of three experiments +/- standard error.

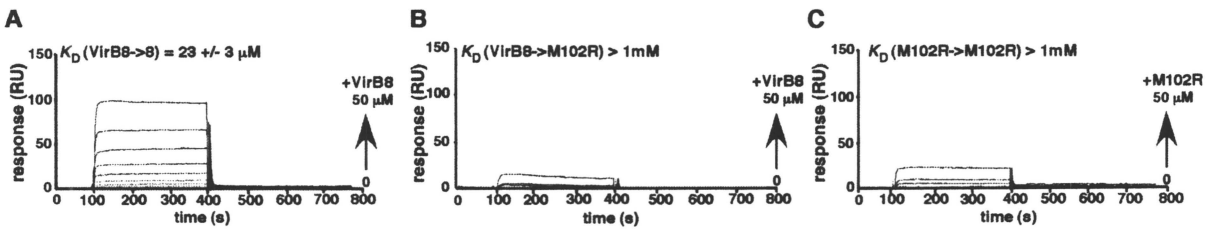

Figure 4.5. Quantitative analysis of VirB8^{M102R} self-association using label-free, real-time SPR. Purified periplasmic VirB domains were amine coupled to CM4 sensor chips to final surface densities of 900 RU each. A, VirB8 was flowed over VirB8 immobilized surface; B, VirB8^{M102R} was flowed over VirB8 immobilized surface; C, VirB8^{M102R} was flowed over VirB8^{M102R} immobilized surface. VirB8 and VirB8^{M102R} protein were titrated using a 2-fold dilution series and the binding was monitored as a function of RU over time (sec): 0 – 50 μM, 10 min association + 10 min dissociation. Apparent equilibrium dissociation constants (K_D) were determined by plotting steady-state binding responses (Req) as a function of VirB concentration (C); resultant binding isotherms were fitted to a "steady-state affinity" model using BIAevaluation software (v4.1). The results represent the average of three experiments +/- standard error.

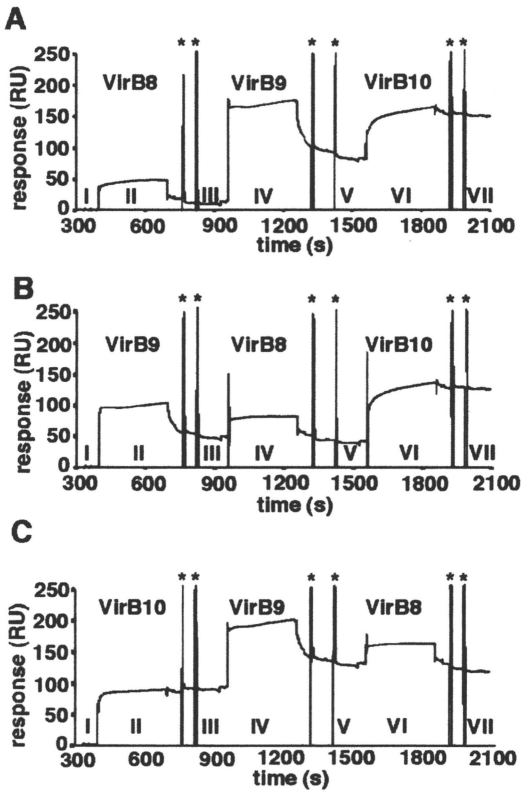

Figure 4.6. Observation of ternary complex formation between VirB proteins using multicomponent SPR. Purified periplasmic domains of VirB8, VirB9, or VirB10 (5 μM each, different injection orders) were flowed over ~900 RU, amine-coupled VirB8 surface: I, starting baseline; II, injection of first protein; III, stable complex after two 0.5 M NaCl pulses to elute loosely bound proteins indicated by stars; IV, inject second protein; V, stable complex after two 0.5 M NaCl pulses to elute loosely bound proteins indicated by stars; VI, inject third protein; VII, stable complex after 0.5 M NaCl pulses indicated by stars to elute loosely bound proteins and assess the final stable complex. A, Binding responses beginning with VirB8 injection followed by VirB9 and VirB10 injections. B, Binding responses beginning with VirB9 injection followed by VirB8 and VirB10 injections. C, Binding responses beginning with VirB10 injection followed by VirB9 and VirB8 injections.

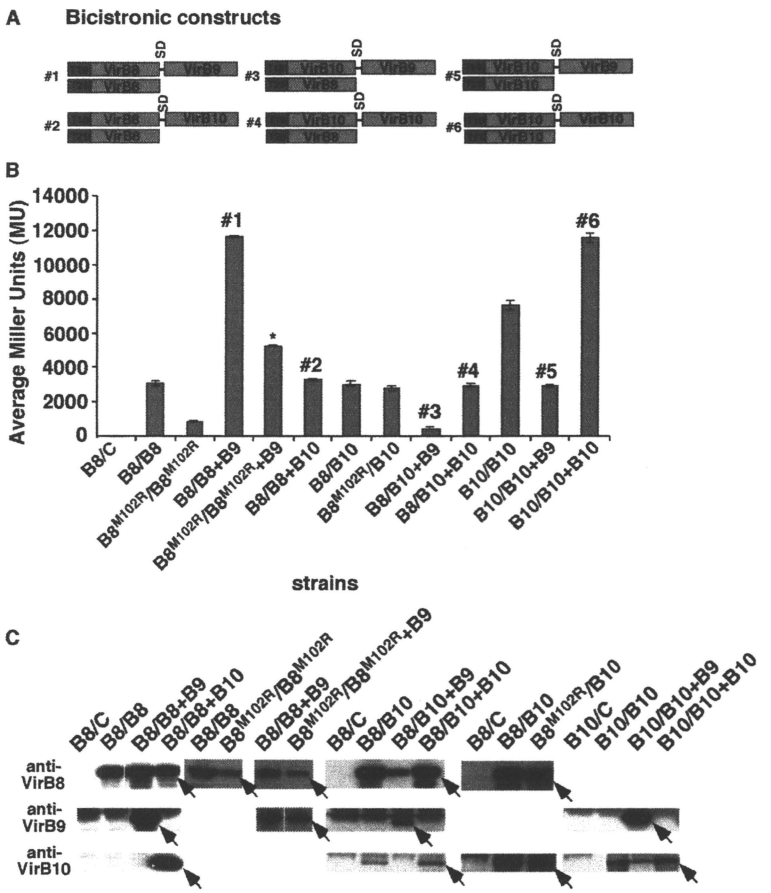

Figure 4.7. *In vivo* analysis of VirB protein interactions using the bacterial two-hybrid assay. As simplified model system to study T4SS core complex interactions, VirB8, VirB8^{M102R} and VirB10 were fused to the T18 and T25 domains of adenylate cyclase (AC) and we determined and the impacts of co-expression of a third protein produced in the periplasm. **A**. Schematic view of the bicistronic constructs generated to test the effects of a third VirB protein on pair wise interactions, T18 and T25 designate the two domains of AC and SD, the Shine Dalgarno sequence. **B**. Quantification of VirB interactions in *E. coli* strain BTH101 carrying plasmids encoding T18 and T25 fusions to VirB8/VirB10 and bicistronic constructs. Error bars represent the standard deviation of three independent measurements. C = negative control plasmid expressing T18 fragment not fused to a protein. The numbers above the bars correspond to the strains carrying the constructs represented schematically in A. * denotes the bicistronic construct in which variant VirB8^{M102R} is co-expressed with VirB9. **C**. Western blot detection of VirB8, VirB8^{M102R}, VirB9 and VirB10 protein levels using specific VirB antisera from *E. coli* strain BTH101 carrying the plasmids encoding T18 and T25 fusions to VirB8/VirB10 and bicistronic constructs as analyzed in B. Arrows indicate the VirB proteins identified with the VirB-specific antisera.

CHAPTER FIVE: Current progress on the identification of residues important for VirB8-VirB9, VirB8-VirB10 and other VirB8 interaction partners.

Preface:

The work in this chapter involves identification of residues in VirB8 that are important for interaction with VirB9 and VirB10. Figure 5.1 was contributed towards the publication entitled 'Dimerization and interactions of *Brucella suis* VirB8 with VirB4 and VirB10 are required for biological activity' in PNAS (Paschos *et al.* 2006). The phage display experiments were performed in Dr. James Coulton's lab (McGill University) in joint collaboration with Dr. Christian Baron. I performed the phage display experiments using the (constrained) Ph.D.-C7C phage library for both periplasmic domain of VirB8 from *B. suis*. Eruno Cheung, a student in Dr. James Coulton's lab performed the phage display experiments using the Ph.D.-12 phage library for periplasmic domain of VirB8 of *B. suis*. I purified the wild type VirB8 proteins; whereas the VirB8 variants of *B. suis* were purified by Dr. Athanasios Paschos (McMaster University).

CHAPTER FIVE: Current progress on the identification of residues important for VirB8-VirB9, VirB8-VirB10 and other VirB8 interaction partners.

Abstract

Type IV secretion systems (T4SS) are multicomponent complexes that span the inner and outer membrane to facilitate transport of effectors to host cells. Ternary complex formation between VirB8, VirB9 and VirB10 was identified recently. In this chapter, the VirB protein domains and residues that are required for interaction with VirB8 were elucidated using various *in vitro* and *in vivo* experiments. A cross-linking assay between VirB10 and VirB8 variants revealed that residue T201 of VirB8 is important for interaction with VirB10. Bacterial two-hybrid assays confirmed that VirB8^{M102}, VirB8^{Y105}, and VirB8^{E214} are involved in dimerization. Finally, phage display experiments using the VirB8 periplasmic domain from *B. suis* selected peptides from the Ph.D.-C7C phage display library and Ph.D.-12 phage display library aligned to the C-terminus of VirB6, the N-terminus of VirB9 and of VirB10. In addition, phage display experiments with the VirB8 periplasmic domain selected peptides aligned with the globular domain of VirB5. The information identified here could be used to probe the dynamics of VirB interactions and of T4SS assembly.

5.1 Introduction

The architecture of Type IV secretion systems (T4SSs) is slowly coming into light. T4SSs are composed of up to 12 VirB proteins depending on the organism and they are divided into three groups of proteins. The first group comprises the NTPases (VirD4, VirB4 and VirB11) that energize the assembly and substrate transfer; the second group comprises the core complex components (VirB1, VirB3, VirB6, VirB7, VirB8, VirB9 and VirB10) that span the inner-membrane and the outer-membrane. The third group, the extracellular components (VirB2 and VirB5), mediates attachment to and/or provides a channel for substrate transfer into host cells (Alvarez-Martinez & Christie, 2009; Baron, 2005; P.J. Christie et al., 2005).

Structural insights of the VirB proteins have suggested potential roles for the T4SS (Fronzes, Christie et al., 2009). In addition, recent structural characterization of the outer-membrane core complex composed of fragments of VirB7-VirB9-VirB10 homologues from the conjugative plasmid pKM101 provided novel information (Chandran et al., 2009). The outer-membrane complex is 590 kDa large consisting of 14 copies of each of the three proteins. VirB7 (TraN) full length binds to VirB9 (TraO) and the C-terminal domain of VirB9 binds to the C-terminus of VirB10 (TraF) (Figure 1.3). The researchers attempted to crystallize the complex in the presence of VirB8, however, VirB8 failed to co-localize with the VirB7-VirB9-VirB10 complex. This result is surprising since VirB8 is known to interact with VirB9 and VirB10 ((Das & Xie, 2000; Paschos et al., 2006), Chapter 4). Moreover, VirB8 is found to functionally interact with VirB6 to transfer the T-DNA substrate to VirB9/VirB2 (Cascales & Christie, 2004b).

Therefore, it is possible that VirB8/VirB6/VirB9/VirB10 are components of the inner-membrane attached core complex.

The molecular resolution of the outer-membrane core complex (VirB7-VirB9-VirB10) structure is excellent; but questions remain unanswered regarding the inner-membrane core complex. Recently, a ternary complex between VirB8-VirB9-VirB10 was identified using surface plasmon resonance and circular dichroism (Chapter 4). In addition, experiments with the bacterial two-hybrid assay demonstrated that VirB9 stimulates the self-association of VirB8, and VirB9 modulates negatively the VirB8-VirB10 and VirB10-VirB10 interactions. Based on these data, a dynamic model for a inner-membrane core complex assembly was proposed in which VirB8 acts as a scaffolding protein interacting with VirB9 and VirB10 to bring both proteins to the poles of the bacteria, but VirB8 may not remain tightly associated with VirB9 and VirB10 (Chapter 4).

The work described in the current chapter comprises follow up work on chapter 4 and the structure function analysis of VirB8 (Paschos et al., 2006). Here, the VirB protein domains and residues that is specifically required for complex formation between VirB8-VirB9-VirB10 is examined. Using this information, we can probe for the effects of the interactions on T4SS assembly and function. Moreover, information on these sites could be used to identify targets for antimicrobials.

5.2 Materials and Methods

5.2.1 Growth of bacterial strains

The strains used in this study are as follows: *E. coli* strain BL21 (DE3) star for protein overexpression, *E. coli* JM109 for cloning experiments, and *E. coli* ER2738 for phage display. With the exception of *E. coli* ER2738 the other two strains are described in Chapter 4 (Table 4.1). The ER2738 strain is grown in LB (1% tryptone, 0.5% yeast extract, 0.5% NaCl) in the presence of tetracycline at 20 μg/mL. Propagation of the plasmids used in this study is identical to the description in Chapter 4 (4.2.1).

5.2.2 Plasmid construction

Plasmids constructed for the bacterial two-hybrid assay are listed in Table 5.1. The VirB8 variants were PCR amplified using the primers (5B8, 5' CTAGTCTAGACGGGATGTTTGGACGCAAACAATCTCCA) and (3B8, 5' CGGGGTACCTCATTGCACCACTCCCATTTCTGG) and subcloned into pKT25 and pUT18C. The pUT18CB8 variants were then used to subclone *virB9* downstream of the *virB8* gene using the pUT18CB8+B9 construct.

5.2.3 Protein purification

StrepIIVirB8sp, StrepIIVirB9sp and StrepIIVirB10sp were purified as described in Chapter 4 (4.2.2).

5.2.4 Cross-linking assay

The ability of StrepIIVirB8sp and variants to interact with StrepIIVirB10sp was assessed by chemical cross-linking (disuccinimidyl suberate) identical to the description in

Chapter 2.2.6 where similarly the ability of StrepIIVirB5 variants to interact with StrepIIVirB8sp was analyzed.

5.2.5 Bacterial two-hybrid assay

To analyze the effects of VirB8s changes on self-association and the influence on VirB9 on this activity, the bacterial two-hybrid system was utilized. The procedure used here is identical to what is described previously in Chapter 4.2.6.

5.2.6 Phage display experiments

The phage display experiments were performed as described elsewhere (Carter DM, 2006). Briefly, a total volume of 150 μL of purified VirB8sp and VirB8ap diluted to (100 μg/mL) diluted in 0.1 M $NaHCO_3$, pH 8.6 was coated onto polystyrene microtitre plates and incubated overnight at 4°C. Next day, the coated wells were blocked for 2 h at 37°C with 5 mg/mL BSA in 0.1 M $NaHCO_3$, pH 8.6 plus 0.02% NaN_3. The wells were washed with TBS-T (50 mM Tris-HCl, pH 7.5; 150 mM NaCl; Tween-20) six times. Ph.D.-12 or Ph.D-C7C phage libraries at a stock of $4X10^{10}$ plaque forming unit (pfu) were added to the wells and incubated at room temperature (RT) for 1 h, followed by washing with TBS-T ten times. The bound phages were eluted using 0.2 M glycine (pH 2.2) incubating for 10 min at RT. The eluted phages were amplified using the ER2738 *E. coli* strain and used in the second panning with freshly coated protein. Three rounds of panning were performed and Tween-20 concentrations of 0.1%, 0.3%, and 0.5% were used for the 1st, 2nd and 3rd panning, respectively. Individual plaques were picked from the second and third panning, inoculated together with ER2738 *E. coli* strain and incubated at 37 °C for 2-3 h. The supernatant containing the phage was harvested and

subjected to ssDNA isolation using the M13 DNA purification kit (Qiagen) according to the manufacturer's description. The ssDNA was then used as a template in PCR with specific primers for phage DNA to amplify the DNA sequence corresponding to the peptide displayed on the pIII coat. The PCR products were then purified using the MiniElute PCR purification kit (Qiagen) according to the manufacturer's description and sequenced at the IRIC sequencing facility (University of Montréal).

The unique peptide sequences obtained from the sequencing results were aligned to VirB8 interacting proteins such as VirB1, VirB3, VirB4, VirB5, VirB6, VirB8, VirB9, VirB10 and VirB11 using the Receptor Ligand Contacts (RELIC) MATCH program (http://relic.bio.anl.gov). The RELIC MATCH program evaluates the affinity-selected peptides for peptide similarities to target sequences using pair-wise similarity matrix. The sites of interaction between the immobilized target antigen (VirB8sp) and the candidate partner sequence will be identified by alignment of clusters of peptides to the target sequence.

5.3 Results

5.3.1 Residue T201 of VirB8 is important for the interaction with VirB10

To identify the VirB8 residues involved in interaction with VirB9 and VirB10, StrepIIVirB8sp, StrepIIVirB8sp variants, StrepIIVirB9sp and StrepIIVirB10sp were purified. The purified VirB8sp wt and variants were mixed either with VirB9sp or VirB10sp in the absence and presence of 0.1 mM DSS (disuccinimidyl suberate). Reproducible differences to the wild type were not observed when VirB8sp variants were cross-linked to VirB9 (data not shown). A signal corresponding to the wild type VirB8-VirB9 complex was observed in all variants suggesting that the residues changed in VirB8 that were tested in this experiment are not involved in the interaction with VirB9. Alternatively, the changes made may not be sufficient to lead to differences from the wild type VirB8 protein using cross-linking as a method. However, when the various VirB8 variants were mixed with VirB10sp protein in the presence and absence of 0.1 mM DSS, the signal corresponding to wild type complex between VirB8 and VirB10 was reproducibly diminished in the case of two VirB8 variants (T201A/T201Y). (Figure 5.1) (Paschos et al., 2006). This suggests that VirB8^{T201} that is exposed on the beta sheet face of VirB8 is involved in interaction with VirB10.

5.3.2 Residues in VirB8 that are affected in dimerization as determined with the BTH assay.

Next, the VirB8 variants were tested for self-association using the bacterial two-hybrid assay that is based on the reconstitution of adenylate cyclase enzyme activity. VirB8 wild type and variant genes were fused to the genes encoding T18 and T25

fragments, respectively, and analyzed for interaction (Figure 5.2A). Here, we found that as mentioned previously in Chapter 3, VirB8^{M102}, VirB8^{Y105}, VirB8^{E214} are involved in VirB8 self-association. In addition, we found that VirB8^{K182} and VirB8^{T201} were also reduced (Figure 5.2B). This was surprising as purified periplasmic domains of both of these variants were tested previously using gel filtration and both eluted as a dimer under conditions similar to wild type VirB8.

Subsequently, we assessed whether VirB8 variants are disrupted in interaction with VirB9 and VirB10. Previously (Chapter 4), we showed using bicistronic constructs that simultaneously expressed VirB9 not fused to the AC domain (Figure 4.7A and Figure 5.3A) with VirB8 fused to the AC domains, there was strong increase in β-galactosidase activity (3.8 fold) indicating that VirB9 stimulated VirB8 self-association (Figure 4.7B). Here, we use this experimental set up to analyze whether other VirB8 variants would have an effect on the stimulatory effect of VirB9 on VirB8 dimerization. Similar to the results of the VirB8 variants, self-association of VirB8^{M102}, VirB8^{Y105}, VirB8^{E214}, VirB8^{K182} was reduced relative to the wild type. However, VirB9 still stimulated the activity of the dimer variants and only a qualitative analysis could be made since the bacterial two hybrid experiments testing the dimerization of VirB8 variants and the effect of VirB9 on the dimerization of VirB9 variants were not performed at the same time. However, this result is in agreement with that of the cross-linking assay in which none of the variants showed reduced complex formation with VirB9 relative to wild type.

5.3.3 Phage display experiments reveal VirB8 binding domains in VirB5, VirB6, VirB9 and VirB10.

Purified StrepIIVirB8sp was used in phage display experiments with two libraries Ph.D.-12 and Ph.D.-C7C (New England Biolabs, NEB) as prey. VirB8sp was immobilized and incubated with phage display libraries. Ph.D.-12 displays 12 variable amino acids sequence, while Ph.D.-C7C displays seven variable amino acids sequence in a constrained fashion on the surface of M13 phage. The bound peptides were eluted and the process repeated second time (2^{nd} panning) and a third time (3^{rd} panning) followed by sequencing of the peptide encoding DNA fragments. From the second and third panning, 91 unique peptide sequences from the Ph.D.-C7C library from 144 ssDNA sequenced, and 48 unique peptides from the Ph.D.-12 library from 192 ssDNA sequenced were obtained. In total, 139 unique peptides were aligned against VirB1, VirB3, VirB4, VirB5, VirB6, VirB8, VirB9, VirB10 and VirB11 using the Receptor ligand Contacts (RELIC) server MATCH program (http://relic.bio.anl.gov). The algoritm in the MATCH program uses as default a window size of five amino acids to search for maximum similarity and identified twelve peptides aligning in overlapping clusters to the C-terminus of VirB6 amino acids 251-313 (Figure 5.4A). A total of six peptides aligned with the N-terminus (49-100) of VirB9 (Figure 5.4B), and eight peptides aligned to VirB10 in two clusters in the N-terminus (101-150 aa) (Figure 5.4C). In addition, four peptides aligned to VirB5 in two clusters in the globular domain of VirB5 (51-100) (Figure 5.4D), thereby providing further evidence that VirB5 interacts with VirB8 via its globular domain (discussed in Chapter 2 of this thesis).

5.4 Discussion

In this study, the exploration of the VirB8 interaction with VirB9 and VirB10 was taken a step further by analysis of the ability of VirB8 variants to interact with VirB9 and VirB10. A cross-linking experiment of purified VirB8 variants with VirB10 identified that residue T201 of VirB8 as part of the likely site of interaction with VirB10 (Figure 5.1) (Paschos et al., 2006). The periplasmic domains of VirB8 from *B. suis* and *A. tumefaciens* crystallized to show high structural similarity. Both proteins consist of β-sheets and five α-helices (Bailey et al., 2006; Terradot et al., 2005). The dimer interface is largely found in the α-helix 1 with residues M102 and Y105 (Paschos et al., 2006), and the T201 residue is located on the β-sheet face. The dimerization site is distinct from the VirB8-VirB9 interaction interface, but we also found using the BTH assay that VirB8 changed at K182 and T201 had reduced self-association (Figure 5.2). On the other hand, when these proteins were purified and analyzed using analytical gel filtration (performed by Dr. A. Paschos, McMaster University (Paschos et al., 2006)), the variants showed similar dimerization features to wild type VirB8. It is possible that the changes K182 and T201 cause slight changes in conformation in this assay as they are fused to the T18 and T25 fragments of the adenylate cyclase unlike the analytical gel filtration experiments. Therefore, taking all the information together, the interface consisting of M102 and Y105 comprises the dimerization site and the T201 interface is possibly involved in interaction with VirB10. The cross-linking assay determines if two proteins are in near proximity and thus variants of VirB8 that are affected in their interaction with VirB9 may not be detected within the resolution of this assay. It would be important to pursue and follow

up this work using other protein-protein interaction analytic methods such as SPR to validate and identify interaction domains of VirB8 required for binding VirB9 and VirB10.

To complement the protein-protein interaction analysis, the phage display technique was adopted to identify domains of VirB proteins that bind to VirB8. VirB8 is well known to interact with multiple partners (Das & Xie, 2000; Ding et al., 2002; Höppner et al., 2005; Paschos et al., 2006; D. Ward et al., 2002; Yuan et al., 2005), and VirB8 from *B. suis* was used as bait with two combinatorial libraries Ph.D.-12 and Ph.D.-C7C to isolate peptides that bind VirB8. A total of 139 unique peptides isolated from the Ph.D.-12 and Ph.D.-C7C libraries were aligned to VirB1, VirB3, VirB4, VirB5, VirB6, VirB8, VirB9, VirB10 and VirB11. A cluster of overlapping peptides aligned with to VirB6, VirB9 and VirB10 (Figure 5.4). The VirB8 binding site in VirB6 is at the C-terminus of the protein that is suggested to be part of the TM helix according to TMPred (not shown) for VirB6 of *B. suis*. The topology of VirB6 from *B. suis* has not been determined experimentally and the topology from *A. tumefaciens* may not be useful as the proteins are of different length. According to TMPred, VirB6suis consists of 6 postulated TM domains (TMPred, not shown) while VirB6agro is reported to have 5 TM domains (Alvarez-Martinez & Christie, 2009; S.J. Jakubowski et al., 2004). However, it is exciting that this is the first report showing evidence for direct binding of VirB6 to VirB8. To substantiate the significance of these results, peptides that are staggered in the sequence of VirB6 amino acids (251-313) will be synthesized and used in protein-protein interaction assays (SPR, tryptophan fluorescence, isothermal titration calorimetry and the

bacterial two hybrid assay). Once the binding of the VirB6 peptides to VirB8 is established, mutational analysis of the VirB6 proteins could be carried out in the *A. tumefaciens* and *B. suis* system to observe the effects of the changes at the VirB8 binding site on T4SS assembly and function.

Phage display results using VirB8sp as bait showed alignment with VirB9 and VirB10 and this corresponds well to the recently published VirB7-VirB9-VirB10 outer core complex structure (Chandran et al., 2009) even if this complex does contain VirB8. The outer membrane core complex comprises the C-terminus of both VirB9 and VirB10 and our data from the phage display experiments revealed that the VirB8 binding domains of VirB9 and VirB10 are at the N-terminus that was not resolved in the crystal structure. Therefore, VirB8 together with other VirB proteins such as VirB6 and VirB3, could be important to form the inner membrane core complex along with the N-terminus of VirB9 and VirB10. A similar approach described before to validate VirB6-VirB8 binding will be pursued for VirB8-VirB9 and VirB8-VirB10 interactions using the information obtained from the phage display experiments. Interestingly, VirB8 affinity selected peptides aligned with VirB5 in the globular domain. This finding provides support for the significance of the results obtained with the phage display technique as we report in Chapter 2 that the globular domain of *B. suis* VirB5 comprises the VirB8 interaction site. Once the strategy to use peptides of VirB proteins to show interaction were established; this work would be used as a platform for use of cell-penetrating peptides to disrupt the interactions for applications in research and for the development of novel antimicrobials.

Table 5.1. Bacterial strains and plasmids used.

Strains	Genotype or description	Source or reference
E. coli ER2738	F' *proA*$^{+}$*B*$^{+}$ *lacI*^{q} Δ(lacZ) M15 *zzf::Tn10 (Tet*^{R}*)/fhuA2 glnVΔ(lac-proAB) Δ(hsdMS-mcrB)*5 [$r_k^-m_k^-$McrBC$^-$]	NEB
Plasmids		
pKT25	kan^r, pSU40 derivative encodes T25 fragment (amino acids 1-224 of CyaA)	(G. Karimova et al., 2000)
pUT18C	car^r, pUC19 derivative encodes T18 fragment (amino acids 225-399 of CyaA)	(G. Karimova et al., 2000)
pUT18CB8	car^r , pUT18C harboring 720 bp *XbaI/KpnI virB8* fragment from *B. suis* (encoding full-length VirB8)	(Paschos et al., 2009)
pKT25B8	kan^r, pKT25 harboring 720 bp *XbaI/KpnI virB8* fragment from *B. suis* (encoding full-length VirB8)	(Paschos et al., 2009)
pKT25B8^{M102R}	kan^r, pKT25 harboring 720 bp *XbaI/KpnI virB8* fragment from *B. suis* carrying the change at M102->R	Chapter 4
pKT25B8^{Y105R}	kan^r, pKT25 harboring 720 bp *XbaI/KpnI virB8* fragment from *B. suis* carrying the change at Y105->R	Chapter 4
pKT25B8^{E214R}	kan^r, pKT25 harboring 720 bp *XbaI/KpnI virB8* fragment from *B. suis* carrying the change at E214->R	Chapter 4
pKT25B8^{W119A}	kan^r, pKT25 harboring 720 bp *XbaI/KpnI virB8* fragment from *B. suis* carrying the change at W119->A	this work
pKT25B8^{I112R}	kan^r, pKT25 harboring 720 bp *XbaI/KpnI virB8* fragment from *B. suis* carrying the change at I112->R	this work
pKT25B8^{L151R}	kan^r, pKT25 harboring 720 bp *XbaI/KpnI virB8* fragment from *B. suis* carrying the change at L151->R	this work
pKT25B8^{K182E}	kan^r, pKT25 harboring 720 bp *XbaI/KpnI virB8* fragment from *B. suis* carrying the change at K182->E	this work
pKT25B8^{D152R}	kan^r, pKT25 harboring 720 bp *XbaI/KpnI virB8* fragment from *B. suis* carrying the change at D152->R	this work
pKT25B8^{T201A}	kan^r, pKT25 harboring 720 bp *XbaI/KpnI virB8* fragment from *B. suis* carrying the change at T201->A	this work
pKT25B8^{T201Y}	kan^r, pKT25 harboring 720 bp *XbaI/KpnI virB8* fragment from *B. suis* carrying the change at T201->Y	this work
pKT25B8^{R230D}	kan^r, pKT25 harboring 720 bp *XbaI/KpnI virB8* fragment from *B. suis* carrying the change at R230->D	this work

pKT25B8^{Y126E}	kan^r, pKT25 harboring 720 bp *XbaI/KpnI virB8* fragment from *B. suis* carrying the change at Y126->E	this work
pKT25B8^{Q144R}	kan^r, pKT25 harboring 720 bp *XbaI/KpnI virB8* fragment from *B. suis* carrying the change at Q144->R	this work
pUT18CB8^{M102R}	car^r, pUT18C harboring 720 bp *XbaI/KpnI virB8* fragment from *B. suis* carrying the change at M102->R	Chapter 4
pUT18CB8^{Y105R}	car^r, pUT18C harboring 720 bp *XbaI/KpnI virB8* fragment from *B. suis* carrying the change at Y105->R	Chapter 4
pUT18CB8^{E214R}	car^r, pUT18C harboring 720 bp *XbaI/KpnI virB8* fragment from *B. suis* carrying the change at E214->R	Chapter 4
pUT18CB8^{W119A}	car^r, pUT18C harboring 720 bp *XbaI/KpnI virB8* fragment from *B. suis* carrying the change at W119->A	this work
pUT18C8^{I112R}	car^r, pUT18C harboring 720 bp *XbaI/KpnI virB8* fragment from *B. suis* carrying the change at I112->R	this work
pUT18CB8^{L151R}	car^r, pUT18C harboring 720 bp *XbaI/KpnI virB8* fragment from *B. suis* carrying the change at L151->R	this work
pUT18CB8^{K182E}	car^r, pUT18C harboring 720 bp *XbaI/KpnI virB8* fragment from *B. suis* carrying the change at K182->E	this work
pUT18CB8^{D152R}	car^r, pUT18C harboring 720 bp *XbaI/KpnI virB8* fragment from *B. suis* carrying the change at D152->R	this work
pUT18CB8^{T201A}	car^r, pUT18C harboring 720 bp *XbaI/KpnI virB8* fragment from *B. suis* carrying the change at T201->A	this work
pUT18CB8^{T201Y}	car^r, pUT18C harboring 720 bp *XbaI/KpnI virB8* fragment from *B. suis* carrying the change at T201->Y	this work
pUT18CB8^{R230D}	car^r, pUT18C harboring 720 bp *XbaI/KpnI virB8* fragment from *B. suis* carrying the change at R230->D	this work
pUT18CB8^{Y126E}	car^r, pUT18C harboring 720 bp *XbaI/KpnI virB8* fragment from *B. suis* carrying the change at Y126->E	this work
pUT18CB8^{Q144R}	car^r, pUT18C harboring 720 bp *XbaI/KpnI virB8* fragment from *B. suis* carrying the change at Q144->R	this work
pUT18CB8+SD	car^r, pUT18CB8 carrying a Shine Dalgarno sequence downstream of *virB8*	Chapter 4
pUT18CB8+B9	car^r, pUT18CB8+SD harboring 870 bp *NcoI/HindIII virB9* fragment from *B. suis* (encoding full-length VirB9)	Chapter 4
pUT18CB8^{M102R}+B9	car^r, pUT18CB8+B9 where *virB8* fragment from *B. suis* carrying the change at M102->R	Chapter 4
pUT18CB8^{Y105R}+B9	car^r, pUT18CB8+B9 where *virB8* fragment from *B. suis* carrying the change at Y105->R	this work
pUT18CB8^{E214R}+B9	car^r, pUT18CB8+B9 where *virB8* fragment from *B. suis* carrying the change at E214->R	this work
pUT18CB8^{W119A}+B9	car^r, pUT18CB8+B9 where *virB8* fragment from *B. suis* carrying the change at W119->A	this work
pUT18C8^{I112R}+B9	car^r, pUT18CB8+B9 where *virB8* fragment from *B. suis* carrying the change at I112->R	this work

pUT18CB8^{L151R}+B9	car^{r}, pUT18CB8+B9 where *virB8* fragment from *B. suis* carrying the change at L151->R	this work
pUT18CB8^{K182E}+B9	car^{r}, pUT18CB8+B9 where *virB8* fragment from *B. suis* carrying the change at K182->E	this work
pUT18CB8^{D152R}+B9	car^{r}, pUT18CB8+B9 where *virB8* fragment from *B. suis* carrying the change at D152->R	this work
pUT18CB8^{T201A}+B9	car^{r}, pUT18CB8+B9 where *virB8* fragment from *B. suis* carrying the change at T201->A	this work
pUT18CB8^{T201Y}+B9	car^{r}, pUT18CB8+B9 where *virB8* fragment from *B. suis* carrying the change at T201->Y	this work
pUT18CB8^{R230D}+B9	car^{r}, pUT18CB8+B9 where *virB8* fragment from *B. suis* carrying the change at R230->D	this work
pUT18CB8^{Y126E}+B9	car^{r}, pUT18CB8+B9 where *virB8* fragment from *B. suis* carrying the change at Y126->E	this work
pUT18CB8^{Q144R}+B9	car^{r}, pUT18CB8+B9 where *virB8* fragment from *B. suis* carrying the change at Q144->R	this work

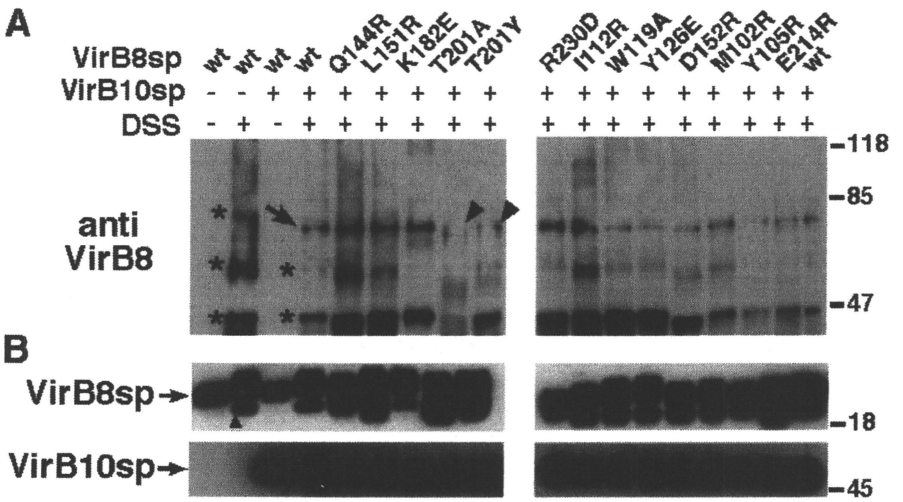

Figure 5.1 Analysis of the interaction between StrepIIVirB8sp variants and StrepIIVirB10sp by cross-linking. **A.** StrepIIVirB8sp and variants were mixed with StrepIIVirB10sp and incubated with 0.1mM DSS followed by SDS-PAGE and Western blotting with VirB8s specific antiserum. An arrow indicates cross-linked products of StrepIIVirB8sp in the absence of StrepIIVirB10sp, and arrowheads indicate reduced amounts of this heterodimer in case of two variants as compared with WT (representative results of three repetitions are shown). **B.** Western blots of SDS gels from cross-linked samples as loading controls. An additional VirB8sp specific signal of lower molecular mass (indicated by triangle) was observed in the presence of DSS that may correspond to an internal crosslink causing the change of migration. Molecular masses of reference proteins are shown on the right (in kDa) (Paschos et al., 2006).

A.

B.

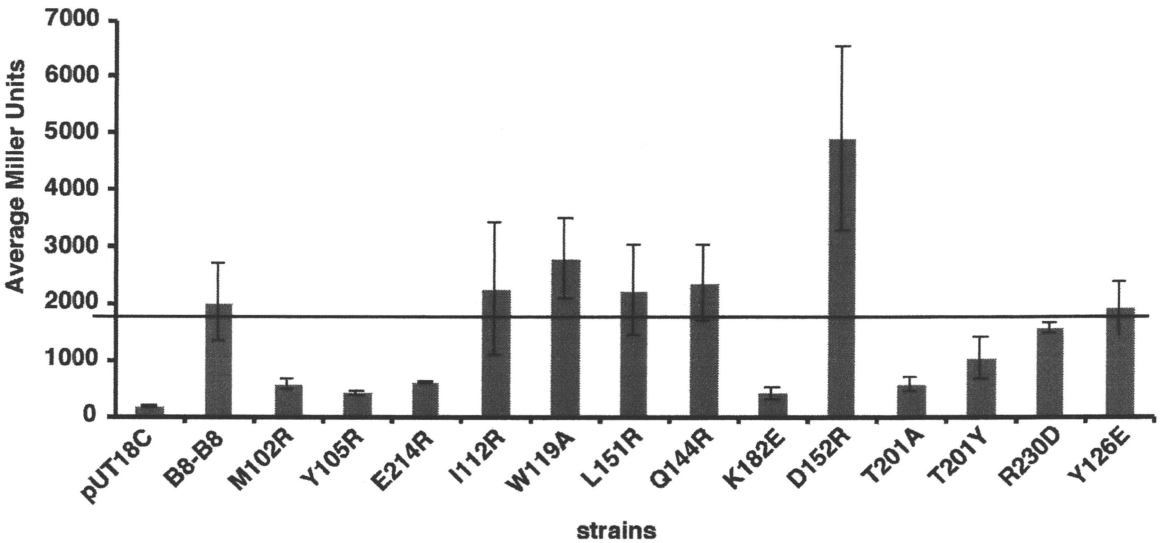

Figure 5.2 Bacterial two-hybrid (BTH) assay to test the self-association of VirB8 and its variants **A.** Schematic view of the constructs generated to test the effects of VirB8 variants on VirB8 dimerization. T18 and T25 designate the two domains of AC. **B.** Quantification of VirB8s and VirB8s variants' ability to self-associate. The strains displayed in the chart were co-transformed with plasmids encoding VirB8s wild type and variants fused to both the T25 fragment and the T18 fragment are labeled below the corresponding bar. Error bars represent the standard deviation of three independent measurements.

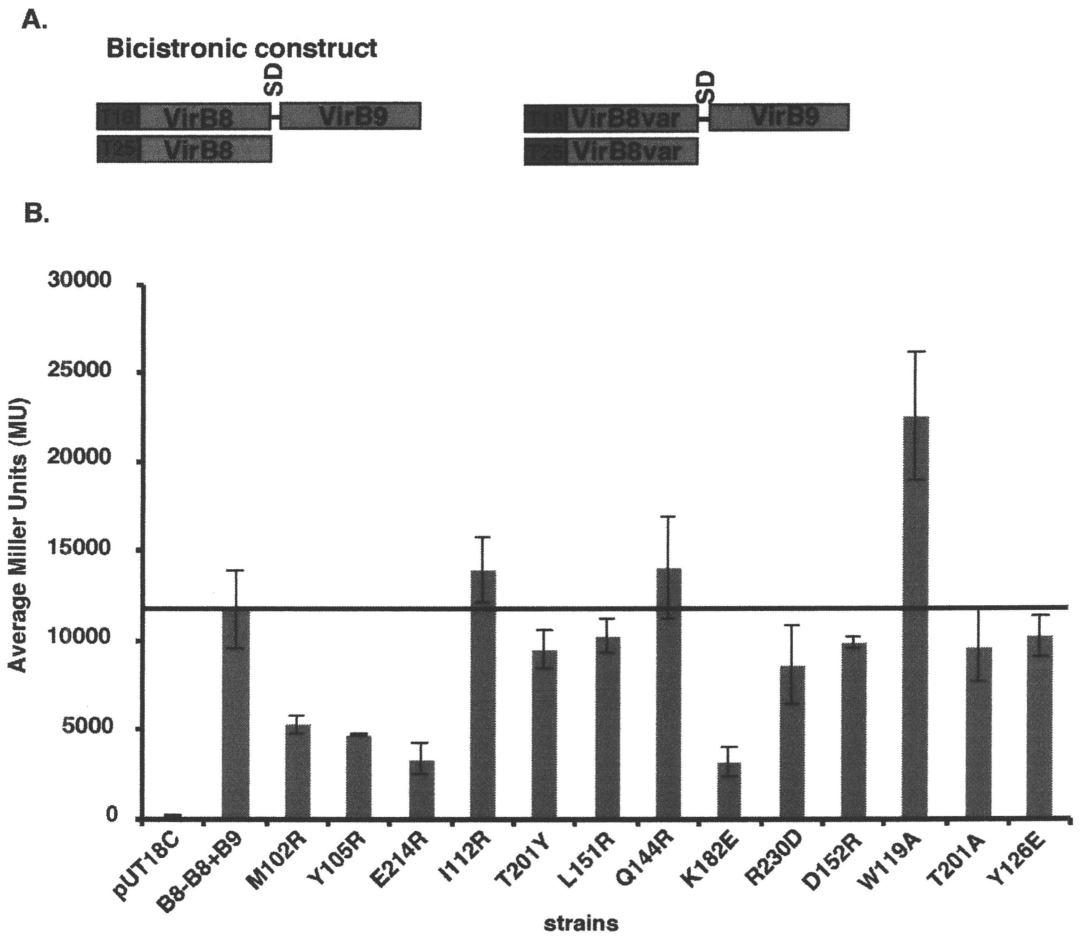

Figure 5.3 Bacterial two-hybrid (BTH) assay of VirB8 self-association stimulated by the presence of VirB9. **A.** Schematic view of the constructs generated to test the effects of VirB8 variants on ability of VirB9 to stimulate VirB8 dimerization. T18 and T25 designate the two domains of AC and SD, the Shine Dalgarno sequence. **B.** Quantification of VirB8s and VirB8s variants' dimerization to be stimulated by VirB9. The strains displayed in the chart were co-transformed with plasmids encoding VirB8s wild type and variants fused to both the T25 fragment and the T18 fragment are labeled below the corresponding bar. Error bars represent the standard deviation of three independent measurements.

A. VirB6 suis

B. VirB9 suis

C. VirB10 suis

D. VirB5 suis

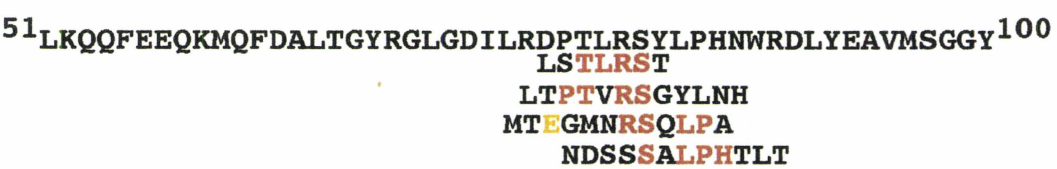

Figure 5.4 Alignment of peptides selected after phage display experiments using VirB8 as bait. Peptides were selected from both Ph.D-12 and Ph.D-C7C phage libraries with the periplasmic domain of VirB8 from *B. suis* as the bait and aligned against VirB6 protein sequence (**A**), VirB9 protein sequence (**B**), VirB10 protein sequence (**C**) and VirB5 protein sequence (**D**). Residues in red represent identical match to the VirB proteins and yellow coloured residues represent conserved match. Alignment of the peptides and maximum similarity scores were performed using the RELIC MATCH server (http://relic.bio.anl.gov). The top sequence displayed corresponds to the primary sequence of the VirB proteins and displayed below are the peptides isolated from the phage display experiments.

CHAPTER SIX: Summary and recommendations for future work.

6.1 Summary

Unraveling the sequence of interactions between VirB proteins that lead to the assembly of a functional T4SS has been tremendously difficult due to the large number of components that constitute them. In our laboratory, we identified an assembly sequence that is dependent on VirB4 (ATPase) and is necessary for pilus assembly and substrate transfer (Yuan et al., 2005). We showed that VirB4 stabilizes VirB8 and VirB3; and that VirB5 interacts directly with VirB8 (Chapter 2). VirB4 was also found to direct VirB5-VirB2 complex formation. Based on the data, we proposed that VirB4 interaction with VirB8 and VirB3 occurs first, followed by VirB5-VirB8 interaction that directs VirB2-VirB5 complexation and pilus formation (Yuan et al., 2005). In parallel, research in another laboratory showed using immuno-fluorescence that VirB8 acts as a scaffold to bring other VirB proteins for T4SS assembly at the poles of bacteria (Judd et al., 2005a). In addition, VirB8 from both *B. suis* and *A. tumefaciens* were crystallized and both were structurally very similar to each other and with nuclear transport factor 2 (NTF2) (Bailey et al., 2006). Along with this, VirB8 is known to interact with many VirB proteins (VirB1, VirB3, VirB4, VirB5, VirB8, VirB9, VirB10 and VirB11) (Das & Xie, 2000; Ding et al., 2002; Judd et al., 2005a; Kumar et al., 2000; Paschos et al., 2006; D. Ward et al., 2002). The main objective of this thesis was to characterize the structure and function of VirB8 in more detail. The second objective was to further characterize the assembly sequence leading to T4SS assembly mediated by VirB8.

Through purification of StrepIIVirB8sp and analysis using biophysical methods, I was able to demonstrate that VirB8 is a concentration dependent dimer with a K_d of 116 +/- 7.5 μM (Chapter 3). This was further confirmed using SPR that calculated a K_d of 26 +/- 5 μM (Chapter 4). Using analytical ultracentrifugation, I was able to show that changes of VirB8 at M102, Y105 and E214 led to monomeric proteins, thus, contributing towards the identification of the dimer interface of VirB8. Similarly, using SPR, I was able to show that M102 was affected in self-association providing further evidence for the identification of dimer interface. Having established the *in vitro* experiments to show that VirB8 self-associates and identified the dimerization site, I successfully adopted the bacterial two-hybrid (BTH) assay to show that VirB8 self-associates in *in vivo* and that the dimer variants are indeed affected (Chapter 3). Dr. Athanasios Paschos further modified the experimental set up and the plasmids for the BTH assay constructed by me to permit testing of the BTH system in anaerobic conditions to identify inhibitors to VirB8 dimerization.

Next, I demonstrated the mechanistic role for VirB8 self-association using the *A. tumefaciens* T4SS (Chapter 3). Here, using cysteine mutagenesis at the VirB8 dimer interface, I showed that VirB8 self-associates under physiological conditions and the dimer interface in VirB8 *suis* corresponds to the interface of VirB8 agro. In addition, I discovered an uncoupling variant changed at the V97 residue in VirB8agro that does not support T-pilus formation if the dimerization is enforced by the introduction of cysteine. In contrast, a change of V97 to T at this residue supports wild type T-pilus formation and dimerization (Chapter 4). Furthermore, I identified that VirB8 self-association is

necessary for VirB2 association with the core complex. In addition, in collaboration with Dr. Anna Carle (peptide array, Chapter 2) and Dr. Athanasios Paschos (competitive cross-linking), I showed that the VirB5 globular domain interacts with VirB8 and dissociates VirB8 dimers. Thus, we hypothesize that VirB8 requires being in a monomer-dimer equilibrium for its function and that it interacts with VirB5 as a monomer and with VirB2 as a dimer to direct VirB2-VirB5 complexes for T-pilus formation (Chapter 3).

Finally, I was able to propose a dynamic model for secretion system assembly in which VirB8 plays a role as assembly factor by interacting with VirB9 and VirB10 and a ternary complex was identified. In addition, a novel role for VirB9 was identified as VirB9 stimulates the self-association of VirB8, but it inhibits the VirB10-VirB10 as well as the VirB8-VirB10 interaction (Chapter 4). Importantly, I successfully established interaction assays (surface plasmon resonance, SPR) and phage display (Chapter 5) that will be used routinely in our laboratory in future.

6.2 Recommendations for future work

Taken together, the results and experimental procedures established in this thesis provide many avenues for further work. Future work leading from Chapter five could identify the VirB protein domains and residues that are important for VirB-VirB interactions. The phage display approach is very exciting and in this report VirB8 was used. In future, other VirB proteins such as VirB9 and VirB10 could be utilized to identify domains that are important for their interactions. Firstly, the information that was obtained from phage display experiments with VirB8 as bait identified a putative VirB9 interaction domain (Chapter 5) and subsequently, the use of VirB9 as bait will

identify the putative interaction domain of VirB8. This information will help us identify whether VirB9 interacts with VirB8 via the same or near the VirB10 binding site. According to the bacterial two hybrid (BTH) results, VirB9 disrupts VirB8-VirB10 interaction, and thus, suggests that VirB9 docks between VirB8 and VirB10 (Chapter 4). The results from phage display will help to test this hypothesis. Therefore, use of phage display technology with other VirB proteins should be examined to obtain high-resolution information regarding the T4SS assembly and architecture.

If the peptide approach to validate interactions between VirB8-VirB6, VirB8-VirB9 and VirB8-VirB10 is successful and validated by ITC, SPR and BTH, then these peptides could be utilized to design peptide inhibitors where target of inhibition is known. This may allow the design of novel inhibitors for therapeutics. In addition, one could utilize these peptides to understand the molecular details of T4SS assembly and function. By disrupting the interaction, for example, between VirB8-VirB9 *in vivo* with cell penetrating peptides one could assess the role of the VirB8-VirB9 interaction towards T4SS complex formation on T4SS function. On the same note, information on the T4SS architecture would be further advanced by the identification of the inner membrane core complex. Recently, the outer membrane core complex (VirB7-VirB9-VirB10) was crystallized, however, VirB8 the interaction partner of VirB9 and VirB10 was missing from this structure (Chandran et al., 2009). However, the phage display experiments using VirB8 (Chapter 5) as prey provided a clue to this perplexing result. VirB8 interacts with the N-terminus of VirB9 and VirB10, which are not crystallized in this complex and in addition, VirB8 interacts with VirB6, an inner membrane polytopic protein. Therefore,

it is possible that there are two major complexes that are formed in the membranes, one being the outer membrane complex that is crystallized (VirB7-VirB9-VirB10) and the second being the inner membrane complex formed between VirB8-VirB6/VirB3- VirB9 (N-terminus) -VirB10 (N-terminus). In order to test this hypothesis one could use the information gleaned from phage display and attempt to crystallize fragments of VirB6 along with VirB8-VirB9 and VirB10. Another question that is intriguing regarding T4SS structure is pilus assembly.

How does pilus assembly gets energized? What interactions among the VirB proteins and energizers of T4SS (VirB4 and VirB11) mediate the assembly of VirB2-VirB5 (pilus components) complexes to elongate into a pilus structure? Information regarding the interactions between the VirB proteins and the ATPases are limited. VirB4 is dispensable for pilus assembly as variant with changes at its active site still allowed pilus formation suggesting that VirB11 plays the major role for pilus assembly (Yuan et al., 2005). Therefore, interactions of VirB11 with inner membrane VirB proteins and assessment of the ATPase activity of VirB11 in the presence of these VirB proteins will provide initial clues towards answering this question.

On a broader topic in T4SS research, the regulation of VirB proteins' stoichiometry still remains a mystery. An observation that is intriguing is when a VirB protein such as VirB8 is absent; levels of VirB3 and VirB6 were strongly reduced in the cells (Chapter 3). Thus, it would be interesting to identify whether the levels of VirB proteins are regulated at the transcriptional level or if cellular proteases are activated by formation of unproductive complexes.

References

Alvarez-Martinez, C. E., & Christie, P. J. (2009). Biological diversity of prokaryotic type IV secretion systems. *Microbiol Mol Biol Rev, 73*(4), 775-808.

Aly, K., & Baron, C. (2007). VirB5 initiates T-pilus assembly in *Agrobacterium tumefaciens* and localizes at the pilus tip. *Microbiology, 153*, 3766-3775.

Anderson, L. B., Vogel Hertzel, A., & Das, A. (1996). *Agrobacterium tumefaciens* VirB7 and VirB9 form a disulfide-linked protein complex. *Proc. Natl. Acad. Sci. USA, 93*, 8889-8894.

Ansaldi, M., Lepelletier, M., & Mejean, V. (1996). Site-specific mutagenesis by using an accurate recombinant polymerase chain reaction method. *Anal. Biochem., 234*, 110-111.

Atmakuri, K., Cascales, E., & Christie, P. J. (2004). Energetic components VirD4, VirB11 and VirB4 mediate early DNA transfer reactions required for bacterial type IV secretion. *Mol. Microbiol., 54*, 1199-1211.

Atmakuri, K., Ding, Z., & Christie, P. J. (2003). VirE2, a type IV secretion substrate, interacts with the VirD4 transfer protein at cell poles of *Agrobacterium tumefaciens*. *Mol. Microbiol., 49*, 1699-1713.

Austin, J. W., Sanders, G., Kay, W. W., & Collinson, S. K. (1998). Thin aggregative fimbriae enhance *Salmonella enteritidis* biofilm formation. *FEMS Microbiol Lett, 162*(2), 295-301.

Backert, S., Fronzes, R., & Waksman, G. (2008). VirB2 and VirB5 proteins: specialized adhesins in bacterial type-IV secretion systems? *Trends Microbiol, 16*(9), 409-413.

Bailey, S., Ward, D., Middleton, R., Grossmann, J. G., & Zambryski, P. (2006). *Agrobacterium tumefaciens* VirB8 structure reveals potential protein-protein interactions sites. *Proc. Natl. Acad. Sci. USA, 103*(8), 2582-2587.

Balakrishnan, L., Hughes, C., & Koronakis, V. (2001). Substrate-triggered recruitment of the TolC channel-tunnel during type I export of hemolysin by *Escherichia coli*. *J Mol Biol, 313*(3), 501-510.

Balsinger, S., Ragaz, C., Baron, C., & Narberhaus, F. (2004). Replicon-specific regulation of small heat shock genes in *Agrobacterium tumefaciens*. *J. Bacteriol., 186*, 6824-6829.

Banta, L. M., Bohne, J., Lovejoy, S. D., & Dostal, K. (1998). Stability of the *Agrobacterium tumefaciens* VirB10 protein is modulated by growth temperature and periplasmic osmoadaption. *J. Bacteriol., 180*, 6597-6606.

Baron, C. (2005). From bioremediation to biowarfare: On the impact and mechanism of type IV secretion systems. *FEMS Microbiol. Lett., 253*, 163-170.

Baron, C. (2006). VirB8: a conserved type IV secretion system assembly factor and drug target. *Biochem Cell Biol, 84*(6), 890-899.

Baron, C., O'Callaghan, D., & Lanka, E. (2002). Bacterial secrets of secretion: EuroConference on the biology of type IV secretion processes. *Mol. Microbiol., 43*, 1359-1366.

Baron, C., Thorstenson, Y. R., & Zambryski, P. C. (1997). The lipoprotein VirB7 interacts with VirB9 in the membranes of *Agrobacterium tumefaciens*. *J. Bacteriol., 179*, 1211-1218.

Baron, C., & Zambryski, P. C. (1996). Plant Transformation: A pilus in *Agrobacterium* T-DNA transfer. *Curr. Biol., 6*, 1567-1569.

Bayliss, R., Harris, R., Coutte, L., Monier, A., Fronzes, R., Christie, P. J., et al. (2007). NMR structure of a complex between the VirB9/VirB7 interaction domains of the pKM101 type IV secretion system. *Proc Natl Acad Sci U S A, 104*(5), 1673-1678.

Beaupré, C. E., Bohne, J., Dale, E. M., & Binns, A. N. (1997). Interactions between VirB9 and VirB10 membrane proteins involved in movement of DNA from *Agrobacterium tumefaciens* into plant cells. *J. Bacteriol., 179*, 78-89.

Beijersbergen, A., Smith, S. J., & Hooykaas, P. J. J. (1994). Localization and topology of VirB proteins of *Agrobacterium tumefaciens*. *Plasmid, 32*, 212-218.

Berger, B. R., & Christie, P. J. (1994). Genetic complementation analysis of the *Agrobacterium tumefaciens* virB operon: virB2 through virB11 are essential virulence genes. *J. Bacteriol., 176*, 3646-3660.

Bhandari, P., & Gowrishankar, J. (1997). An *Escherichia coli* host strain useful for efficient overproduction of cloned gene products with NaCl as the inducer. *J. Bacteriol., 179*, 4403-4406.

Bohne, J., Yim, A., & Binns, A. N. (1998). The Ti plasmid increases the efficiency of *Agrobacterium tumefaciens* as a recipient in virB-mediated conjugal transfer of an IncQ plasmid. *Proc. Natl. Acad. Sci. USA, 95*, 7057-7062.

Bourg, G., Sube, R., O'Callaghan, D., & Patey, G. (2009). Interactions between *Brucella suis* VirB8 and its homolog TraJ from the plasmid pSB102 underline the dynamic nature of type IV secretion systems. *J Bacteriol, 191*(9), 2985-2992.

Brok, R., Van Gelder, P., Winterhalter, M., Ziese, U., Koster, A. J., de Cock, H., et al. (1999). The C-terminal domain of the *Pseudomonas* secretin XcpQ forms oligomeric rings with pore activity. *J Mol Biol, 294*(5), 1169-1179.

Carle, A., Höppner, C., Aly, K. A., Yuan, Q., den Dulk-Ras, A., Vergunst, A., et al. (2006). The *Brucella suis* type IV secretion system assembles in the cell envelope of the heterologous host *Agrobacterium tumefaciens* and increases IncQ plasmid pLS1 recipient competence. *Infect. Immun., 74*, 108-117.

Carter DM, I. M., JN Gagnon, E. Martinez, A. Clements, J. Lee, MA Hancock, H. Gagnon, PD. Pawelek, and JW Coulton. (2006). Interactions between TonB from *Escherichia coli* and the periplasmic protein FhuD. *Journal of Biological Chemistry, 281*(46), 35413-35424.

Cascales, E., & Christie, P. J. (2003). The versatile bacterial type IV secretion systems. *Nat. Rev. Microbiol., 1*, 137-149.

Cascales, E., & Christie, P. J. (2004a). *Agrobacterium* VirB10, an ATP energy sensor required for type IV secretion. *Proc. Natl. Acad. Sci. USA, 101*, 17228-17233.

Cascales, E., & Christie, P. J. (2004b). Definition of a bacterial type IV secretion pathway for a DNA substrate. *Science, 304*, 1170-1173.

Celli, J., de Chastellier, C., Franchini, D. M., Pizarro-Cerda, J., E., M., & Gorvel, J. P. (2003). *Brucella* evades macrophage killing via VirB-dependent sustained interactions with the endoplasmic reticulum. *J. Exp. Med., 198*, 545-556.

Celli, J., & Gorvel, J. P. (2004). Organelle robbery: *Brucella* interactions with the endoplasmic reticulum. *Curr. Opin. Microbiol., 7*, 93-97.

Chaillan-Huntington, C., Butler, P. J., Huntington, J. A., Akin, D., Feldherr, C., & Stewart, M. (2001). NTF2 monomer-dimer equilibrium. *J. Mol. Biol., 314*, 465-477.

Chandran, V., Fronzes, R., Duquerroy, S., Cronin, N., Navaza, J., & Waksman, G. (2009). Structure of the outer membrane complex of a type IV secretion system. *Nature, 29*, 29.

Christie, P. J. (2001). Type IV secretion: intercellular transfer of macromolecules by systems ancestrally related to conjugation machines. *Mol. Microbiol., 40*, 294-305.

Christie, P. J. (2004). Type IV secretion: the *Agrobacterium* VirB/D4 and related conjugation systems. *Biochim. Biophys. Acta, 1694*, 219-234.

Christie, P. J., Atmakuri, K., Krishnamoorthy, V., Jakubowski, S., & Cascales, E. (2005). Biogenesis, Architecture, and Function of Bacterial Type IV Secretion Systems. *Annu. Rev. Microbiol., 59*, 415-485.

Cianciotto, N. P. (2005). Type II secretion: a protein secretion system for all seasons. *Trends Microbiol, 13*(12), 581-588.

Cowie, A., Jiujun Cheng, Christopher D. Sibley, Ying Fong, Rahat Zaheer, Cheryl L. Patten, Richard M. Morton, G. Brian Golding, and Turlough M. Finan. (2006). An Integrated Approach to Functional Genomics: Construction of a Novel Reporter Gene Fusion Library for *Sinorhizobium meliloti*. *Applied and Environmental Microbiology, 72*(11), 7156-7167.

Dang, T. A., & Christie, P. J. (1997). The VirB4 ATPase of *Agrobacterium tumefaciens* is a cytoplasmic membrane protein exposed at the periplasmic surface. *J. Bacteriol., 179*, 453-462.

Das, A., Anderson, L. B., & Xie, Y.-H. (1997). Delineation of the interaction domains of *Agrobacterium tumefaciens* VirB7 and VirB9 by use of the yeast two-hybrid assay. *J. Bacteriol., 179*, 3404-3409.

Das, A., & Xie, Y.-H. (1998). Construction of transposon Tn3phoA: its application in defining the membrane topology of the *Agrobacterium tumefaciens* DNA transfer proteins. *Mol. Microbiol., 27*, 405-414.

Das, A., & Xie, Y.-H. (2000). The *Agrobacterium* T-DNA transport pore proteins VirB8, VirB9 and VirB10 interact with one another. *J. Bacteriol., 182*, 758-763.

Das, A., & Xie, Y. H. (1998). Construction of transposon Tn3phoA: its application in defining the membrane topology of the *Agrobacterium tumefaciens* DNA transfer proteins. *Mol Microbiol, 27*(2), 405-414.

De Crescenzo, G., Boucher, C., Durocher, Y., & Jolicoeur, M. (2008). Kinetic characterization by surface plasmon resonance-based biosensors: principle and emerging trends. *Cell. Mol. Bioeng., 1*, 204-215.

de Jong, M. F., Sun, Y. H., den Hartigh, A. B., van Dijl, J. M., & Tsolis, R. M. (2008a). Identification of VceA and VceC, two members of the VjbR regulon that are translocated into macrophages by the *Brucella* type IV secretion system. *Mol Microbiol, 70*(6), 1378-1396.

de Jong, M. F., Sun, Y. H., den Hartigh, A. B., van Dijl, J. M., & Tsolis, R. M. (2008b). Identification of VceA and VceC, two members of the VjbR regulon that are translocated into macrophages by the *Brucella* type IV secretion system. *Mol. Microbiol. , 70*(6), 1378-1396.

de Paz, H. D., Sangari, F. J., Bolland, S., Garcia-Lobo, J. M., Dehio, C., de la Cruz, F., et al. (2005). Functional interactions between type IV secretion systems involved in DNA transfer and virulence. *Microbiology, 151*(Pt 11), 3505-3516.

Delrue, R. M., Deschamps, C., Leonard, S., Nijskens, C., Danese, I., Schaus, J. M., et al. (2005). A quorum-sensing regulator controls expression of both the type IV secretion system and the flagellar apparatus of *Brucella melitensis*. *Cell. Microbiol., 7*, 1151-1161.

den Hartigh, A. B., Rolan, H. G., de Jong, M. F., & Tsolis, R. M. (2008). VirB3 to VirB6 and VirB8 to VirB11, but not VirB7, are essential for mediating persistence of *Brucella* in the reticuloendothelial system. *J Bacteriol, 190*(13), 4427-4436.

den Hartigh, A. B., Sun, Y. H., Sondervan, D., Heuvelmans, N., Reinders, M. O., Ficht, T. A., et al. (2004). Differential requirements for VirB1 and VirB2 during *Brucella abortus* infection. *Infect. Immun., 72*, 5143-5149.

Desvaux, M., Hebraud, M., Talon, R., & Henderson, I. R. (2009). Secretion and subcellular localizations of bacterial proteins: a semantic awareness issue. *Trends Microbiol, 17*(4), 139-145.

Ding, Z., Zhao, Z., Jakubowski, S., Krishnamohan, A., Margolin, W., & Christie, P. J. (2002). A novel cytology-based, two-hybrid screen for bacteria applied to protein-protein interaction studies of a type IV secretion system. *J. Bacteriol., 184*(20), 5572-5582.

Fernandez, D., Dang, T. A. T., Spudich, G. M., Zhou, X.-R., Berger, B. R., & Christie, P. J. (1996). The *Agrobacterium tumefaciens* virB7 gene product, a proposed component of the T-complex transport apparatus, is a membrane-associated lipoprotein exposed at the periplasmic surface. *J. Bacteriol., 178*, 3156-3167.

Fernandez, D., Spudich, G. M., Zhou, X.-R., & Christie, P. J. (1996). The *Agrobacterium tumefaciens* virB7 lipoprotein is required for stabilization of VirB proteins during assembly of the T-complex transport apparatus. *J. Bacteriol., 178*, 3168-3176.

Filloux, A. (2004). The underlying mechanisms of type II protein secretion. *Biochim Biophys Acta, 1694*(1-3), 163-179.

Filloux, A., Hachani, A., & Bleves, S. (2008). The bacterial type VI secretion machine: yet another player for protein transport across membranes. *Microbiology, 154*(Pt 6), 1570-1583.

Foulongne, V., Bourg, G., Cazevieille, C., Michaux-Charachon, S., & O'Callaghan, D. (2000). Identification of *Brucella suis* genes affecting intracellular survival in an in vitro human macrophage infection model by signature-tagged transposon mutagenesis. *Infect. Immun., 68*, 1297-1303.

Fronzes, R., Christie, P. J., & Waksman, G. (2009). The structural biology of type IV secretion systems. *Nat Rev Microbiol, 7*(10), 703-714.

Fronzes, R., Schafer, E., Wang, L., Saibil, H. R., Orlova, E. V., & Waksman, G. (2009). Structure of a type IV secretion system core complex. *Science, 323*(5911), 266-268.

Garcillan-Barcia, M. P., Francia, M. V., & de la Cruz, F. (2009). The diversity of conjugative relaxases and its application in plasmid classification. *FEMS Microbiol Rev, 33*(3), 657-687.

Greenfield, N. J., & Fowler, V. M. (2002). Tropomyosin requires an intact N-terminal coiled coil to interact with tropomodulin. *Biophys J, 82*(5), 2580-2591.

Guo, M., Jin, S., Sun, D., Hew, C. L., & Pan, S. Q. (2007). Recruitment of conjugative DNA transfer substrate to *Agrobacterium* type IV secretion apparatus. *Proc Natl Acad Sci U S A, 104*(50), 20019-20024.

Hamilton, C. M., Lee, H., Li, P. L., Cook, D. M., Piper, K. R., von Bodman, S. B., et al. (2001). TraG from RP4 and TraG and VirD4 from Ti plasmids confer relaxosome specificity to the conjugal transfer system of pTiC58. *J. Bacteriol., 182*, 1541-1548.

Hapfelmeier, S., Domke, N., Zambryski, P. C., & Baron, C. (2000). VirB6 is required for stabilization of VirB5, VirB3 and formation of VirB7 homodimers in *Agrobacterium tumefaciens*. *J. Bacteriol., 182*, 4505-4511.

Hare, S., Bayliss, R., Baron, C., & Waksman, G. (2006). A large domain swap in the VirB11 ATPase of *Brucella suis* leaves the hexameric assembly intact. *J Mol Biol, 360*(1), 56-66.

Harlow, E., & Lane, D. (Eds.). (1988). *Antibodies: A laboratory manual*. Cold Spring Harbor, NY: Cold Spring Harbor Laboratory.

Henderson, I. R., Cappello, R., & Nataro, J. P. (2000). Autotransporter proteins, evolution and redefining protein secretion. *Trends Microbiol, 8*(12), 529-532.

Höppner, C., Carle, A., Sivanesan, D., Hoeppner, S., & Baron, C. (2005). The putative lytic transglycosylase VirB1 from *Brucella suis* interacts with the type IV secretion system core components VirB8, VirB9 and VirB11. *Microbiology, 151*, 3469-3482.

Höppner, C., Liu, Z., Domke, N., Binns, A. N., & Baron, C. (2004). VirB1 orthologs from *Brucella suis* and pKM101 complement defects of the lytic transglycosylase required for efficient type IV secretion from *Agrobacterium tumefaciens*. *J. Bacteriol., 186*, 1415-1422.

Hudson, M. E., & Nodwell, J. R. (2003). Membrane association and kinase-like motifs of the RamC protein of *Streptomyces coelicolor*. *J. Bacteriol., 186*, 1330-1336.

Hung, D. L., Knight, S. D., Woods, R. M., Pinkner, J. S., & Hultgren, S. J. (1996). Molecular basis of two subfamilies of immunoglobulin-like chaperones. *Embo J, 15*(15), 3792-3805.

Hwang, H. H., & Gelvin, S. B. (2004). Plant proteins that interact with VirB2, the *Agrobacterium tumefaciens* pilin protein, mediate plant transformation. *Plant Cell, 16*, 3148-3167.

Jakubowski, S. J., Cascales, E., Krishnamoorthy, V., & Christie, P. J. (2005). *Agrobacterium tumefaciens* VirB9, an outer-membrane-associated component of a type IV secretion system, regulates substrate selection and T-Pilus biogenesis. *J. Bacteriol., 187*, 3486-3495.

Jakubowski, S. J., Kerr, J. E., Garza, I., Krishnamoorthy, V., Bayliss, R., Waksman, G., et al. (2009). *Agrobacterium* VirB10 domain requirements for type IV secretion and T pilus biogenesis. *Mol Microbiol, 71*(3), 779-794.

Jakubowski, S. J., Krishnamoorthy, V., Cascales, E., & Christie, P. J. (2004). *Agrobacterium tumefaciens* VirB6 domains direct the ordered export of a DNA substrate through a type IV secretion System. *J. Mol. Biol., 341*, 961-977.

Jakubowski, S. J., Krishnamoorthy, V., & Christie, P. J. (2003). *Agrobacterium tumefaciens* VirB6 protein participates in formation of VirB7 and VirB9 complexes required for type IV secretion. *J. Bacteriol., 185*, 2867-2878.

Jones, A. L., Shirasu, K., & Kado, C. I. (1994). The product of the virB4 gene of *Agrobacterium tumefaciens* promotes accumulation of VirB3 protein. *J. Bacteriol., 176*, 5255-5261.

Jose, J., Jahnig, F., & Meyer, T. F. (1995). Common structural features of IgA1 protease-like outer membrane protein autotransporters. *Mol Microbiol, 18*(2), 378-380.

Judd, P. K., Kumar, R. B., & Das, A. (2005a). Spatial location and requirements for the assembly of the *Agrobacterium tumefaciens* type IV secretion apparatus. *Proc. Natl. Acad. Sci. USA*(102), 11498-11503.

Judd, P. K., Kumar, R. B., & Das, A. (2005b). The type IV secretion apparatus protein VirB6 of *Agrobacterium tumefaciens* localizes to a cell pole. *Mol. Microbiol., 55*, 115-124.

Karimova, G., Josette Pidoux, Agnes Ullmann and Daniel Ladant. (1998). A bacterial two-hybrid system based on a reconstituted signal transduction pathway. *Proc Natl Acad Sci U S A, 95*(10), 5752-5756.

Karimova, G., Ullmann, A., & Ladant, D. (2000). A bacterial two-hybrid system that exploits a cAMP signaling cascade in *Escherichia coli. Methods Enzymol, 328*, 59-73.

Krall, L., Wiedemann, U., Unsin, G., Weiss, S., Domke, N., & Baron, C. (2002). Detergent extraction identifies different VirB protein subassemblies of the type IV secretion machinery in the membranes of *Agrobacterium tumefaciens. Proc. Natl. Acad. Sci. USA, 99*, 11405-11410.

Krause, S., Pansegrau, W., Lurz, R., de la Cruz, F., & Lanka, E. (2000). Enzymology of type IV macromolecule secretion systems: the conjugative transfer regions of plasmids RP4 and R388 and the cag pathogenicity island of *Helicobacter pylori* encode structurally and functionally related nucleoside triphosphate hydrolases. *J. Bacteriol., 182*, 2761-2770.

Kromayer, M., Wilting, R., Tormay, P., & Böck, A. (1996). Domain structure of the prokaryotic selenocysteine-specific elongation factor SelB. *J. Mol. Biol., 262*, 413-420.

Kumar, R. B., & Das, A. (2001). Functional analysis of the *Agrobacterium tumefaciens* T-DNA transport pore protein VirB8. *J. Bacteriol., 183*, 3636-3641.

Kumar, R. B., Xie, Y.-H., & Das, A. (2000). Subcellular localization of the *Agrobacterium tumefaciens* T-DNA transport pore proteins: VirB8 is essential for assembly of the transport pore. *Mol. Microbiol., 36*, 608-617.

Laemmli, U. K. (1970). Cleavage of structural proteins during the assembly of the head of bacteriophage T4. *Nature, 227*, 680-685.

Lai, E. M., Eisenbrandt, R., Kalkum, M., Lanka, E., & Kado, C. I. (2002). Biogenesis of T pili in *Agrobacterium tumefaciens* requires precise VirB2 propilin cleavage and cyclization. *J Bacteriol, 184*(1), 327-330.

Lai, W. C., & Hazelbauer, G. L. (2007). Analyzing transmembrane chemoreceptors using *in vivo* disulfide formation between introduced cysteines. *Methods Enzymol, 423*, 299-316.

Letoffe, S., Ghigo, J. M., & Wandersman, C. (1994). Secretion of the *Serratia marcescens* HasA protein by an ABC transporter. *J Bacteriol, 176*(17), 5372-5377.

Liu, Z., & Binns, A. N. (2003). Functional subsets of the VirB type IV transport complex proteins involved in the capacity of *Agrobacterium tumefaciens* to serve as a recipient in virB-Mediated conjugal transfer of plasmid RSF1010. *J. Bacteriol., 185*, 3259-3269.

Llosa, M., & O'Callaghan, D. (2004). Euroconference on the Biology of Type IV Secretion Processes: bacterial gates into the outer world. *Mol. Microbiol., 53*, 1-8.

Llosa, M., Roy, C., & Dehio, C. (2009). Bacterial type IV secretion systems in human disease. *Mol Microbiol, 73*(2), 141-151.

Maniatis, T. A., Fritsch, E. F., & Sambrook, J. (1982). *Molecular Cloning: A Laboratory Manual*. Cold Spring Harbor, NY: Cold Spring Harbor Laboratory.

Marlovits, T. C., & Stebbins, C. E. (2009). Type III secretion systems shape up as they ship out. *Curr Opin Microbiol, 16*, 16.

Middleton, R., Sjölander, K., Krishnamurthy, N., Foley, J., & Zambryski, P. (2005). Predicted hexameric structure of the *Agrobacterium* VirB4 C terminus suggests VirB4 acts as a docking site during type IV secretion. *Proc. Natl. Acad. Sci. USA, 102*, 1685-1690.

Mota, L. J., & Cornelis, G. R. (2005). The bacterial injection kit: type III secretion systems. *Ann Med, 37*(4), 234-249.

Mourino, M., Munoa, F., Balsalobre, C., Diaz, P., Madrid, C., & Juarez, A. (1994). Environmental regulation of alpha-haemolysin expression in *Escherichia coli*. *Microb Pathog, 16*(4), 249-259.

Mudrak, B., & Kuehn, M. J. Specificity of the type II secretion systems of enterotoxigenic *Escherichia coli* and *Vibrio cholerae* for heat-labile enterotoxin and cholera toxin. *J Bacteriol, 2010*, 22.

Myszka, D. G. (1999). Improving biosensor analysis. *J Mol Recognit, 12*(5), 279-284.

Nanao, M., Ricard-Blum, S., Di Guilmi, A. M., Lemaire, D., Lascoux, D., Chabert, J., et al. (2003). Type III secretion proteins PcrV and PcrG from *Pseudomonas aeruginosa* form a 1:1 complex through high affinity interactions. *BMC Microbiol, 3*(21), 21.

Novick, R. P. (1987). Plasmid incompatibility. *Microbiol Rev, 51*(4), 381-395.

O´Callaghan, D., Cazevieille, C., Allardet-Servent, A., Boschiroli, M. L., Bourg, G., Foulongne, V., et al. (1999). A homologue of the *Agrobacterium tumefaciens* VirB and *Bordetella pertussis* Ptl type IV secretion systems is essential for intracellular survival of *Brucella suis*. *Mol. Microbiol., 33*, 1210-1220.

O'Callaghan, D., Cazevieille, C., Allardet-Servent, A., Boschiroli, M. L., Bourg, G., Foulongne, V., et al. (1999). A homologue of the *Agrobacterium tumefaciens* VirB and *Bordetella pertussis* Ptl type IV secretion systems is essential for intracellular survival of Brucella suis. *Mol. Microbiol., 33*, 1210-1220.

Parsot, C., Hamiaux, C., & Page, A. L. (2003). The various and varying roles of specific chaperones in type III secretion systems. *Curr Opin Microbiol, 6*(1), 7-14.

Paschos, A., den Hartig, A., Coincon, M., Sivanesan, D., Sygusch, J., Tsolis, R. M., et al. (2009). An *in vivo* high-throughput screening approach targeting the type IV secretion system component VirB8 identified inhibitors of intracellular proliferation of *Brucella*. *Plos Pathogens, In revision.*

Paschos, A., Patey, G., Sivanesan, D., Bayliss, R., Waksman, G., O'Callaghan, D., et al. (2006). Dimerization and interactions of *Brucella suis* VirB8 with VirB4 and VirB10 are required for its biological activity. *Proc Natl Acad Sci U S A, 103*(19), 7252-7257.

Paulsen, I. T., Seshadri, R., Nelson, K. E., Eisen, J. A., Heidelberg, J. F., Read, T. D., et al. (2002). The *Brucella suis* genome reveals fundamental similarities between animal and plant pathogens and symbionts. *Proc. Natl. Acad. Sci. USA, 99*, 13148-13153.

Quinaud, M., Chabert, J., Faudry, E., Neumann, E., Lemaire, D., Pastor, A., et al. (2005). The PscE-PscF-PscG complex controls type III secretion needle biogenesis in *Pseudomonas aeruginosa*. *J Biol Chem, 280*(43), 36293-36300.

Rambow-Larsen, A. A., Petersen, E. M., Gourley, C. R., & Splitter, G. A. (2009). *Brucella* regulators: self-control in a hostile environment. *Trends Microbiol, 17*(8), 371-377.

Rouot, B., Alvarez-Martinez, M.-T., Marius, C., Mentanteau, P., Guilloteau, L., Boigegrain, R.-A., et al. (2003). Production of the type IV secretion system differs among *Brucella* species as revealed with VirB5- and VirB8-specific antisera. *Infect. Immun., 71*, 1075-1082.

Roux, C. M., Rolan, H. G., Santos, R. L., Beremand, P. D., Thomas, T. L., Adams, L. G., et al. (2007). *Brucella* requires a functional Type IV secretion system to elicit innate immune responses in mice. *Cell Microbiol, 9*(7), 1851-1869.

Sagulenko, E., Sagulenko, V., Chen, J., & Christie, P. J. (2001). Role of *Agrobacterium* VirB11 ATPase in T-pilus assembly and substrate selection. *J. Bacteriol., 183*, 5813-5825.

Salmond, G. P. C. (1994). Secretion of extracellular virulence factors by plant pathogenic bacteria. *Annu. Rev. Phytopathol., 32*, 181-200.

Sauer, F. G., Remaut, H., Hultgren, S. J., & Waksman, G. (2004). Fiber assembly by the chaperone-usher pathway. *Biochim. Biophys. Acta, 1694*, 259-267.

Savvides, S. N., Yeo, H. J., Beck, M. R., Blaesing, F., Lurz, R., Lanka, E., et al. (2003). VirB11 ATPases are dynamic hexameric assemblies: new insights into bacterial type IV secretion. *EMBO J., 22*, 1969-1980.

Schägger, H., & von Jagow, G. (1987). Tricine-sodium dodecyl sulfate-polyacrylamide gel electrophoresis for the separation of proteins in the range of 1 to 100 kDa. *Anal. Biochem., 166*, 368-379.

Schmidt-Eisenlohr, H., Domke, N., Angerer, C., Wanner, G., Zambryski, P. C., & Baron, C. (1999). Vir proteins stabilize VirB5 and mediate its association with the T pilus of *Agrobacterium tumefaciens*. *J. Bacteriol., 181*, 7485-7492.

Schmidt-Eisenlohr, H., Domke, N., & Baron, C. (1999). TraC of IncN plasmid pKM101 associates with membranes and extracellular high molecular weight structures in *Escherichia coli*. *J. Bacteriol., 181*, 5563-5571.

Schröder, G., & Dehio, C. (2005). Virulence-associated type IV secretion systems of *Bartonella*. *Trends Microbiol., 13*, 336-342.

Schröder, G., & Lanka, E. (2005). The mating pair formation system of conjugative plasmids-A versatile secretion machinery for transfer of proteins and DNA. *Plasmid, 54*, 1-25.

Seubert, A., Hiestand, R., de la Cruz, F., & Dehio, C. (2003). A bacterial conjugation machinery recruited for pathogenesis. *Mol. Microbiol., 49*, 1253-1266.

Shamaei-Tousi, A., Cahill, R., & Frankel, G. (2004). Interaction between protein subunits of the type IV secretion system of *Bartonella henselae*. *J. Bacteriol., 186*, 4796-4801.

Shirasu, K., & Kado, C. I. (1993). Membrane localization of the Ti plasmid VirB proteins involved in the biosynthesis of a pilin-like structure in *Agrobacterium tumefaciens*. *FEMS Microbiol. Lett., 111*, 287-294.

Sivanesan, D., Hancock, M. A., Villamil Giraldo, A. M., & Baron, C. (2010). Quantitative Analysis of VirB8-VirB9-VirB10 Interactions Provides a Dynamic Model of Type IV Secretion System Core Complex Assembly. *Biochemistry*.

Sreerama, N., & Woody, R. W. (2000). Estimation of protein secondary structure from circular dichroism spectra: comparison of CONTIN, SELCON, and CDSSTR Methods with an expanded reference set. *Anal. Biochem., 287*, 252-260.

Stachel, S. E., & Zambryski, P. C. (1986). virA and virG control the plant-induced activation of the T-DNA transfer process of A. tumefaciens. *Cell, 46*(3), 325-333.

Stahl, L. E., Jacobs, A., & Binns, A. N. (1998). The conjugal intermediate of plasmid RSF1010 inhibits *Agrobacterium tumefaciens* virulence and VirB-dependent export of VirE2. *J. Bacteriol., 180*, 3933-3939.

Sun, Y. H., Garcia-Rolan, H., den Hartigh, A. B., Sondervan, D., & Tsolis, R. M. (2005). *Brucella abortus* VirB12 is expressed during infection, but it is not an essential component of the type IV secretion system. *Infect. Immun., 73*, 6048-6054.

Surana, N. K., Cutter, D., Barenkamp, S. J., & St Geme, J. W., 3rd. (2004). The *Haemophilus influenzae* Hia autotransporter contains an unusually short trimeric translocator domain. *J Biol Chem, 279*(15), 14679-14685.

Taneva, S., Joanne E. Johnson, and Rosemary B. Cornell. (2003). Lipid-Induced Conformational Switch in the Membrane Binding Domain of

CTP:Phosphocholine Cytidyltransferase: A Circular Dichroism Study. *Biochemistry, 42*, 11768-11776.

Terradot, L., Bayliss, R., Oomen, C., Leonard, G., Baron, C., & Waksman, G. (2005). Crystal Structures of the periplasmic domains of two core subunits of the bacterial type IV secretion system, VirB8 from *Brucella suis* and ComB10 from *Helicobacter pylori*. *Proc. Natl. Acad. Sci. USA, 102*, 4596-4601.

van Larebeke, N., Engler, G., Holsters, M., van den Elsacker, S., Zaenen, I., Schilperoort, R. A., et al. (1974). Large plasmids in *Agrobacterium tumefaciens* essential for crown gall-inducing ability. *Nature, 252*, 169-170.

Vetsch, M., Erilov, D., Moliere, N., Nishiyama, M., Ignatov, O., & Glockshuber, R. (2006). Mechanism of fibre assembly through the chaperone-usher pathway. *EMBO Rep, 7*(7), 734-738.

Vitagliano, L., Ruggiero, A., Pedone, C., & Berisio, R. (2007). A molecular dynamics study of pilus subunits: insights into pilus biogenesis. *J Mol Biol, 367*(4), 935-941.

Ward, D., Draper, O., Zupan, J. R., & Zambryski, P. C. (2002). Peptide linkage mapping of the *A. tumefaciens* vir-encoded type IV secretion system reveals novel protein subassemblies. *Proc. Natl. Acad. Sci. USA, 99*, 11493-11500.

Ward, J. E., Dale, E. M., Nester, E. W., & Binns, A. N. (1990). Identification of a VirB10 protein aggregate in the inner membrane of *Agrobacterium tumefaciens*. *Journal of Bacteriology, 172*, 5200-5210.

Watarai, M., Makino, S., Fujii, Y., Okamoto, K., & Shirahata, T. (2002). Modulation of *Brucella*-induced macropinocytosis by lipid rafts mediates intracellular replication. *Cell Microbiol, 4*, 341-355.

Winans, S. C. (1992). Two-way chemical signalling in *Agrobacterium*-plant interactions. *Microbiol. Rev., 56*, 12-31.

Yanisch-Perron, C., Viera, J., & Messing, J. (1985). Improved M13 phage cloning vectors and host strains: nucleotide sequence of the M13mp18 and pUC18 vectors. *Gene, 33*, 103-119.

Yeo, H.-J., Yuan, Q., Beck, M. R., Baron, C., & Waksman, G. (2003). Structural and functional characterization of the VirB5 protein from the type IV secretion system encoded by the conjugative plasmid pKM101. *Proc. Natl. Acad. Sci. USA, 100*, 15947-15962.

Yeo, H. J., Savvides, S. N., Herr, A. B., Lanka, E., & Waksman, G. (2000). Crystal structure of the hexameric traffic ATPase of the *Helicobacter pylori* type IV secretion system. *Mol. Cell, 6*, 1461-1472.

Yuan, Q., Carle, A., Gao, C., Sivanesan, D., Aly, K., Höppner, C., et al. (2005). Identification of the VirB4-VirB8-VirB5-VirB2 pilus assembly sequence of type IV secretion systems. *J. Biol. Chem., 280*, 26349-26359.

Zahrl, D., Wagner, M., Bischof, K., Bayer, M., Zavecz, B., Beranek, A., et al. (2005a). Peptidoglycan degradation by specialized lytic transglycosylases associated with type III and type IV secretion systems. *Microbiology, 151*, 3455-3467.

Zahrl, D., Wagner, M., Bischof, K., Bayer, M., Zavecz, B., Beranek, A., et al. (2005b). Peptidoglycan degradation by specialized lytic transglycosylases associated with type III and type IV secretion systems. *Microbiology, 151*(Pt 11), 3455-3467.

Zhou, X. R., & Christie, P. J. (1997). Suppression of mutant phenotypes of the *Agrobacterium tumefaciens* VirB11 ATPase by overproduction of VirB proteins. *J Bacteriol, 179*(18), 5835-5842.

Zupan, J., Hackworth, C. A., Aguilar, J., Ward, D., & Zambryski, P. (2007). VirB1* promotes T-pilus formation in the vir-Type IV secretion system of *Agrobacterium tumefaciens. J Bacteriol, 189*(18), 6551-6563.

Zupan, J., Muth, T. R., Draper, O., & Zambryski, P. C. (2000). The transfer of DNA from *Agrobacterium tumefaciens* into plants: A feast of fundamental insights. *Plant J., 23*, 11-28.